

MATHEMATICAL MODELLING AND ANALYSIS OF CALCIUM
OSCILLATIONS
IN EXCITABLE AND NON-EXCITABLE CELL LINES

A Thesis

by

BHARATI KRISHNA HEGDE

Submitted to the Office of Graduate Studies of
Texas A&M University
in partial fulfillment of the requirements for the degree of
MASTER OF SCIENCE

May 2003

Major Subject: Biomedical Engineering

MATHEMATICAL MODELLING AND ANALYSIS OF CALCIUM
OSCILLATIONS
IN EXCITABLE AND NON-EXCITABLE CELL LINES

A Thesis

by

BHARATI KRISHNA HEGDE

Submitted to Texas A&M University
in partial fulfillment of the requirements
for the degree of

MASTER OF SCIENCE

Approved as to style and content by:

Roula Mouneimne
(Co-Chair of Committee)

John Criscione
(Co-Chair of Committee)

Robert Burghardt
(Member)

Hsin-I Wally Wu
(Member)

William Hyman
(Head of Department)

May 2003

Major Subject: Biomedical Engineering

ABSTRACT

Mathematical Modelling And Analysis of Calcium Oscillations
in Excitable and Non-Excitable Cell Lines. (May 2003)

Bharati Krishna Hegde, B.E., University of Pune, India

Co-Chairs of Advisory Committee: Dr. Roula Mouneimne
Dr. John Criscione

Information is transmitted from the cell surface to various specific targets in the cell via several cellular signaling pathways. Cytosolic free calcium (Ca^{2+}) is one of the most versatile and ubiquitous intracellular messengers since it is able to regulate diverse number of functions such as proliferation, secretion, fertilization, metabolism, learning and memory. In the last couple of years, evidence has been accumulating that Ca^{2+} ion is able to integrate information from multiple signaling pathways and convert this information into a code which regulates events ranging from contraction to modification of gene expression (Berridge et al. 1998). It was shown that Ca^{2+} concentration displays oscillatory behavior in response to agonist stimulation in a variety of cells (Goldbeter 1996) and the frequency of these oscillations increases with the concentration of agonist, a behavior called frequency encoding which has led to the concept that many Ca^{2+} -regulated processes are controlled by these codes (Berridge 1998).

Although the presence of Ca^{2+} oscillations and the sources of Ca^{2+} pools involved is known in many cell types, it is yet not known how the various frequencies of Ca^{2+} oscillations are converted into codes that regulate the numerous cellular events. Recently a number of cellular targets that decode Ca^{2+} signals and are tuned to

the frequency of Ca^{2+} oscillations have been identified. Prominent among them are calcium-calmodulin kinase II (CAM II) and protein kinase C (PKC).

The objective of this work is to study and mathematically model the oxytocin and vasopressin-induced Ca^{2+} oscillations in cells of normal rat liver (Clone 9) and cells of pregnant human myometrium. The proposed model accounts for the receptor-controlled Ca^{2+} oscillations involving positive feedback leading to activation of phospholipase C (PLC) and negative feedback from PKC onto G-proteins which simulates many of the features of observed intracellular Ca^{2+} . The model also incorporates the concept that coordinated Ca^{2+} signals in a group of hepatocytes require both effective gap junctions and the presence of agonist at each cell surface. Another objective of this research is to understand the relevance of frequency-encoded signals by performing an analysis of frequencies of Ca^{2+} oscillations using the Fast Fourier Transform and the Wavelet Transform. The validity of the model was confirmed by using statistical tests to check if the frequencies and amplitudes of the experimental Ca^{2+} oscillations match with those of the modelled oscillations.

To my parents.

ACKNOWLEDGMENTS

I wish to thank several people without whose help and support it would have been difficult for me to work towards my goal. Firstly I am deeply indebted to Dr. Roula Barhoumi Mouneimne for having given me this opportunity. Her constant guidance and advice and in-depth discussions on all important issues have helped me immensely. I also express my heartfelt gratitude to Dr. John Criscione, Dr. Jay Humphrey and Dr. Robert Burghardt for providing valuable insights. I would like to thank my family members who have seen me through all times and have been an unending source of inspiration. I am also grateful to the faculty and staff of both the Biomedical Engineering Department and the Image Analysis Lab for extending their helping hand whenever needed. Last but not least, I would like to thank all my friends for all the enlightening discussions and fruitful arguments.

TABLE OF CONTENTS

CHAPTER		Page
I	INTRODUCTION	1
	A. CALCIUM SIGNALLING	1
	1. Some Important Aspects Of Calcium Signalling	9
II	BACKGROUND	14
	A. MODELS FOR Ca^{2+} OSCILLATIONS	14
	1. Incorporation Of Gap Junction Diffusion	26
III	PROPOSED MODEL	28
	A. EXPERIMENTAL PROCEDURE FOR EXCITABLE CELLS	28
	B. EXPERIMENTAL PROCEDURE FOR NON-EXCITABLE CELLS	30
	C. DESCRIPTION OF THE PROPOSED MODEL	33
	1. Gap Junction Diffusion In Non-Excitable Cell Model	36
IV	RESULTS OF DATA MODELLING	38
	A. EXCITABLE (PHM1-41) CELL LINE	38
	1. Results Of Proposed Model Fit With PHM1-41 (Excitable) Cell Line	39
	2. Time Domain Statistical Tests	43
	3. Frequency Domain Statistical Tests	46
	B. NON-EXCITABLE (CLONE 9) CELL LINE	51
	1. Results Of Proposed Model Fit With Non-Excitable Cells	52
	2. Results To Show Effect Of Gap Junction	57
	3. Time Domain Statistical Tests	62
	4. Frequency Domain Statistical Tests	65
	C. DISCUSSION	72
V	RESULTS OF DATA ANALYSIS	74
	A. FAST FOURIER TRANSFORM	74
	1. Analysis Of Excitable Cells Using FFT	76

CHAPTER	Page
2. Analysis Of Non-Excitable Cells Using FFT	83
B. WAVELET TRANSFORMS	88
1. Analysis Of Excitable Cells Using 1-D DWT	92
C. DISCUSSION	115
VI SUMMARY AND CONCLUSIONS	116
A. SUMMARY	116
B. CONCLUSIONS	118
REFERENCES	119
APPENDIX A	122
VITA	143

LIST OF TABLES

TABLE		Page
I	Time Domain Test For Excitable Cells.	44
II	Fundamental Frequencies Of Excitable Cells.	46
III	Statistical Frequency Test For Excitable Cells.	48
IV	Fundamental Amplitudes Of Excitable Cells.	49
V	Statistical Amplitude Test For Excitable Cells.	51
VI	Time Domain Test For Non-Excitable Cell Line.	63
VII	Fundamental Frequencies Of Non-Excitable Cell Line.	66
VIII	Statistical Frequency Test For Non-Excitable Cell Line.	68
IX	Fundamental Amplitudes Of Excitable Cells.	69
X	Statistical Amplitude Test For Excitable Cells.	71

LIST OF FIGURES

FIGURE		Page
1	The Four Units Of The Ca^{2+} Signalling Toolkit[3].	2
2	Details Of The Signalling Toolkit[3]	3
3	Elementary And Global Events[6]	10
4	Basic Mechanisms Of Ca^{2+} Signalling[6]	12
5	The CICR Model[12]	16
6	IP_3 - Ca^{2+} Crosscoupling (ICC) Model[13]	19
7	Shen And Larter Model[14]	21
8	Cytosolic Calcium Oscillations.[14]	23
9	Gap Junction Diffusion In A Group Of Three Hepatocytes.[9]	24
10	The Proposed Model	34
11	PHM1-41 Cell 1	39
12	PHM1-41 Cell 2	39
13	PHM1-41 Cell 3	40
14	PHM1-41 Cell 4	40
15	PHM1-41 Cell 5	41
16	PHM1-41 Cell 6	41
17	PHM1-41 Cell 7	42
18	PHM1-41 Cell 8	42
19	PHM1-41 Cell 9	42

FIGURE	Page
20	PHM1-41 Cell 10 43
21	Clone 9 Cell 1 52
22	Clone 9 Cell 2 53
23	Clone 9 Cell 3 54
24	Clone 9 Cell 4 54
25	Clone 9 Cell 5 55
26	Clone 9 Cell 6 55
27	Clone 9 Cell 7 55
28	Clone 9 Cell 8 56
29	Clone 9 Cell 9 56
30	Clone 9 Cell 10 56
31	With Gap Junction Clone 9 Cell 1 57
32	Without Gap Junction Clone 9 Cell 1 57
33	With Gap Junction Clone 9 Cell 2 58
34	Without Gap Junction Clone 9 Cell 2 58
35	With Gap Junction Clone 9 Cell 3 59
36	Without Gap Junction Clone 9 Cell 3 59
37	With Gap Junction Clone 9 Cell 4 60
38	Without Gap Junction Clone 9 Cell 4 60
39	With Gap Junction Clone 9 Cell 5 60
40	Without Gap Junction Clone 9 Cell 5 61
41	With Gap Junction Clone 9 Cell 6 61

FIGURE	Page
42	Without Gap Junction Clone 9 Cell 6 62
43	Original Cell 1 In Time Domain 76
44	Fast Fourier Transform(FFT) Of Cell 1 76
45	Reconstructed Cell 1 After IFFT 77
46	Original Cell 2 In Time Domain 77
47	Fast Fourier Transform(FFT) of Cell 2 77
48	Reconstructed Cell 2 After IFFT 78
49	Original Cell 3 In Time Domain 78
50	Fast Fourier Transform(FFT) Of Cell 3 78
51	Reconstructed Cell 3 After IFFT 79
52	Original Cell 4 In Time Domain 79
53	Fast Fourier Transform(FFT) Of Cell 4 80
54	Reconstructed Cell 4 After IFFT 80
55	Original Cell 5 In Time Domain 81
56	Fast Fourier Transform(FFT) Of Cell 5 81
57	Reconstructed Cell 5 After IFFT 81
58	Original Cell 6 In Time Domain 82
59	Fast Fourier Transform(FFT) Of Cell 6 82
60	Reconstructed Cell 6 After IFFT 82
61	Original Cell 1 In Time Domain 83
62	Fast Fourier Transform(FFT) Of The Cell 1 83
63	Reconstructed Cell 1 After IFFT 84

FIGURE	Page
64	Original Cell 2 In Time Domain 84
65	Fast Fourier Transform(FFT) Of The Cell 2 85
66	Reconstructed Cell 2 After IFFT 85
67	Original Cell 3 In Time Domain 86
68	Fast Fourier Transform(FFT) Of The Cell 3 86
69	Reconstructed Cell 3 After IFFT 86
70	Original Cell 4 In Time domain 87
71	Fast Fourier Transform(FFT) Of The Cell 4 87
72	Reconstructed Cell 4 After IFFT 87
73	Scaling[19] 88
74	Shifting[19] 89
75	Continuous Wavelet Transform.[19] 90
76	Filtering For One-d Discrete Wavelet Transform.[19] 91
77	Decomposition And Reconstruction.[19] 91
78	Original Cell 1 In Time Domain 92
79	Denoised Experimental Cell 1 93
80	Denoised Model Cell 1 94
81	1-D DWT Of Cell 1 94
82	1-D Inverse DWT Of Cell 1 95
83	Expt Cell 1 Decomposition: Approximations 97
84	Expt Cell 1 Decomposition: Details 98
85	Details Of Coefficients Of Expt Cell 1 99

FIGURE	Page
86	Model Cell 1 Decomposition: Approximations 101
87	Model Cell 1 Decomposition: Details 102
88	Details Of Coefficients Of Model Cell 1 103
89	Original Cell 2 In Time Domain 104
90	Denoised Experimental Cell 2 105
91	Denoised Model Cell 2 106
92	1-D DWT Of Cell 2 107
93	1-D Inverse DWT Of Cell 2 107
94	Expt Cell 2 Decomposition: Approximations 108
95	Expt Cell 2 Decomposition: Details 109
96	Details Of Coefficients Of Expt Cell 2 110
97	Model Cell 2 Decomposition: Approximations 112
98	Model Cell 2 Decomposition: Details 113
99	Details Of Coefficients Of Model Cell 2 114
100	PHM1 Cell 11 122
101	PHM1 Cell 12 122
102	PHM1 Cell 13 123
103	PHM1 Cell 14 123
104	PHM1 Cell 15 123
105	PHM1 Cell 16 124
106	PHM1 Cell 17 125
107	PHM1 Cell 18 125

FIGURE	Page
108	PHM1 Cell 19 126
109	PHM1 Cell 20 126
110	PHM1 Cell 21 127
111	PHM1 Cell 22 127
112	PHM1 Cell 23 128
113	PHM1 Cell 24 128
114	PHM1 Cell 25 129
115	PHM1 Cell 26 129
116	PHM1 Cell 27 130
117	PHM1 Cell 28 130
118	PHM1 Cell 29 131
119	PHM1 Cell 30 131
120	PHM1 Cell 31 132
121	PHM1 Cell 32 132
122	PHM1 Cell 33 133
123	PHM1 Cell 34 133
124	PHM1 Cell 35 134
125	PHM1 Cell 36 135
126	PHM1 Cell 37 135
127	Clone 9 Cell 19 136
128	Clone 9 Cell 20 136
129	Clone 9 Cell 21 136

FIGURE	Page
130	Clone 9 Cell 22 137
131	Clone 9 Cell 23 137
132	Clone 9 Cell 24 137
133	Clone 9 Cell 25 138
134	Clone 9 Cell 26 138
135	Clone 9 Cell 27 139
136	Clone 9 Cell 28 139
137	Clone 9 Cell 29 139
138	Clone 9 Cell 30 140
139	Clone 9 Cell 31 140
140	Clone 9 Cell 32 140
141	Clone 9 Cell 33 141
142	Clone 9 Cell 34 141
143	Clone 9 Cell 35 141
144	Clone 9 Cell 36 142

CHAPTER I

INTRODUCTION

A. CALCIUM SIGNALLING

Almost everything that we do is controlled by Ca^{2+} – how we move, how our hearts beat and how our brains process information and store memories. To do all of this, Ca^{2+} acts as an intracellular messenger, relaying information within cells to regulate their activity. It is a versatile signal responsible for controlling a diverse range of cellular processes such as gene transcription, muscle contraction and cell proliferation. For example, Ca^{2+} triggers life at fertilization and controls the development and differentiation of cells into specialized types [1]. It mediates the subsequent activity of these cells and finally is invariably involved in cell death. The ability of a simple ion such as Ca^{2+} to play a pivotal role in cell biology results from the facility that cells have to shape Ca^{2+} signals in the dimensions of space, time and amplitude [2]. Cells at rest have a Ca^{2+} concentration of approximately 100 nM but are activated when this level rises as high as 1000 nM (Fig.1). At this elevation Ca^{2+} can regulate a number of processes. This is possible because of its use of numerous signalling components, which comprise the "signalling toolkit", an array of signalling, homeostatic and sensory mechanisms that can be assembled in various combinations to create signals with widely different spatial and temporal profiles (Fig.2)[3]. By mixing and matching components from the toolkit, cells can obtain Ca^{2+} signals that suit their physiology. Many variations are achieved through the cross talk between Ca^{2+} and other signalling pathways, which results in the regulation of diverse cellular responses. Given below is a brief description of the elements that form the basic building blocks

The journal model is *IEEE Transactions on Automatic Control*.

of the calcium signalling toolkit:

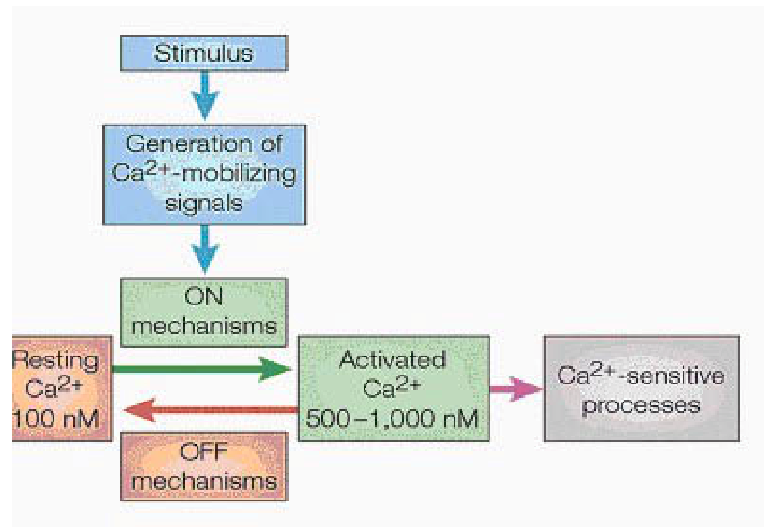


Fig. 1. The Four Units Of The Ca^{2+} Signalling Toolkit[3].

- Signalling is triggered by a stimulus that generates various Ca^{2+} -mobilizing signals.
- These Ca^{2+} -mobilizing signals activate the ON mechanisms that feed Ca^{2+} into the cytoplasm.
- Ca^{2+} functions as a messenger to stimulate numerous Ca^{2+} -sensitive processes.
- The OFF mechanisms, composed of pumps and exchangers, remove Ca^{2+} from the cytoplasm to restore the resting state of Ca^{2+} .

The following is a more detailed description of the above four units:

- Generation of Ca^{2+} mobilizing signals:

Cells generate their Ca^{2+} signals by using both internal and external sources of Ca^{2+} . The internal stores are held within the membrane systems of the endoplasmic reticulum (ER) or the sarcoplasmic reticulum (SR) of muscle cells.

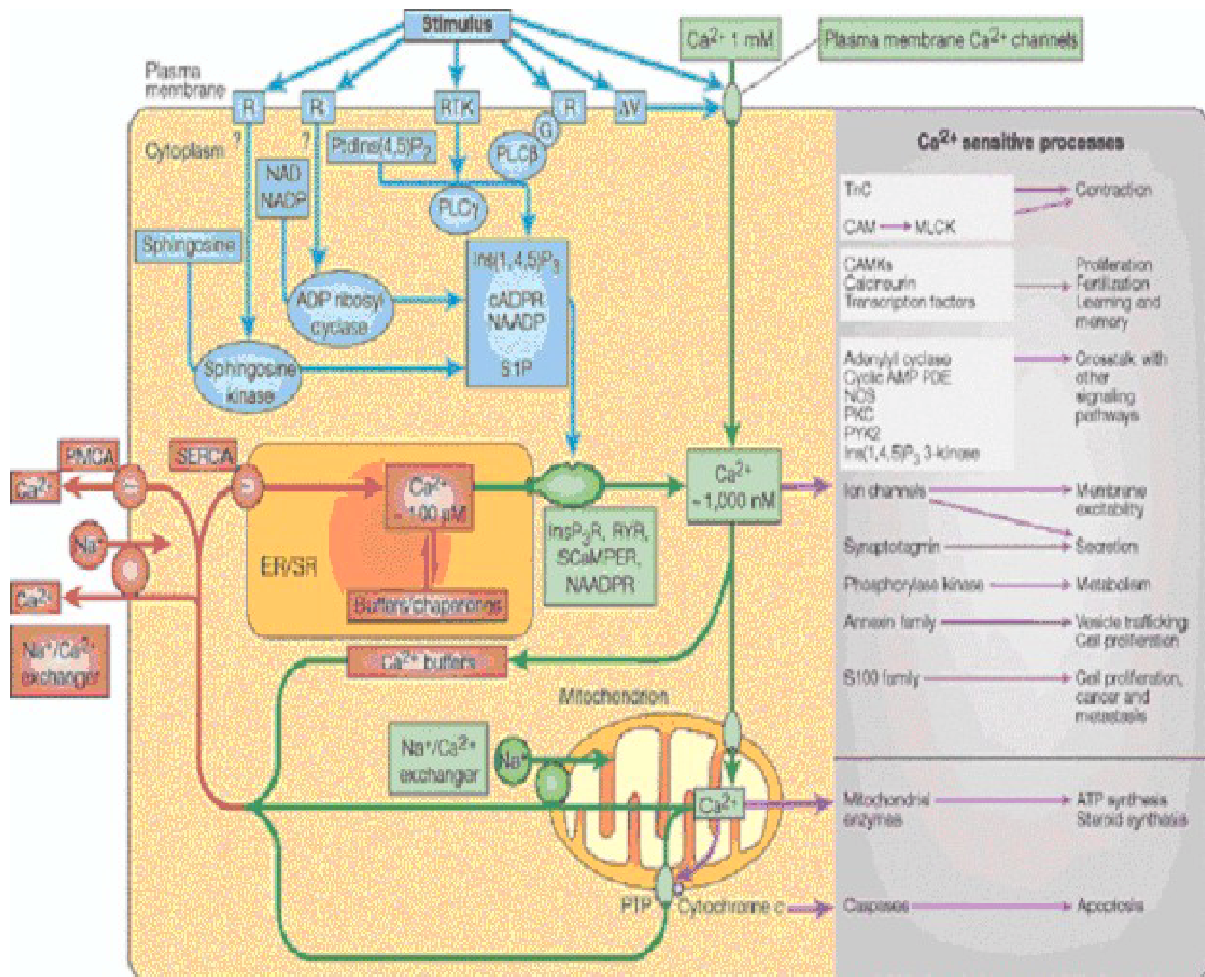


Fig. 2. Details Of The Signalling Toolkit[3]

The release from these internal stores is controlled by various channels, of which the inositol-1,4,5-triphosphate receptor (InsP₃R) and ryanodine receptor (RYR) families have been studied most extensively. Ca²⁺ is the main activator of these channels and this process of Ca²⁺-Induced-Ca²⁺-Release is central to the mechanism of Ca²⁺ signalling. Ca²⁺-mobilizing second messengers that are generated when stimuli bind to cell surface receptors (Fig.2) determine whether Ca²⁺ can activate these channels. These Ca²⁺-mobilizing signals are generated by stimuli acting through a variety of cell-surface receptors (R), including G-protein (G)-linked receptors and receptor tyrosine kinases (RTK). The signals generated include:

1. Inositol-1,4,5-trisphosphate(Ins(1,4,5)P₃), generated by the hydrolysis of phosphatidylinositol-4,5-bisphosphate (PtdIns(4,5)P₂) by a family of phospholipase C enzymes (PLC, PLC); Ins(1,4,5)P₃ diffuses into the cell to engage the InsP₃Rs and release Ca²⁺ from the ER.
2. Cyclic ADP ribose (cADPR) and nicotinic acid dinucleotide phosphate (NAADP)[4], are both generated from nicotinamide-adenine dinucleotide (NAD) and its phosphorylated derivative NADP by ADP ribosyl cyclase. NAADP acts on a separate, as yet uncharacterized channel.
3. Sphingosine 1-phosphate (S1P), generated from sphingosine by a sphingosine kinase, which releases Ca²⁺ from the ER - by binding to a sphingolipid Ca²⁺ release-mediating protein of the ER (SCaMPER)[5].

These different Ca²⁺-mobilizing messengers can co-exist in cells, where they seem to be controlled by different receptors. For example, human SH-SY5Y cells have acetylcholine receptors linked through Ins(1,4,5)P₃ whereas lysophos-

phatidic acid acts through S1P[3].

- ON Mechanisms:

The Ca^{2+} 'On' mechanisms include channels located at the plasma membrane (PM) which regulate the supply of Ca^{2+} from extra cellular space, and channels on the endoplasmic reticulum and sarcoplasmic reticulum (ER and SR respectively.) The On mechanisms depend on Ca^{2+} channels that control the entry of external Ca^{2+} or the release of Ca^{2+} from internal stores Cells utilize several different types of Ca^{2+} influx channels, which can be grouped on the basis of their activation mechanisms[2]. There are several types of channels:

- Voltage-Operated Ca^{2+} Channels (VOCCs): These are plasma-membrane ion channels that are activated by plasma membrane depolarization. VOCCs are employed largely by excitable cell types such as muscle and neuronal cells, where they are activated by depolarization of the PM. Mammalian VOCCs are comprised of 5 protein subunits (a1,a2,b,g,d), with one member (the a1 subunit) acting as the Ca^{2+} channel, and the others serving to regulate channel gating. Multiple isoforms of these subunits have been detected, raising the possibility of a myriad of different combinations.
- Receptor-Operated Ca^{2+} Channels (ROCCs): These are plasma-membrane ion channels that are activated by the binding of an agonist to the extracellular domain of the channel. These channels open on binding external stimuli, usually transmitters such as glutamate, ATP or acetylcholine. ROCCs comprise a range of structurally and functionally diverse channels that are particularly prevalent on secretory cells and nerve terminals. Well-known ROCCs include the nicotinic acetylcholine receptor and the

N-methyl-D-aspartate receptor.

- Store-Operated Ca^{2+} Channels (SOCCs): These are plasma-membrane ion channels, of uncertain identity, that open in response to depletion of intracellular Ca^{2+} stores, either by physiological Ca^{2+} -mobilising messengers or pharmacological agents. The mechanism by which the SOCCs 'sense' the filling status of the intracellular pool is unknown. In response to a Ca^{2+} -mobilizing signal such as inositol-1, 4,5-trisphosphate ($\text{Ins}(1,4,5)\text{P}_3$), Ca^{2+} is released from the endoplasmic reticulum. Emptying of the store is detected by a protein, most probably an inositol-1,4,5-trisphosphate receptor (InsP_3R) or a ryanodine receptor (RZR), which undergoes a conformational change that is transmitted to the store-operated channel to induce Ca^{2+} entry across the plasma membrane. Since many different types of cells have been shown to have an enhanced Ca^{2+} entry following Ca^{2+} pool depletion, SOCCs may be one of the most ubiquitous PM Ca^{2+} channels.
- Mechanically activated Ca^{2+} channels are present on many cell types and respond to cell deformation. Such channels convey information into the cell concerning the stress/ shape changes that a cell is experiencing. An example of this type of channel was observed in epithelial cells from the trachea, where deformation of a single cell led to a radial Ca^{2+} wave that synchronized the Ca^{2+} -sensitive beating of cilia on many neighboring cells [2].

In addition to the established mechanisms described above, evidence is accumulating in favor of Ca^{2+} channels that are activated by intracellular lipid messengers such as diacylglycerol and arachdonic acid. These unknown channels

activate substantial Ca^{2+} influx in the absence of Ca^{2+} store release. Increasing the level of Ca^{2+} within the lumen of the ER/SR enhances the sensitivity of the RYRs and the same may apply to the InsP_3Rs . The cytosolic action of Ca^{2+} is more complex: it can be both stimulatory and inhibitory and can vary between the different InsP_3R isoforms. In general, the InsP_3Rs have a bell-shaped Ca^{2+} dependence when treated with low concentrations of $\text{Ins}(1,4,5)\text{P}_3$: low concentrations of Ca^{2+} (100-300 nM) are stimulatory but above 300 nM, Ca^{2+} becomes inhibitory and switches the channel off. Evidence indicates that InsP_3Rs are sometimes not inhibited by high cytosolic Ca^{2+} concentrations. Instead of a bell-shape, the relationship between InsP_3R activity and cytosolic Ca^{2+} is sigmoidal. This is particularly true in the presence of high $\text{Ins}(1,4,5)\text{P}_3$ levels, indicating that $\text{Ins}(1,4,5)\text{P}_3$ acts as a molecular switch and that once the receptor binds $\text{Ins}(1,4,5)\text{P}_3$, it becomes sensitive to the stimulatory, but not the inhibitory, action of Ca^{2+} . The autocatalytic process of Ca^{2+} -induced Ca^{2+} release enables the InsP_3Rs and RYRs to communicate with each other to establish coordinated Ca^{2+} signals, often organized into propagating waves. The main function of the Ca^{2+} -mobilizing messengers, therefore, is to alter the sensitivity of the InsP_3Rs and RYRs to this stimulatory action of Ca^{2+} .

- Ca^{2+} sensitive processes:

Once the ON mechanisms have generated a Ca^{2+} signal, various Ca^{2+} -sensitive processes translate this into a cellular response. The Ca^{2+} signalling toolkit has numerous Ca^{2+} -binding proteins, which can be divided into Ca^{2+} buffers and Ca^{2+} sensors, on the basis of their main functions. The latter respond to an increase in Ca^{2+} by activating diverse processes (Fig.2). The classical sensors are troponin C (TnC) (Contraction in striated muscle is regulated by the calcium-

ion-sensitive, multiprotein complex troponin) and calmodulin(CAM)(CAM binds Ca^{2+} , regulates proteins and enzymes in a Ca^{2+} -dependent manner), which have four EF hands (many calcium-binding proteins belong to the same evolutionary family and share a type of calcium-binding domain known as the EF-hand. In an EF-hand loop the calcium ion is coordinated in a pentagonal bipyramidal configuration) that bind Ca^{2+} and undergo a pronounced conformational change to activate various downstream effectors. TnC has a limited function to control the interaction of actin and myosin during the contraction cycle of cardiac and skeletal muscle. CAM is used more generally to regulate many processes such as the contraction of smooth muscle, cross talk between signalling pathways, gene transcription, ion channel modulation and metabolism. The same cell can use different sensors to regulate separate processes. In skeletal muscle, for example, TnC regulates contraction whereas CAM stimulates phosphorylase kinase to ensure a parallel increase in ATP production. In addition to the above proteins, which act generally, there are numerous Ca^{2+} -binding proteins designed for more specific functions. For example, synaptotagmin is associated with membrane vesicles and is a Ca^{2+} sensor for exocytosis. The versatility of Ca^{2+} signalling is greatly enhanced by some of the Ca^{2+} -sensitive processes linking into other signalling pathways.

- OFF Mechanisms:

Once Ca^{2+} has carried out its signalling functions, it is rapidly removed from the cytoplasm by various pumps and exchangers (Fig.2). The plasma membrane Ca^{2+} -ATPase (PMCA) pumps and $\text{Na}^{2+}/\text{Ca}^{2+}$ exchangers extrude Ca^{2+} to the outside whereas the sarco-endoplasmic reticulum ATPase (SERCA) pumps return Ca^{2+} to the internal stores. The mitochondrion is an important component

of the OFF mechanism. It sequesters Ca^{2+} rapidly during the development of the Ca^{2+} signal and then releases it back slowly during the recovery phase (Fig.2). Mitochondria extrude protons to create the electrochemical gradient that allows ATP synthesis. This gradient is used to drive Ca^{2+} uptake that has a low sensitivity to Ca^{2+} (half-maximal activation around 15M) which means that mitochondria accumulate Ca^{2+} more effectively when they are close to Ca^{2+} -releasing channels. Here, they form a 'quasi-synapse', which allows them to directly sense the high local Ca^{2+} concentration that builds up in the vicinity of open Ca^{2+} channels, such as the InsP_3Rs and RYRs . Reciprocal interactions between the two organelles arise from the fact that the ER/SR provides the Ca^{2+} that enters the mitochondria, which in turn modifies the Ca^{2+} feedback mechanisms that regulate Ca^{2+} release from the ER/SR. The mitochondrion has an enormous capacity to accumulate Ca^{2+} and the mitochondrial matrix contains buffers that prevent the concentration from rising too high. Once the cytosolic Ca^{2+} has returned to its resting level, a mitochondrial $\text{Na}^{2+}/\text{Ca}^{2+}$ exchanger pumps the large load of Ca^{2+} back into the cytoplasm, from which it is either returned to the ER or removed from the cell (Fig.2).

1. Some Important Aspects Of Calcium Signalling

1. Spatial Aspects:

Improvements in imaging technology mean that cell physiologists can see how the Ca^{2+} signals are generated. When a Ca^{2+} channel opens, a highly concentrated plume of Ca^{2+} forms around its mouth and then dissipates rapidly by diffusion after the channel is closed. Such localized signals, which can originate from channels in the plasma membrane or on the internal stores, represent the elementary events. Essentially, these elementary signals have two functions.

They can either activate highly localized cellular processes in the immediate vicinity of the channels (Fig.3a) or by recruiting channels throughout the cell, they can activate processes at the global level.(Fig.3b,c). For sites of elementary Ca^{2+} release to produce global responses, the individual channels must communicate with each other to set up Ca^{2+} waves. If cells are connected, such intracellular waves can spread into neighboring cells and become intercellular waves to coordinate cellular responses within a tissue.

A striking example of how spatial organization enables Ca^{2+} to activate opposing cellular responses in the same cell is seen in smooth muscle cell where Ca^{2+} sparks that arise locally near the plasma membrane activate potassium (K^+) channels causing the muscle to relax but when elementary release events deeper in the cell are coordinated to create a global Ca^{2+} signal, the muscle contracts.

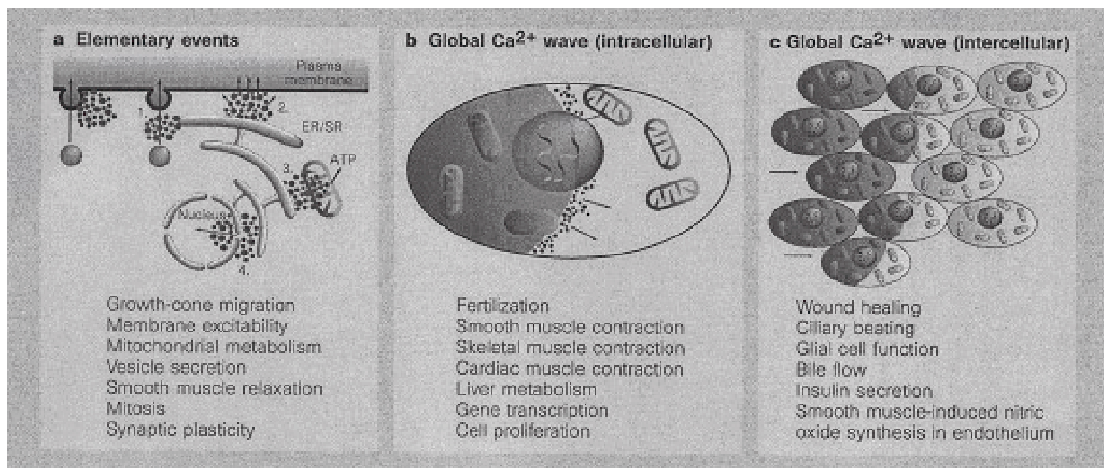


Fig. 3. Elementary And Global Events[6]

2. Temporal Aspects:

Although elevations in Ca^{2+} are necessary for it to act as a signal, prolonged increases in the concentration of Ca^{2+} can be lethal. Cells avoid death by using

low-amplitude Ca^{2+} signals or by delivering the signals as brief transients. This holds true for both elementary as well as global signals. Both kinds of events can oscillate, but they have widely different periods. For example, whereas the period of elementary Ca^{2+} sparks in arterial smooth muscle is 0.1-0.5 seconds; it is 10-60 seconds for global waves in liver cells, 1-35 minutes for Ca^{2+} waves in human eggs after fertilization and 10-20 hours for the spontaneous Ca^{2+} that control cell division[1]. Cells use frequency modulation to vary the intensity of the physiological output and by varying the frequency of global Ca^{2+} signals, different genes can be activated.(Berridge et al. 1998). To use FM signalling, cells have developed decoders that respond to the frequency of the Ca^{2+} signals. The best known example of a frequency decoder is an enzyme called calmodulin-dependent protein kinase II, which is found in both animal and plant cells and which regulates other enzymes that rely on Ca^{2+} .

3. Cell Proliferation:

A prolonged period of calcium signalling is an important growth signal for many cells. Alterations in calcium signalling can underlie defects in cell growth and are implicated in some cancers. Because the internal Ca^{2+} stores are finite, prolonged bouts of signalling depend on the influx of external Ca^{2+} through the store-operated calcium channels (SOCCs) in the plasma membrane (Fig.4). Ca^{2+} is also involved in the proliferation of immune cells(lymphocytes) in response to foreign antigens. Both T and B-lymphocytes detect antigens through complex receptors on their surface. When a foreign molecule binds to an antigen receptor, $\text{Ins}(1,4,5)\text{P}_3$ is produced, stimulating the release of Ca^{2+} from internal stores. Once these stores are empty, entry of external Ca^{2+} is activated through the SOCCs (Fig.4) allowing lymphocytes to maintain a prolonged increase of

Ca^{2+} . This increase, which often occurs as a series of Ca^{2+} oscillations activates factors such as NF-AT, which enter the nucleus and cause genes to be turned on.

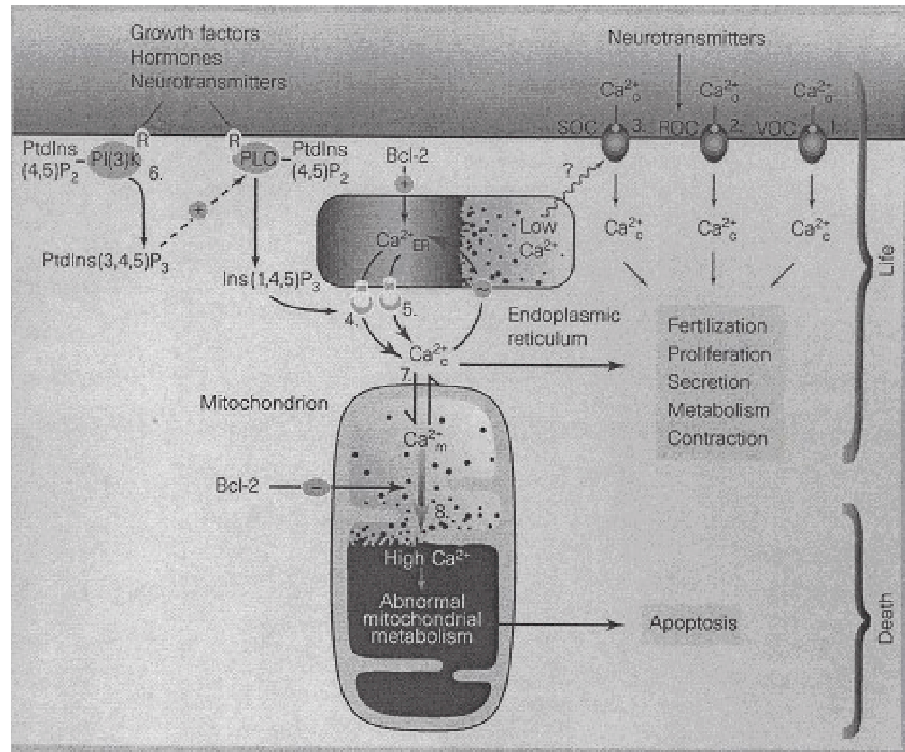


Fig. 4. Basic Mechanisms Of Ca^{2+} Signalling[6]

4. Cell Death:

Very high concentrations of Ca^{2+} can lead to the disintegration of cells (necrosis) through the activity of Ca^{2+} -sensitive protein-digesting enzymes. Calcium has also been implicated in the orderly programme of cell death called apoptosis. Apoptosis is important during both normal development and pathological conditions such as AIDS, Alzheimer's disease and cancer. A protein that is mutated in cancerous cells, called Bcl-2, prevents the cell death that would nor-

mally limit the survival and proliferation of cancer cells. Bcl-2 mediates some of its anti-apoptotic action by modifying the way in which organelles such as the endoplasmic reticulum and mitochondria handle Ca^{2+} (Fig.4). In many cells, mitochondria participate in the recovery phase of normal Ca^{2+} transients—they sequester some of the Ca^{2+} signal, which is later returned to the endoplasmic reticulum. Normal Ca^{2+} signalling involves continuous shuttling of Ca^{2+} between these two organelles. Normally, most of the Ca^{2+} resides within the lumen of the endoplasmic reticulum, with very little in the mitochondria. These high levels of Ca^{2+} are essential as they form a reservoir of signal Ca^{2+} in the endoplasmic reticulum and also are essential for the synthesis and processing of proteins there. If the Ca^{2+} stored within the endoplasmic reticulum was depleted, the mitochondria would become overloaded and there would be two main consequences for the cells. Firstly, the decline in the Ca^{2+} levels in the endoplasmic reticulum would lead to the activation of stress signals, which switch on the genes associated with cell death. Since some of the genes also specify the proteins that bind Ca^{2+} in the endoplasmic reticulum, this could be a desperate attempt by the cell to restore the correct balance of Ca^{2+} between the endoplasmic reticulum and the mitochondria. Secondly, the build-up of mitochondrial Ca^{2+} initiates a programme of events that leads to cell death (Fig.4). In normal cells, Bcl-2 may modify the Ca^{2+} -handling properties of the endoplasmic reticulum and the mitochondria (Fig.4) to restore the correct Ca^{2+} balance.

The above processes illustrate the universality of the signalling mechanism, which triggers a new life at fertilization and is used over and over again to regulate the developmental programme as it unfolds to produce a new organism.

CHAPTER II

BACKGROUND

There are several reasons for developing mathematical models of calcium oscillations. Mathematical modeling is important in the study of oscillations of free calcium because of their inherent nonlinear nature and unreliability of intuitive approaches. This chapter discusses the important models in the literature whose concepts have been used in this research for the development of the final model.

A. MODELS FOR Ca^{2+} OSCILLATIONS

The first and the simplest reason for modeling calcium oscillations, is to demonstrate that informal hypotheses for the oscillators do indeed have the necessary structure to produce oscillations with the right characteristics. Another purpose of modeling is to establish what aspects of a class of model can be varied and what aspects are essential. Also, the modeling can establish what will not work. There are three basic types of models [7], each with its own part to play. First, qualitative models, presented in diagrammatic rather than mathematic form, are widely used for discussion of initial hypotheses. The advantage of these models is ease of construction and their disadvantage is lack of precision. Next, are the phenomenological models that mimic the observed behavior but are not precise on the underlying biology. Another disadvantage being that since a number of mathematical models can mimic the same behavior, hence the agreement between model and experiment cannot be a very reliable guide to underlying mechanisms. Lastly, there are the quantitative or mechanistic models, which are based on known parameters. These models develop with the help of experimental data. Hence, they have the advantage of providing precise predictions but their disadvantage is that these predictions can be sensitive to any variation in the

parameters of the model.

It has been suggested that Ca^{2+} oscillations play an important role in signal transduction [8],[9]. The receipt of an external signal might be encoded in the frequency of oscillations and the cellular response might depend on this frequency. Several theoretical models for the generation of oscillations have been proposed. All the models fall into three broad categories: 1) Ca^{2+} -initiated Ca^{2+} -release, 2) Agonist(external hormone)-receptor oscillations mediated by G proteins, diacylglycerol and protein kinase C [10] and 3) positive feedback of Ca^{2+} on the production of inositol 1,4,5-triphosphate (IP_3) through membrane-bound phospholipase C (PLC).

The *calcium-induced calcium-release model* invokes a positive feedback loop that was discovered by Endo et al. in 1970[11]. They found that calcium release from the sarcoplasmic reticulum of skinned skeletal muscle fibers is directly induced by calcium itself. Given below is an example of a CICR model as proposed by Goldbeter et al.[12].

According to their model, cells contain two kinds of nonmitochondrial calcium stores: an IP_3 -sensitive store and a Ca^{2+} -sensitive (but IP_3 -insensitive) store. In their model (Fig.5) IP_3 is formed because of receptor activation, which releases Ca^{2+} at a nearly constant rate from the IP_3 -sensitive store. The Ca^{2+} level in this store is kept constant by Ca^{2+} influx from the extracellular medium. Release of Ca^{2+} from the Ca^{2+} -sensitive pool is directly triggered by Ca^{2+} itself. Ca^{2+} is released until the Ca^{2+} -sensitive pool is depleted. The spike begins when the Ca^{2+} -sensitive pool is replenished. In the CICR model, the cytosolic calcium level is determined by IP_3 -induced calcium release ($J_{\text{IP}_3\text{channel}}$). Ca^{2+} influx ($J_{\text{PMchannel}}$) and efflux (J_{PMpump}) across the plasma membrane; calcium-induced calcium release ($J_{\text{CICRchannel}}$) from the Ca^{2+} -sensitive store; and Ca^{2+} uptake by this store (J_{CICRpump}):

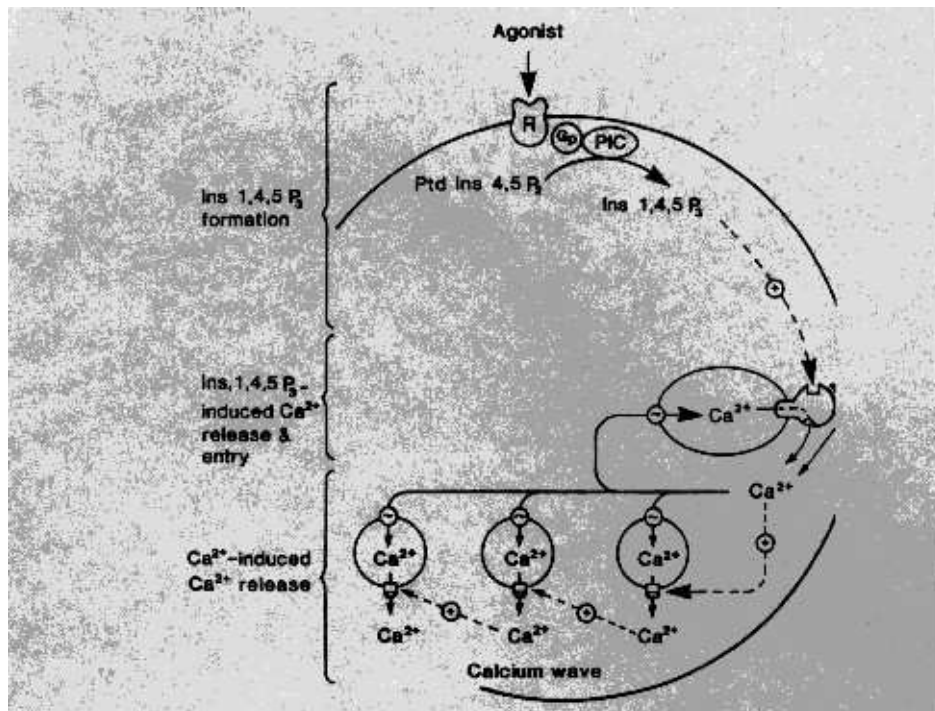


Fig. 5. The CICR Model[12]

$$\frac{dCa_i}{dt} = J_{IP_3channel} + J_{PMchannel} - J_{PMpump} + J_{CICRchannel} - J_{CICRpump} \quad (2.1)$$

The channel is gated by Ca^{2+} , both on the cytosolic side (Ca_i) and the store side (Ca_s) of the membrane. The assumption is that Ca^{2+} release depends on Ca_i^2 and Ca_s^2 and is given by:

$$J_{CICRchannel} = A * \left[\frac{Ca_i^4}{K_1^4 + Ca_i^4} \right] * \left[\frac{Ca_s}{K_2^2 + Ca_s^2} \right] \quad (2.2)$$

where A is the maximal rate and K_1 and K_2 are constants that determine the concentration dependence of the fluxes.

The Ca^{2+} level in the Ca^{2+} -sensitive store is given by:

$$\frac{dCa_s}{dt} = J_{CICRpump} + J_{CICRchannel} \quad (2.3)$$

One of the main features of the CICR models is that IP_3 oscillations are not needed for the calcium oscillations. The only role of IP_3 is to induce a constant efflux of Ca^{2+} from the other store.

In the IP_3 - Ca^{2+} crosscoupling model, positive feedback comes from the mutual reinforcement of IP_3 -induced Ca^{2+} release and Ca^{2+} -stimulated IP_3 formation. T. Meyer and L. Stryer [13] developed this model based on earlier work of others that showed that IP_3 cooperatively opens calcium channels in the ER and that Ca^{2+} activates PLC. The positive feedback loop of the ICC model can be described by the following equations:

$$\frac{dCa_i}{dt} = J_{channel} - J_{pump} \quad (2.4)$$

$$\frac{dIP_3}{dt} = k_{PLC} - k_{phosphate} \quad (2.5)$$

where t is the time and k is a rate constant. Both the flow of Ca^{2+} through channels that are cooperatively opened by the binding of molecules of IP_3 and L , an independent leak, contribute to $J_{channel}$, the efflux of calcium from the ER into the cytosol:

$$J_{channel} = \left[\frac{A * IP_3^4}{IP_3 + K_1^4 + L} \right] * Ca_s \quad (2.6)$$

where Ca_s is the concentration of calcium in the ER store. J_{pump} , the sequestration of Ca^{2+} by the Ca^{2+} -ATPase pump, is given by

$$J_{pump} = \frac{B * Ca_i^2}{Ca_i^2 + K_2^2} \quad (2.7)$$

In equations 2.3 and 2.4 the maximal rates are A and B, and are constants that determine the concentration dependence of the fluxes. Spiking can occur in the absence of extra-cellular Ca^{2+} . Over longer times, channels, pumps and exchangers in the plasma membrane control Ca_i . In the ICC model shown in Fig.6 below, the rate of formation of IP_3 by PLC is assumed to depend on both, the R, the fractional activation of the cell-surface receptor and on the cytosolic level of Ca^{2+} . An approximation for the relationship between PLC, R and Ca_i is:

$$k_{PLC} = C \left[1 - \left[\frac{K_3}{Ca_i + K_3} \right] \left[\frac{1}{1 + R} \right] \right] \quad (2.8)$$

where C is the maximal rate of IP_3 formation and K_3 is the dissociation constant of the Ca^{2+} -sensing component of PLC. Finally, the degradation of IP_3 is given by a first-order decay with a rate constant D:

$$k_{phosphatase} = D[IP_3] \quad (2.9)$$

The system defined by the above equations cannot exhibit spiking because deactivation and reactivation processes are needed. Several studies indicate that cytosolic Ca^{2+} levels can directly terminate IP_3 -induced Ca^{2+} efflux in oocytes and neurons. This inhibition directly senses the spike height and can be modeled with an inhibition parameter g that equals 0 when the channel is fully responsive and 1 when the channel is totally inactive:

$$\frac{dCa_i}{dt} = (1 - g)J_{channel} - J_{pump} \quad (2.10)$$

and

$$\frac{dg}{dt} = ECa_i^4(1 - g) - Fg \quad (2.11)$$

where E and F are inactivation and activation rates, respectively.

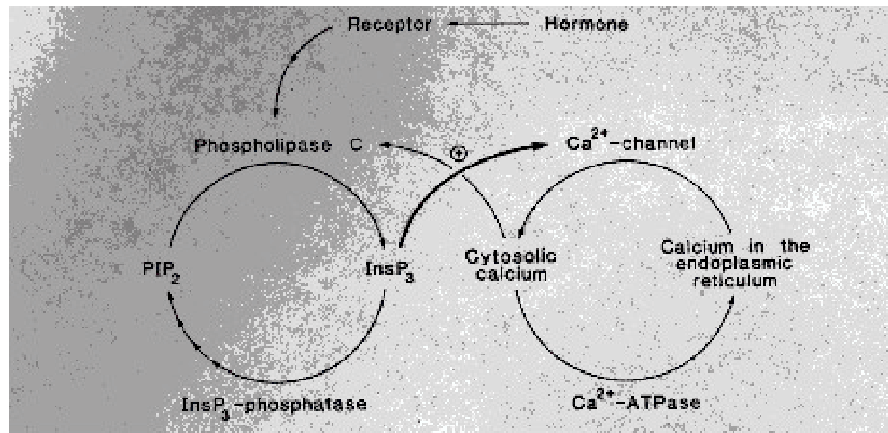


Fig. 6. IP_3 - Ca^{2+} Crosscoupling (ICC) Model[13]

The model proposed by Shen and Larter[14](Fig.7) consists of three variables and

two coupled positive feedback loops, which generate Ca^{2+} in the cytosol along with the inhibition of both loops at high $[\text{Ca}^{2+}]$. In Fig.7 we see a schematic of the proposed model. The three variables in the model are the cytosolic Ca^{2+} concentration(x), the Ca^{2+} concentration inside the endoplasmic reticulum ER or store(y), and the IP_3 concentration in the cytosol(z). The ICC mechanism provides the first positive feedback while the second is given by the CICR mechanism. The three differential equations governing the system are:

$$\frac{dx}{dt} = \nu_0 + \nu_1 R - \nu_2 + (\nu_3 + k_s)y - k_c x \quad (2.12)$$

$$\frac{dy}{dt} = \nu_2 - (\nu_3 + k_s)y \quad (2.13)$$

$$\frac{dz}{dt} = J_+ - J_- \quad (2.14)$$

where

$$\nu_2 = V_{M2} * \frac{x^n}{x^n + K_2^n} \quad (2.15)$$

$$\nu_3 = V_{M3} * \frac{z^n}{z^n + K_1^n} \frac{K_4 x}{(x + K_4)(x + K_5)^p} \quad (2.16)$$

$$J_+ = AR \frac{x}{K_3 + x} \quad (2.17)$$

$$J_- = Bz \quad (2.18)$$

The fractional activation of the cell surface receptor, R , reflects the degree of stimulation of the cell by the agonist and is taken to be between 0 and 1. The value

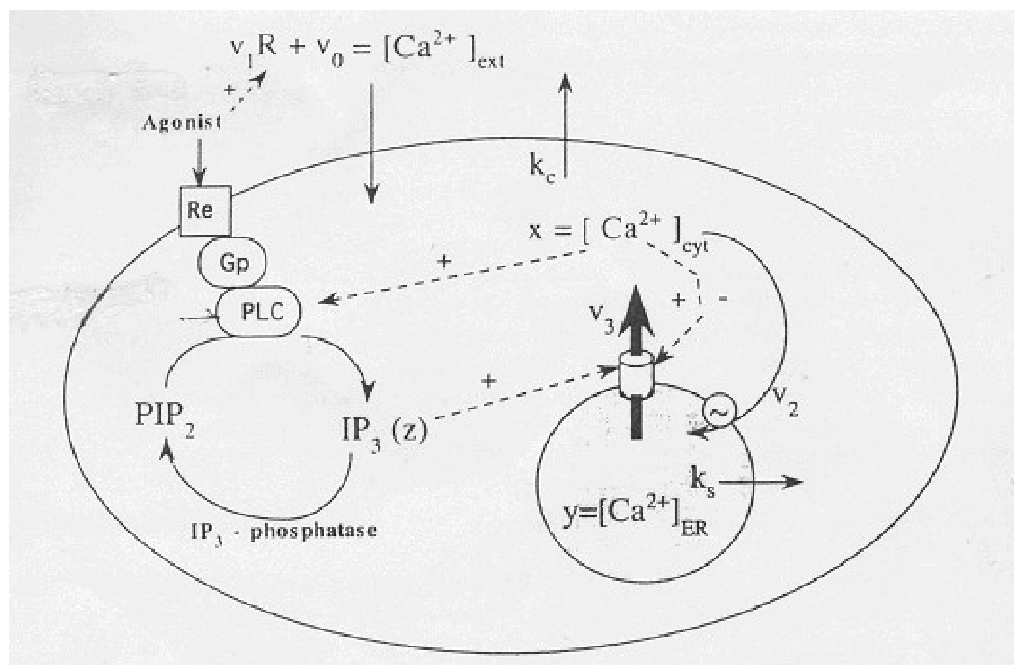


Fig. 7. Shen And Larter Model[14]

of R has an important influence on the dynamics of the model. The quantities $\nu_0 + \nu_1 R$ and k_{cx} are respectively the influx and efflux of Ca^{2+} into and out of the cell; ν_0 is the constant influx of Ca^{2+} from the extracellular space and $\nu_1 R$ is the agonist-dependent influx. As seen the Fig.7, ν_2 is the Ca^{2+} -ATPase pumping rate of Ca^{2+} back into the store and $\nu_3 y$ is the Ca^{2+} release rate from the intracellular Ca^{2+} stores. The latter is dependent on three elements: $\text{IP}_3(z)$, the Ca^{2+} concentration in the store(y), and the cytosolic Ca^{2+} concentration(x). In ν_2 and ν_3 , VM_3 is the maximum rate of efflux, K_1 is the IP_3 concentration at which half the IP_3 sites are filled and K_2 is the threshold constant for pumping. The parameters m and n are the Hill coefficients, K_4 and K_5 are the Ca^{2+} binding constants for the activation and inhibition sites and p is the number of Ca^{2+} -binding subunits. The term $k_s y$ refers to a nonactivated, leaky transport of Ca^{2+} from the ER. The rate of change of IP_3 (dz/dt) is taken to be of the same form as in the ICC model [13]; J_+ , the production rate of IP_3 by PLC, is assumed to depend both on R , the fractional activation of the cell surface receptor, and on the cytosolic level of Ca^{2+} (x). The quantity A is the maximal rate of IP_3 formation and K_3 is the dissociation constant of the Ca^{2+} -dependent component of PLC. Finally, J_- , the degradation of IP_3 is given by a first order decay with a rate constant B . Some observations made were as follows:

As seen in the Fig.8, the cytosolic Ca^{2+} begins to oscillate when R reaches 0.25 and stops spiking at $R=0.70$. As R increases, the simple oscillations which arise at $R=0.25$ become more complex between $R=0.60$ and $R=0.63$. Also, the frequency increases with R . This model incorporates features of the ICC and CICR models, both of which can generate calcium oscillations. An IP_3 -sensitive Ca^{2+} channel with bell-shaped Ca^{2+} dependence is also incorporated. As the cytosolic Ca^{2+} concentration increases above the critical (maximum) level, it inhibits any further release of Ca^{2+} , which leads to oscillatory behavior. Hence, this model shows that when complex

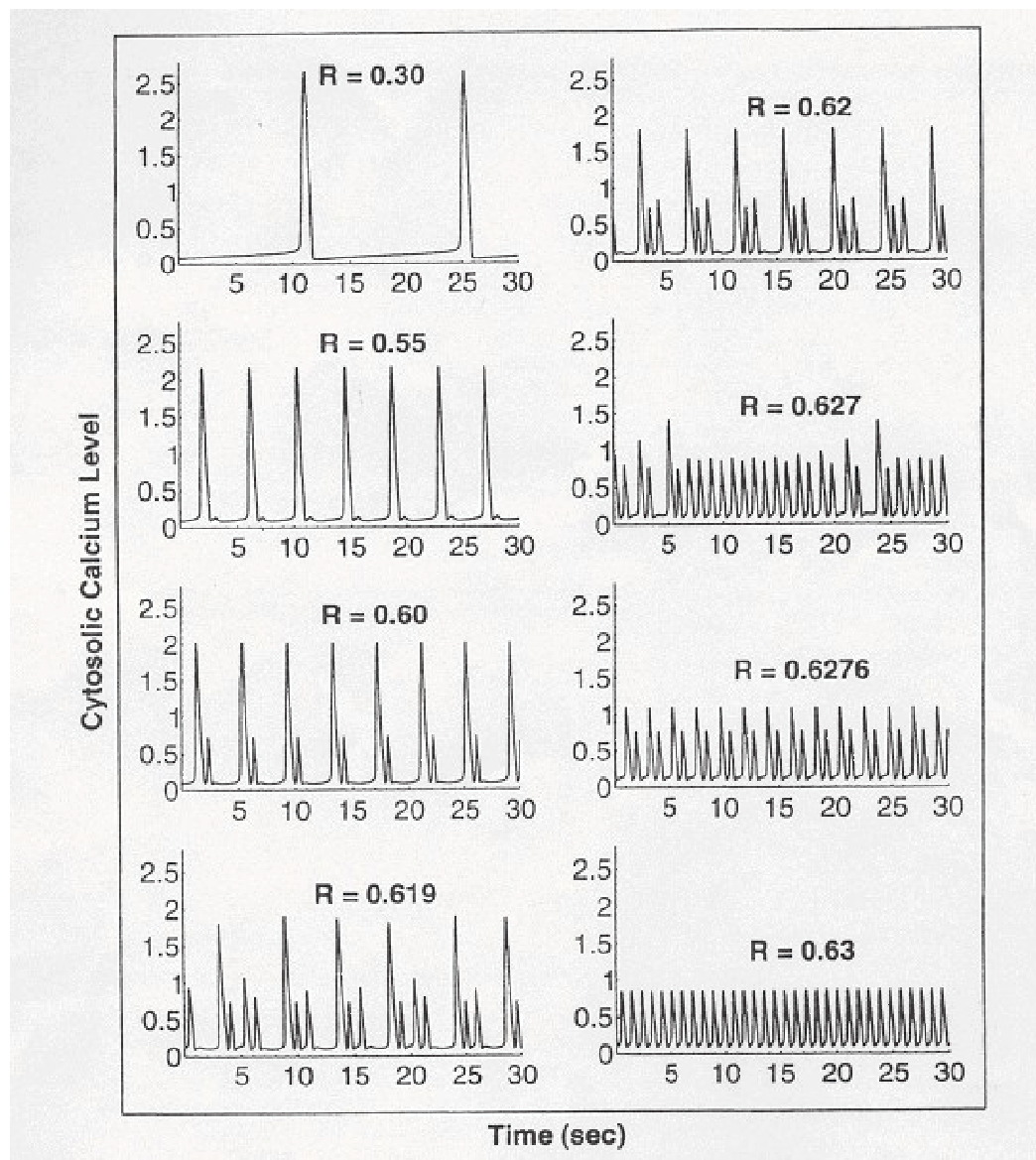


Fig. 8. Cytosolic Calcium Oscillations.[14]

intracellular Ca^{2+} oscillations are produced, the frequency of spiking is proportional to the concentration of agonist (R), and the latency of the Ca^{2+} , which is observed to decrease with increasing agonist concentrations.

G. Dupont et al.[9] (Fig.9) proposed a model to explain intercellular Ca^{2+} wave propagation in hepatocytes. Co-ordination of Ca^{2+} signals between neighboring cells requires the presence of the agonist at each cell surface as well as gap junctional permeability. Their model was based on the junctional coupling of several hepatocytes differing in sensitivity to the agonist and thus in the intrinsic period of Ca^{2+} oscillations and also on the passive diffusion of InsP_3 between adjacent cells through gap junctions. IP_3 is produced in the mechanically stimulated cell and provokes the release of calcium from the internal stores, in the form of an intracellular Ca^{2+} wave propagating via Ca^{2+} -induced- Ca^{2+} -release. Because IP_3 is supposed to move through gap junctions, similar Ca^{2+} waves are initiated in adjacent cells. This phenomenon then keeps being repeated as long as the amount of IP_3 entering the cell is large enough to induce a Ca^{2+} wave. The following is a description of the model:

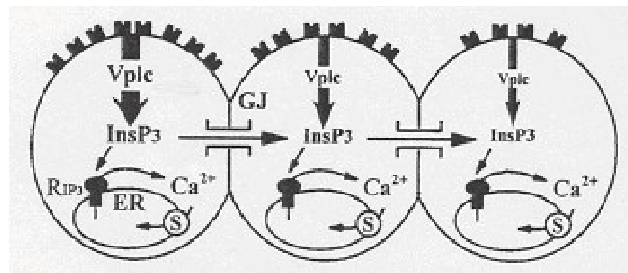


Fig. 9. Gap Junction Diffusion In A Group Of Three Hepatocytes.[9]

It is assumed that IP_3 and Ca^{2+} -mediated activation are instantaneous whereas Ca^{2+} -induced inactivation develops slowly. Activation and inactivation being co-operative processes, the change in the fraction of inactive IP_3 receptors (R_{des}) obeys the follow-

ing equation:

$$\frac{dR_{des}}{dt} = k_+ C_{cyto}^n i \frac{1 - R_{des}}{1 + \left(\frac{C_{cyto}}{K_{act}}\right)} - k_- R_{des} \quad (2.19)$$

where k_+ and k_- are the kinetic constants of Ca^{2+} association to and dissociation from the inhibitory Ca^{2+} binding site of IP_3 receptor, C_{cyto} represents the concentration of cytosolic Ca^{2+} and K_{act} is the dissociation constant of Ca^{2+} binding to the activating Ca^{2+} binding site of the InsP_3 receptor. The time evolution of the concentration of cytosolic Ca^{2+} is given by:

$$\frac{dC_{cyto}}{dt} = k_1(b + IR_a)[C_{a_{tot}} - C_{cyto}(\alpha + 1)] - V_{MP} \frac{C_{cyto}^{np}}{C_{cyto}^{np} + K_p^{np}} \quad (2.20)$$

in which IR_a represents the fraction of active i.e. open IP_3 receptor and is given by:

$$IR_a = IR_{able} \frac{1}{1 + \left(\frac{K_{act}}{C_{cyto}}\right)^{np}} \quad (2.21)$$

where IR_{able} is the fraction of receptors that can be activated.

$$IR_{able} = (1 - R_{des}) \frac{IP^{n_r}}{K_{IP}^{n_r} + IP^{n_r}} \quad (2.22)$$

and IP is the intracellular concentration of IP_3 , k_1 is the kinetic constant governing the flux of Ca^{2+} from the lumen into the cytosol and k_{1b} is the basal efflux in the absence of IP_3 . K_{IP} is the dissociation constant of IP_3 binding to its receptor. In view of the fact that in the model IP_3 can diffuse through gap junctions, its progression over time is considered. The change in IP_3 over time is determined by:

$$\frac{dIP}{dt} = V_{PLC} - V_K \frac{I_p}{K_k + I_p} \frac{C_{cyto}^{nd}}{K_d^{nd}} - V_{PH} \frac{I_p}{K_{PH} + I_p} \quad (2.23)$$

where V_{PLC} is the velocity of IP_3 synthesis by PLC, which depends on the level of simulation. V_K and V_{PH} are the maximal velocities of IP_3 metabolism and K_k and K_{PH} are the Michaelis constants. In the above equation, the rate of IP_3 synthesis is assumed to be independent of the level of cytosolic Ca^{2+} . K_d reflects stimulation of IP_3 by Ca^{2+} in the above equation, which is the threshold constant for activation and nd , the hill coefficient characterizing the above process.

1. Incorporation Of Gap Junction Diffusion

In hepatocytes, cells are tightly coupled by gap junctions, which allow the diffusion of diverse small-sized molecules between adjacent cells. It is assumed that at each cell boundary the flux is dependent on both the concentration difference across the membrane and on the permeability of the gap junction to the IP_3 . Hence at each boundary between two cells the following equation applies:

$$D_{IP} \frac{\delta IP^-}{\delta x} = D_{IP} \frac{\delta IP^+}{\delta x} = F_{IP} (IP^+ - IP^-) \quad (2.24)$$

where the subscripts $+$ and $-$ indicate the IP_3 concentrations at the left and the right limits of the border respectively. The spatial co-ordinate is indicated by x . The intracellular diffusion coefficient for IP_3 is represented by D_{IP} . The junctional permeability to IP_3 , F_{IP} is an unknown parameter whose value was chosen to mimic experimental observations. If $F_{IP} = 0$, no IP_3 can diffuse between the cells and the above equation reduces to no flux boundary conditions. Infinitely large values for F_{IP} correspond to the absence of any cell membrane. The above models are some of the prominent models in the literature, which have been used to model Ca^{2+} oscillations

for excitable and non-excitable cells.

CHAPTER III

PROPOSED MODEL

The proposed model is based on the concept of agonist-receptor oscillations mediated by G proteins similar to the model by Cuthbertson and Chay[10]. This model is applicable to both excitable and non-excitable cells with additions to the non-excitable cell model to incorporate the concepts of intercellular coupling based on gap junctional diffusion[9]. This first part of this chapter describes the experimental procedure of data collection for both the excitable and non-excitable cells. The latter part of the chapter deals with description of the proposed model.

A. EXPERIMENTAL PROCEDURE FOR EXCITABLE CELLS

For the excitable cells, the human myometrial cell line, (PHM1-41)[15] was chosen and the following were the materials used for collecting the data.

Materials and Methods

Dulbecco's Modified Eagle's medium with F-12 salts (DME-F12), Dulbecco's PBS, nifedipine, neomycin, thapsigargin, Bay K 8644, ryanodine, caffeine, oxytocin, vasopressin, prostaglandins E1 and E2 (PGE1, PGE2)[16], EGTA, and all general chemical reagents were purchased from Sigma Chemical Co. (St. Louis, MO). Fetal bovine serum (FBS) was purchased from Equitech, Inc. (Ingram, TX). Tissue culture flasks were obtained from Corning (Oneonta, NY), and 2-well LabTek Chambered Coverglass slides were purchased from Nunc, Inc. (Naperville, IL). Fluo 3-AM and 8-bromo-cAMP were purchased from Molecular Probes, Inc. (Eugene, OR). Stock solution of 1.0mM fluo 3-AM was prepared in dimethyl sulfoxide (DMSO) and diluted with medium to 3.0 μ M (0.3% final DMSO concentration) for loading in cultured cells.

Thapsigargin stock (1.0mM) was prepared in DMSO and used at a concentration of 1.0 μ M (0.1% DMSO). Nifedipine was prepared in ethanol (10mM) and diluted in medium to 10 μ M (0.1% ethanol); ryanodine was prepared in ethanol (10mM) and diluted in medium to 5M for experiments. Bay K 8644 was prepared in ethanol and diluted to 1 μ M. The 8-bromo-cAMP was prepared as a 10mM stock, and neomycin and caffeine were prepared in 100mM stocks in DME-F12. PGE1 and PGE2 stocks (1 and 50mM, respectively) were prepared in ethanol and diluted to 50 μ M-10 η M in DME-F12.

Cell Culture:

The myometrial cell line, PHM1-41[15], was derived from term-pregnant human myometrium (patient not in labor) and immortalized using a vector expressing human papilloma virus E6 and E7 proteins[18]. Cells were cultured in DME-F12 plus 10% fetal calf serum and used between passages 15 and 23. The primary human myometrial cells, like PHM1-41 cells, are communication competent and exhibit comparable properties including connexin43 gap junctions and estrogen, progesterone, and oxytocin receptors [19], [19]. First-passage normal myometrial cells were analyzed 72h after plating on Chambered Coverglass slides. Oxytocin-induced changes in intracellular Ca²⁺ in myometrial cultures 72h after plating were monitored with the Ca²⁺-sensitive fluorophore, fluo 3-AM[20], using a Meridian Ultima Confocal Microscope (Meridian Instruments, Okemos, MI). To minimize differences in fluo 3-AM[21] loading from experiment to experiment, cells were seeded at the same density, all experiments were performed with the same fluo 3-AM stock, and each treatment was compared to a separate control. Cells were loaded with 3.0 μ M fluo 3-AM for 1 h in serum- and phenol red-free medium at 37C and then washed with serum- and phenol red-free medium. Cells were then placed on the stage of the confocal microscope, and an area of the

chamber slide was selected for analysis. For image collection, scan parameters were adjusted for maximum detection of fluorescence with minimal cellular photo bleaching. Fluorescence was generated in the cells by excitation at 488nm , and fluorescence emission from scanned individual cells was collected (530nm) by means of a photo multiplier tube. The basal fluorescence intensity was obtained from 5 image scans recorded from about 5-10 cells every 10 sec. After the fifth scan, cells were exposed to oxytocin, and image scans were acquired at the same sampling interval. Scanning continued until the cells established a uniform pattern of oscillations. At this time, a pharmacological agent was added to the cells, and scanning was continued at the same sampling interval used with the hormone treatment. Control experiments were performed similarly with the addition of the corresponding solvent for each pharmacological agent. The fluorescence intensity of fluo 3 obtained from each cell was collected with a sampling frequency f_s (one scan every 10 sec) and analyzed using FFT to identify the frequency or frequencies of Ca^{2+} oscillations if they exist. It was found that the 10-sec interval was good enough to produce Ca^{2+} oscillations at even very high concentrations of oxytocin.

B. EXPERIMENTAL PROCEDURE FOR NON-EXCITABLE CELLS

For the non-excitable cells, the Clone9[16] cell line was chosen and the following were the materials used for collecting the data:

Materials and Methods

Culture media, Dulbecco's phosphate-buffered saline (PBS), serum, patulin, gossypol (gossypol-acetic acid), nifedipine, thapsigargin, ryanodine, 1-octanol, and all general chemical reagents were purchased from Sigma Chemical Co. (St. Louis, MO). Both

2,3,7,8-TCDD and 1,2,3,4-tetrachlorodibenzo-p-dioxin (1,2,3,4-TCDD) were synthesized to greater than 98% purity as determined by chromatography and spectroscopic analysis (Mason et al., 1986). Tissue culture flasks were obtained from Corning (Oneonta, NY) and LabTek Coverglass chamber slides were purchased from Nunc, Inc. (Naperville, IL). Fluo-3, AM and rhodamine 123 were purchased from Molecular Probes, Inc. (Eugene, OR). Patulin was dissolved in dimethyl sulfoxide (DMSO) and stored at -20C until used. For use in cell cultures, patulin was dissolved in Ham's Nutrient Mixture F-12 culture medium for dilution (100mM, 0.1% DMSO). Gossypol stock (20mM) was prepared in ethanol and diluted in media (3.0mM, $\leq 0.05\%$ ethanol) immediately before each experiment. TCDD stocks (100mM) were prepared in DMSO and diluted to 1.0 μ M in media for treatment of cells. Stock solution of 1.0mM fluo-3, AM was prepared in DMSO and diluted with medium to 3.0mM (0.3% final DMSO concentration) for loading in cultured cells. Rhodamine 123 was prepared as a 5 mg/ml stock in ethanol and diluted to 5 mg/ml in medium (0.1% ethanol). Thapsigargin stock (1.0mM) was prepared in DMSO and used at a concentration of 1.0mM (0.1% DMSO). Nifedipine was prepared in ethanol(10mM) and diluted in medium to 10mM (0.1% ethanol); ryanodine was prepared in ethanol(2.0 mM) and diluted in medium to 2mM for experiments. Octanol was mixed with ethanol at a ratio of 1:10 (v:v) and prepared as a 10mM stock in serum and phenol red-free culture medium for dilution to 1.0mM during experiments.

Cell Culture:

Clone 9 (ATCC, CRL 1439, passage 17) normal rat liver cells were used between passages 25 and 35. Cells were grown in Ham's Nutrient Mixture F-12 with 10% fetal bovine serum and plated on Lab-Tek chambered coverglass slides (Nunc, Inc., Naperville, IL) for 48 hr prior to laser cytometry. Laser cytometry experiments were

performed with a Meridian ACAS Ultima work station (Meridian Instruments, Okemos, MI) using an excitation wavelength of 488nm. Fluo-3, AM and rhodamine 123 were used to monitor intracellular Ca^{2+} and mitochondrial membrane potential, respectively. Fluo-3, AM is a nonratiometric, visible-wavelength probe that exhibits about a 40-fold enhancement of fluorescence intensity with Ca^{2+} binding (Tsien, 1989). To minimize differences in Fluo-3, AM loading from experiment to experiment, cells were seeded at the same density, all experiments, were performed with the same Fluo-3, AM stock, and each treatment was compared to a separate control. Cells were loaded with either 3.0mM fluo-3, AM or 5.0 mg/ml rhodamine 123 for 1 hr or 20 min, respectively, in serum-and phenol red-free medium at 37°C. Following repeated washing with serum- and phenol red-free medium, cells were placed on the ACAS stage and basal fluorescence intensity was obtained from four image scans recorded from about 4 cells every 3 sec. Following the fourth scan, cells were exposed to the various treatments and image scans were acquired at the same sampling interval for about 7 min. For image collection, the laser excited fluorescence in cells from a two-dimensional raster pattern generated by a scanning mirror and a stepper motor-driven microscope stage (scan parameters were optimized for maximum detection of fluorescence with minimum cellular photo bleaching). Excitation and detection parameters were kept constant for all experiments. To evaluate the effect of the presence or absence of gap junction-mediated intercellular coupling on the Ca^{2+} oscillations, the aliphatic alcohol 1-octanol was used as a specific inhibitor of gap junction permeability (Burt, 1991). Cells were pretreated for 3 min with 1.0mM octanol, which is sufficient to uncouple cells (Burghardt et al., 1995). Fluorescence intensities of fluo-3 and rhodamine 123, collected from each cell in the time domain with a sampling frequency f_s (0.333 sec⁻¹, i.e., one scan every 3 sec), were analyzed using FFT.

C. DESCRIPTION OF THE PROPOSED MODEL

The proposed model is based on the model proposed by Cuthbertson and Chay[10]. Ca^{2+} signals due to the intracellular release of Ca^{2+} are mediated by a small metabolite, inositol (1,4,5) triphosphate (IP_3)[10]. IP_3 is released from a membrane phospholipid, phosphatidylinositol (4,5)-biphosphate (PIP_2), by a phospholipase C, which is activated by GTP-bound G-proteins, which are in turn activated by agonist-occupied receptors. The IP_3 binds rapidly [22] to a receptor on part of the endoplasmic reticulum (ER), which then releases Ca^{2+} . IP_3 is degraded by a phosphatase and by a kinase, which produces inositol (1,3,4,5)-tetrakiphosphate (IP_4) which may have a role in promoting the refilling of the Ca^{2+} store from extracellular Ca^{2+} . The other product of the hydrolysis of PIP_2 is diacylglycerol (DAG), which activates protein kinase C (PKC) and is degraded by DAG kinase. PKC can phosphorylate receptors and perhaps the G-proteins.

Given below as seen from Fig.10 is the description of the proposed model:

In this model, the transients activated by GTP-binding proteins, combine with positive feedback processes and cause a sudden activation of phospholipase C (PLC) followed by negative feedback processes which switch off the Ca^{2+} rise and lead to a fall in free Ca^{2+} back to resting levels. This model has negative feedback via PKC phosphorylation of G-proteins and positive feedback from diacylglycerol (DAG) (or IP_3 or a metabolite of DAG or IP_3) onto PLC. The model is defined by four simultaneous first order differential equations for activated G-protein, diacylglycerol and IP_3 and Ca^{2+} . Agonist-occupied receptors activate G-proteins at a rate rg . Activated G-protein (Ga-GTP) is inactivated by phosphorylation at a rate proportional to activated protein kinase C (PKC) that depends on DAG and Ca^{2+} and can be stimulated by phorbol esters (PH) at the DAG binding site.

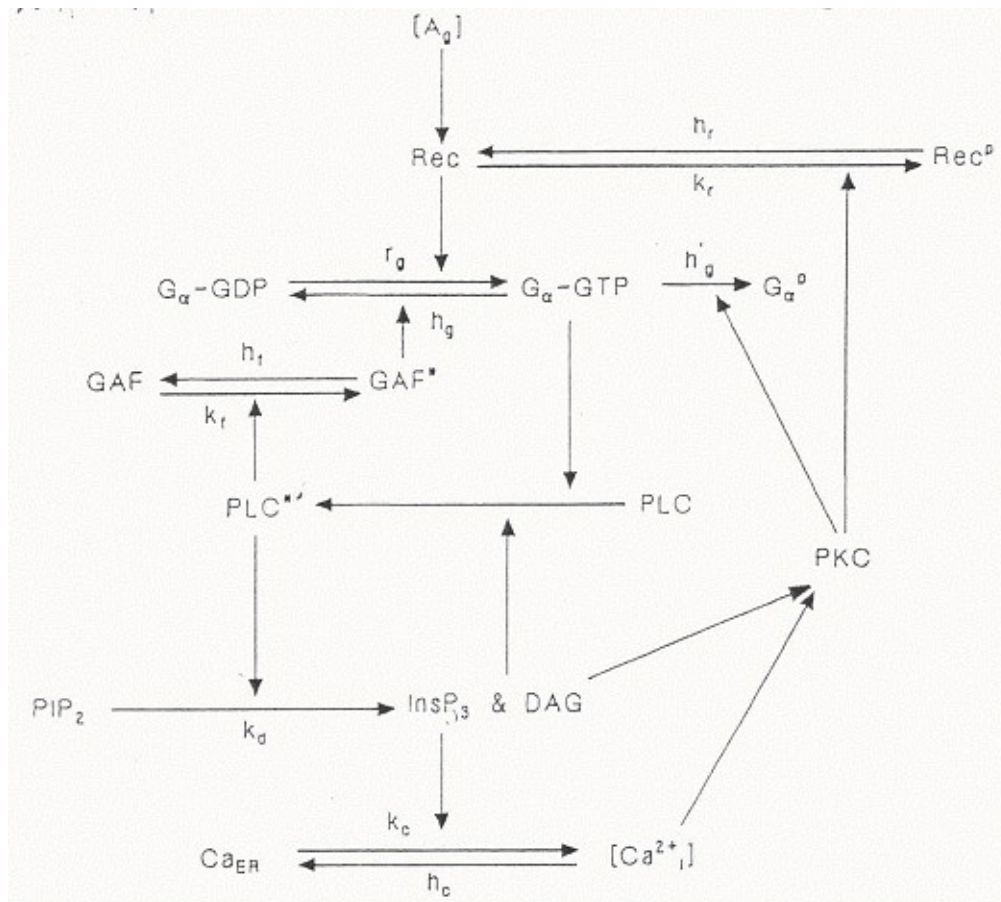


Fig. 10. The Proposed Model

$$\frac{d[G\alpha GTP]}{dt} = rg - hg * Rpkc * [G\alpha GTP] \quad (3.1)$$

where the fraction of activated PKC,

$$Rpkc = \frac{[DAG] + [PH]}{Kp + [DAG] + [PH]} * \frac{[Ca^{2+}]_i}{Kc + [Ca^{2+}]_i} \quad (3.2)$$

DAG and IP₃ are produced from phosphatidylinositol [7],[11] biphosphate (*PIP*₂) by activated phospholipase C (PLC) and at a background rate and are removed at a rate giving the following equation;

$$\frac{d[DAG]}{dt} = kd * Rplc - hd * [DAG] + ld \quad (3.3)$$

where the fraction of activated PLC,

$$Rplc = \frac{(d^*)^n}{1 + (d^*)^n} * \frac{(g^*)^n}{1 + (g^*)^n} \quad (3.4)$$

where

$$g^* = \frac{[G\alpha GTP]}{Kg} \text{ and } d^* = \frac{[DAG]}{Kd} \quad (3.5)$$

Similarly, the equation for IP₃ production is the same as above with *hd* replaced by *hi* where *hi*, is the rate of removal of IP₃ and in the equation for *d**, DAG is replaced by IP₃.

$$\frac{d[IP_3]}{dt} = kd * Rplc - hi * [IP_3] + ld \quad (3.6)$$

IP_3 binds to an IP_3 receptor on the endoplasmic reticulum (ER), which releases Ca^{2+} . Ca^{2+} is pumped back into the ER at a rate hc , which together with a 'leak' influx lc , determines the resting $[Ca^{2+}]$. Ca^{2+} changes are therefore determined by the equation:

$$\frac{d[Ca^{2+}]_i}{dt} = \frac{kc * (s^*)^3}{(1 + (s^*)^3)} hc * [Ca^{2+}]_i + lc \quad (3.7)$$

where

$$s^* = \frac{IP_3}{Ks}; [IP_3] = [DAG] \quad (3.8)$$

Here, the spike frequency is controlled by, the rate of conversion of $[G\alpha GDP]$ to $[G\alpha GTP]$ which in turn depends on the agonist concentration. ld would be increased by the activation of another pathway, which produced DAG, such as the hydrolysis of phosphatidylcholine by another PLC. kd be increased by anything that increased the rate of PIP_2 hydrolysis by activated PLC, such as an increase in PIP_2 . Spike shape depends on hg , Ks , which controls IP_3 binding, and on hc which depends on the Ca^{2+} uptake. Hg determines the rate of PKC phosphorylation of . Spike amplitude is controlled by kc , which determines the rate of Ca^{2+} release induced by each activated IP_3 -receptor. kc might be affected by cAMP-dependent phosphorylation of the IP_3 -receptor or by intra-store $[Ca^{2+}]$.

1. Gap Junction Diffusion In Non-Excitable Cell Model

The above model has been proposed for excitable cells. For non-excitable cells, there is an addition to the above model. It has been observed that in a group of non-excitable cells, when each cell is treated with an agonist, Ca^{2+} oscillations that are

generated are coordinated by a diffusion of small amounts of IP_3 into the neighboring cells. To incorporate this feature in non-excitabile cells the parameter "rcc" has been incorporated into the equation for rate of DAG production in the following form:

$$\frac{d[DAG]}{dt} = kd * Rplc - hd * [DAG] + ld - [DAG] * rcc * e^{-rcc*t} \quad (3.9)$$

The "rcc" parameter corresponds to the gap junction permeability and the e^{-rcc*t} term has been included to mimic the exponential nature of diffusion of IP_3 with time across the gap junction between cells. The inclusion of the $[DAG] * rcc * e^{-rcc*t}$ factor in the above equation results in the formation of intercellular calcium oscillations. For each different cell, the "rcc" value changes depending on the cell's gap junction permeability. The four first order differential equations in the model were solved using MathCAD 6.

CHAPTER IV

RESULTS OF DATA MODELLING

This chapter presents the results obtained using the proposed model for both excitable and non-excitable cells. The first part of the chapter deals with results for the excitable cells followed by statistical time and frequency domain tests to verify the validity of the proposed model. The latter part of the chapter presents the results for the non-excitable cells, again followed by the relevant statistical tests for verifying the validity of the model for both frequency and amplitude.

A. EXCITABLE (PHM1-41) CELL LINE

As mentioned in the experimental procedure, while collecting the data for excitable cells, the sampling rate was 1 scan in every 10 seconds. Hence the sampling frequency f_s is 0.1Hz. The first 128 samples of Ca^{2+} data were analyzed out of the total 256 samples collected. The Nyquist Theorem states that an analog waveform may be uniquely reconstructed, without error, from samples taken at equal intervals. For this, the sampling rate must be equal to, or greater than, twice the highest frequency component in the analog signal. This means that the highest frequency in any of the cells should not exceed 0.1Hz, which is the sampling frequency for the above set of excitable cells. It was found that the 10-second interval was sufficient to observe Ca^{2+} oscillations. Before deciding on the final model a couple of other models already existing in the literature were tried. In the following figures, which show the model being fitted to the experimental data, the Y-axis variable represents Ca^{2+} intensity in the cell while the X-axis represents the time variable. The Ca^{2+} oscillations in the model is labeled as "ca" and is represented by a solid line while that in the cells is labeled by the name of the cell (e.g. "c22k") and is represented by a dashed line.

1. Results Of Proposed Model Fit With PHM1-41 (Excitable) Cell Line

The proposed model was tried on a large number of excitable cells. The following figures (Fig.11 to Fig.20) are the results of the proposed model fit with the experimental data of Ca^{2+} oscillations. The model was tried to fit each cell by adjusting the various parameters of the model for spike amplitude, frequency, height and shape and basal calcium level in the cell. Refer to Appendix A for more results of data fitting with excitable cells.

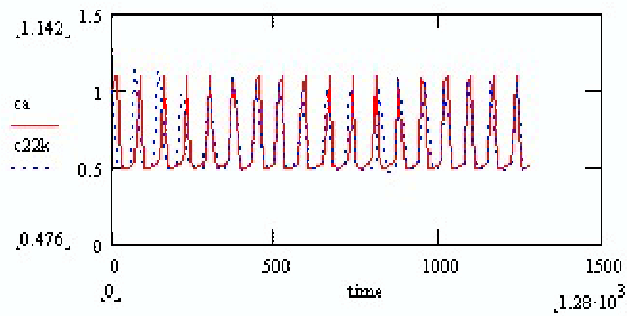


Fig. 11. PHM1-41 Cell 1

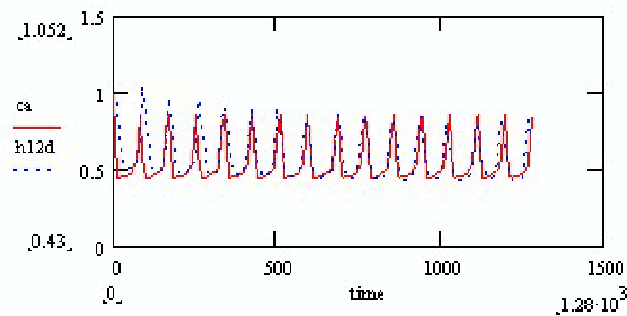


Fig. 12. PHM1-41 Cell 2

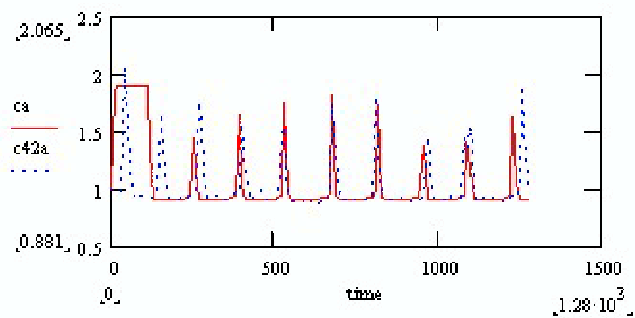


Fig. 13. PHM1-41 Cell 3

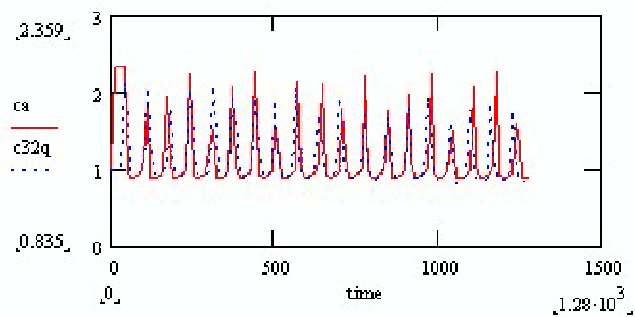


Fig. 14. PHM1-41 Cell 4

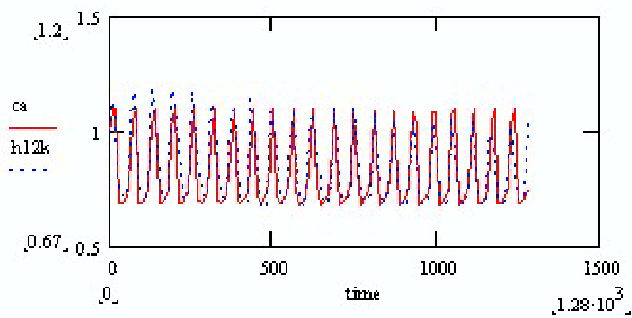


Fig. 15. PHM1-41 Cell 5

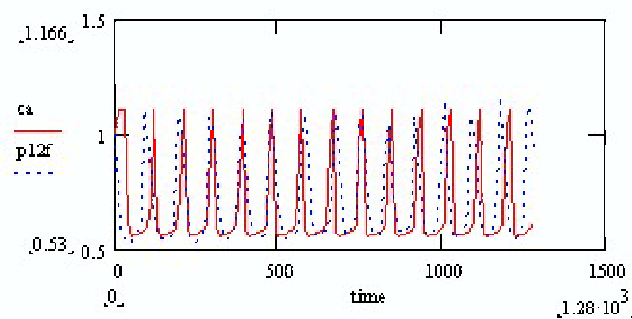


Fig. 16. PHM1-41 Cell 6

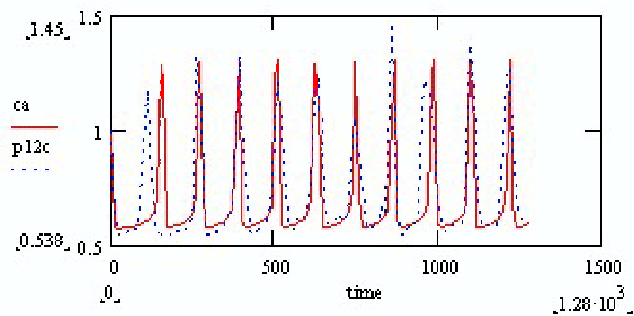


Fig. 17. PHM1-41 Cell 7

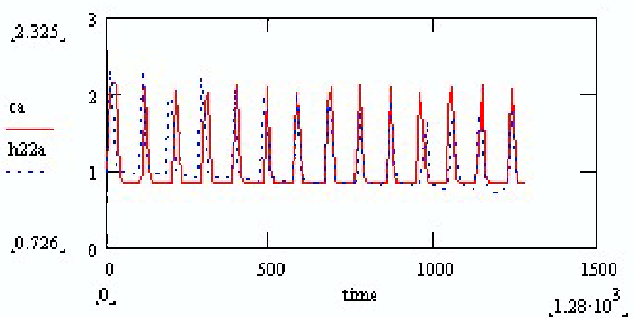


Fig. 18. PHM1-41 Cell 8

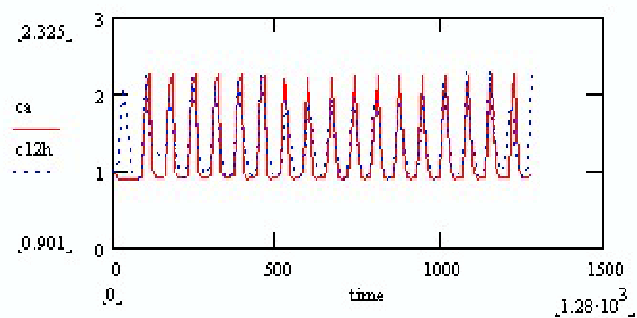


Fig. 19. PHM1-41 Cell 9

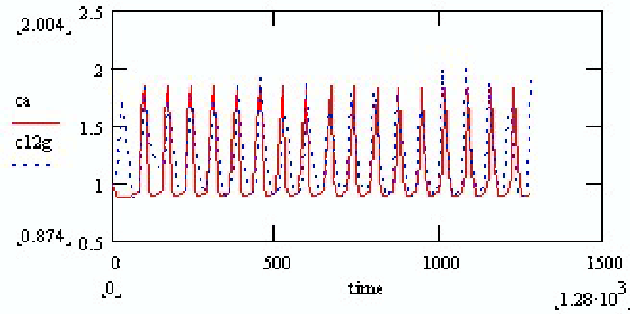


Fig. 20. PHM1-41 Cell 10

2. Time Domain Statistical Tests

After fitting the proposed model to the experimental data, to check the validity of the model before analyzing it in frequency domain, a time domain statistical t-test was carried out on the cell pairs of experimental time series data and model time series data to check if the pairing was effective in the time domain. The Table I shows the results of the t-test. The test carried out was Wilcoxon signed rank t-test.

Table I. Time Domain Test For Excitable Cells.

No.	Name of cell	Was the pairing significantly effective?
1	Cell 1	Yes
2	Cell 2	Yes
3	Cell 3	Yes
4	Cell 4	Yes
5	Cell 5	Yes
6	Cell 6	Yes
7	Cell 7	Yes
8	Cell 8	Yes
9	Cell 9	Yes
10	Cell 10	Yes
11	Cell 11	Yes
12	Cell 12	Yes
13	Cell 13	Yes
14	Cell 14	Yes
15	Cell 15	Yes
16	Cell 16	Yes

Table I. Continued.

No.	Name of cell	Was the pairing significantly effective?
17	Cell 17	Yes
18	Cell 18	Yes
19	Cell 19	Yes
20	Cell 20	Yes
21	Cell 21	No
22	Cell 22	Yes
23	Cell 23	Yes
24	Cell 24	Yes
25	Cell 25	Yes
26	Cell 26	Yes
27	Cell 27	Yes
28	Cell 28	Yes
29	Cell 29	Yes
30	Cell 30	Yes
31	Cell 31	Yes
32	Cell 32	Yes
33	Cell 33	Yes
34	Cell 34	Yes
35	Cell 35	Yes
36	Cell 36	Yes
37	Cell 37	Yes
38	Cell 38	Yes

The cell 21 was not significantly paired hence was discarded.

3. Frequency Domain Statistical Tests

i) Frequency Test:

The Table II gives a list of the fundamental frequencies obtained by doing a spectral analysis of the above excitable cells.

Table II. Fundamental Frequencies Of Excitable Cells.

No.	Name of cell	Fundamental Frequency(Expt)	Fundamental Frequency(Model)
1	Cell 1	36.883	37.055
2	Cell 2	96.173	95.258
3	Cell 3	51.615	53.395
4	Cell 4	40.895	41.791
5	Cell 5	40.895	38.958
6	Cell 6	33.743	34.897
7	Cell 7	96.172	96.255
8	Cell 8	61.733	34.897
9	Cell 9	84.719	85.278
10	Cell 10	63.8	61.435
11	Cell 11	145.388	145.788
12	Cell 12	145.388	101.847
13	Cell 13	107.799	107.961
14	Cell 14	99.039	99.039
15	Cell 15	107.799	107.961
16	Cell 16	115.058	113.592

Table II. Continued.

No.	Name of cell	Fundamental Frequency(Expt)	Fundamental Frequency(Model)
17	Cell 17	59.082	60.579
18	Cell 18	38.399	40.231
19	Cell 19	75.367	148.041
20	Cell 20	73.725	75.592
21	Cell 22	73.998	71.424
22	Cell 23	52.09	50.071
23	Cell 24	90.81	89.84
24	Cell 25	84.684	87.885
25	Cell 26	137.896	137.896
26	Cell 27	136.396	142.235
27	Cell 28	145.116	144.683
28	Cell 29	105.284	107.98
29	Cell 30	86.936	85.161
30	Cell 31	113.656	111.47
31	Cell 32	166.83	170.174
32	Cell 33	118.336	117.209
33	Cell 34	164.878	164.297
34	Cell 35	138.699	140.192
35	Cell 36	152.714	150.722
36	Cell 37	73.833	71.742
37	Cell 38	84.554	165.02

The Table III shows the results of the statistical t-test (Wilcoxon signed rank test) that was performed on the above table to verify the validity of the proposed model for frequency.

Table III. Statistical Frequency Test For Excitable Cells.

Analysis Parameters	Results
P value	0.9510
Exact or approximate P value?	Gaussian Approximation
P value summary	Ns
Are medians significantly different?($P \leq 0.05$)	No
One- or two-tailed P value?	Two-tailed
Sum of positive, negative ranks	311.0 , -319.0
Sum of signed ranks (W)	-8.000
How effective was the pairing?	
rs (Spearman, Approximation)	0.8696
P Value (one tailed)	$P < 0.0001$
P value summary	***
Was the pairing significantly effective?	Yes

ii)Amplitude Test:

The fundamental frequencies mentioned above have the following amplitudes as listed in Table IV below:

Table IV. Fundamental Amplitudes Of Excitable Cells.

No.	Name of cell	Fundamental Amplitude(Expt)	Fundamental Amplitude(Model)
1	Cell 1	265.9600	110.2830
2	Cell 2	563.4710	621.8150
3	Cell 3	249.2830	218.8550
4	Cell 4	586.9860	458.2890
5	Cell 5	586.9860	370.0300
6	Cell 6	452.7050	410.6690
7	Cell 7	343.3250	457.7030
8	Cell 8	352.1000	410.6690
9	Cell 9	288.9830	259.0320
10	Cell 10	316.3720	332.7120
11	Cell 11	618.6480	613.1900
12	Cell 12	618.6480	252.4180
13	Cell 13	568.8110	593.9410
14	Cell 14	518.8180	518.8180
15	Cell 15	7568.8110	593.9410
16	Cell 16	316.9700	347.6780

Table IV. Continued.

No.	Name of cell	Fundamental Amplitude(Expt)	Fundamental Amplitude(Model)
17	Cell 17	138.8890	153.8890
18	Cell 18	381.3760	210.1930
19	Cell 19	387.7450	253.5530
20	Cell 20	191.5430	160.9250
21	Cell 22	198.0300	158.5450
22	Cell 23	228.8180	337.9820
23	Cell 24	603.2620	611.6350
24	Cell 25	209.7530	217.6050
25	Cell 26	202.1420	202.1420
26	Cell 27	222.4930	385.9560
27	Cell 28	504.7520	620.7440
28	Cell 29	330.9200	390.6670
29	Cell 30	244.9410	202.5150
30	Cell 31	207.0550	191.5910
31	Cell 32	217.4210	206.0940
32	Cell 33	185.5650	148.1700
33	Cell 34	202.3200	177.0030
34	Cell 35	214.0340	241.2660
35	Cell 36	369.5250	372.3050
36	Cell 37	159.5040	132.2100
37	Cell 38	247.4120	152.4230

The Table V shows the results of the statistical t-test (Wilcoxon signed rank test) that was performed on the above table to verify the validity of the proposed model for amplitude.

Table V. Statistical Amplitude Test For Excitable Cells.

Analysis Parameters	Results
P value	0.3043
Exact or approximate P value?	Gaussian Approximation
P value summary	Ns
Are medians significantly different?($P \leq 0.05$)	No
One- or two-tailed P value?	Two-tailed
Sum of positive, negative ranks	378.0 , -252.0
Sum of signed ranks (W)	126.0
How effective was the pairing?	
rs (Spearman, Approximation)	0.8032
P Value (one tailed)	$P < 0.0001$
P value summary	***
Was the pairing significantly effective?	Yes

B. NON-EXCITABLE (CLONE 9) CELL LINE

In the case of non-excitable cells, the fluorescence intensity for each cell was collected at the rate of 1 scan every 3 seconds. Hence, the sampling frequency in this case is 0.333Hz. Since 3 seconds is a very short period, it was observed that a little

more than 3 seconds is taken by the computer before proceeding to the next scan. This extra time has been considered while solving for the differential equations. The results for the proposed model fit with the experimental data for non-excitabile cells are summarized below. The solid line represents the model while the dotted line represents the experimental data.

1. Results Of Proposed Model Fit With Non-Excitable Cells

The following figures(Fig.21 to Fig.30) show some of the data fitting results obtained with non-excitabile Clone 9 cell line.

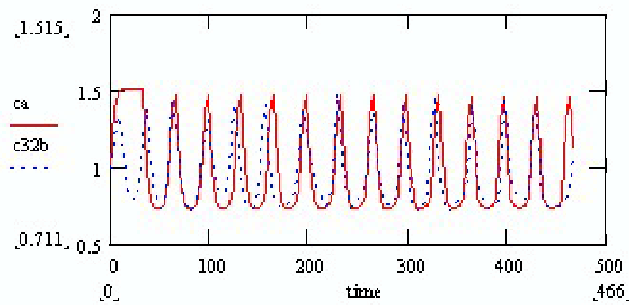


Fig. 21. Clone 9 Cell 1

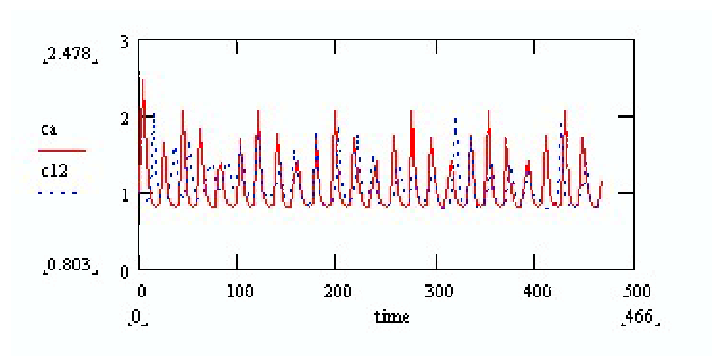


Fig. 22. Clone 9 Cell 2

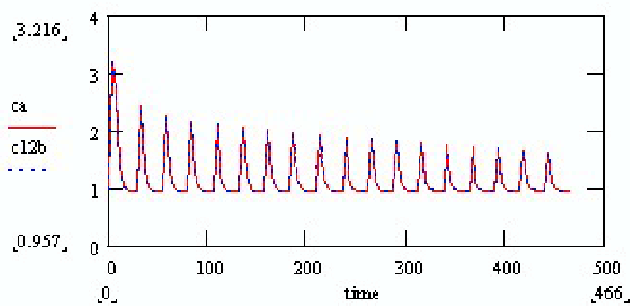


Fig. 23. Clone 9 Cell 3

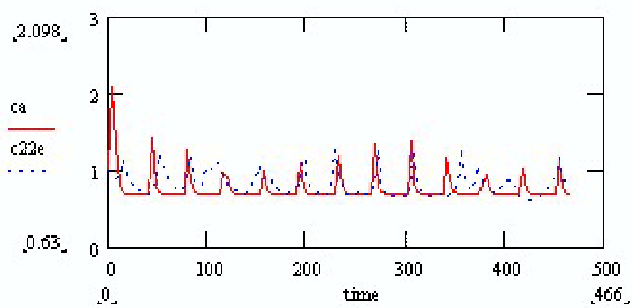


Fig. 24. Clone 9 Cell 4

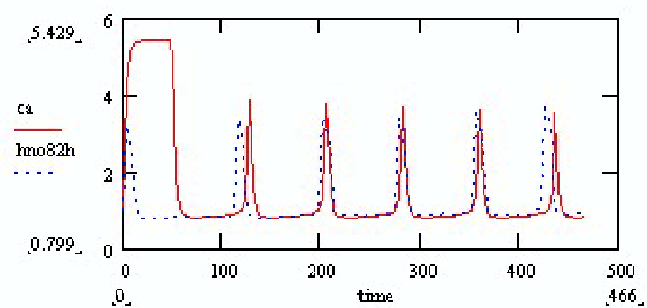


Fig. 25. Clone 9 Cell 5

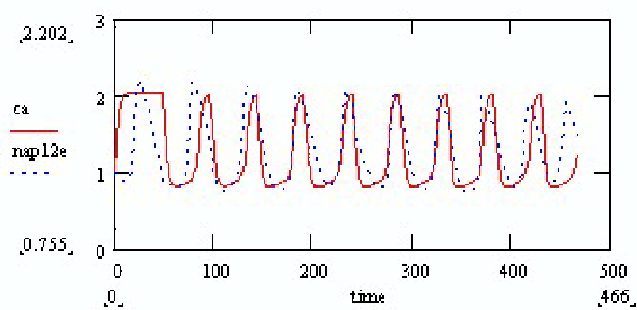


Fig. 26. Clone 9 Cell 6

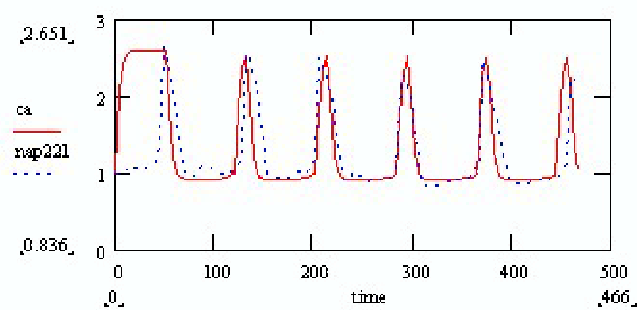


Fig. 27. Clone 9 Cell 7

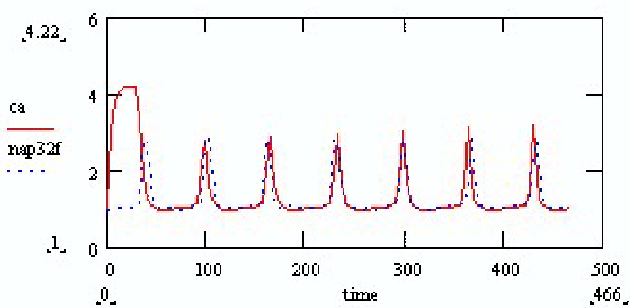


Fig. 28. Clone 9 Cell 8

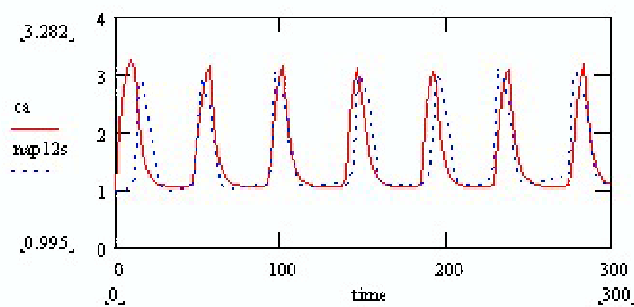


Fig. 29. Clone 9 Cell 9

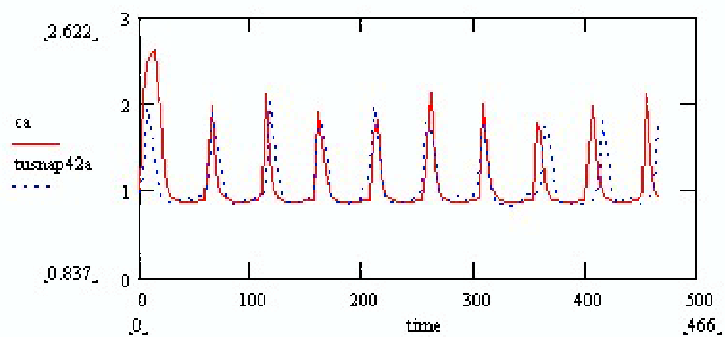


Fig. 30. Clone 9 Cell 10

2. Results To Show Effect Of Gap Junction

In the proposed model, the factor "rcc" has been included to account for the gap junction permeability of the cell. It has been observed that inclusion of the term " $rcc * e^{-rcc*t}$ " causes a slight improvement in the fit. The following non-excitable cells (Fig.31 to Fig.42) show a marked improvement in fit to the model with the gap junction effect included:

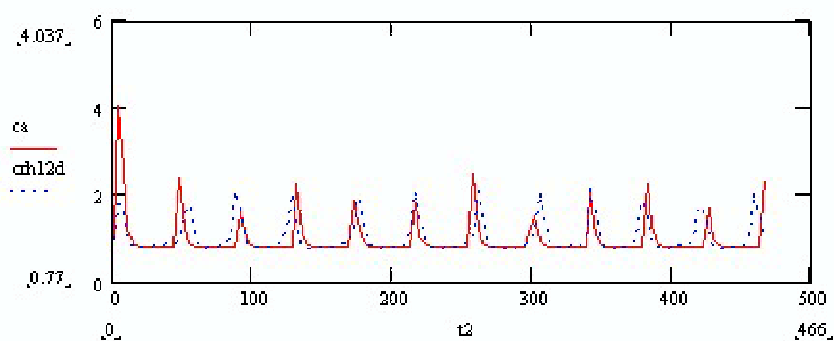


Fig. 31. With Gap Junction Clone 9 Cell 1

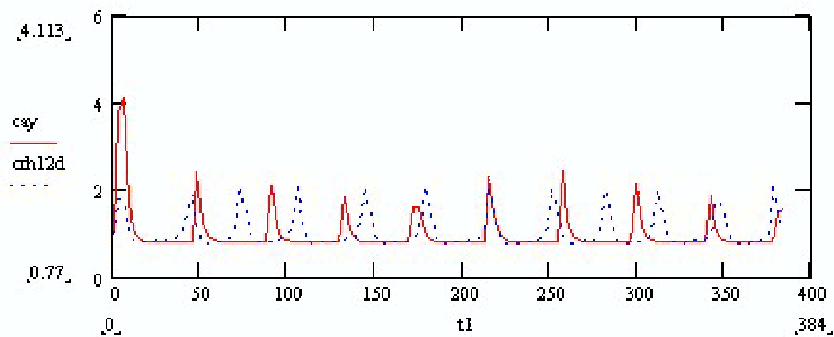


Fig. 32. Without Gap Junction Clone 9 Cell 1

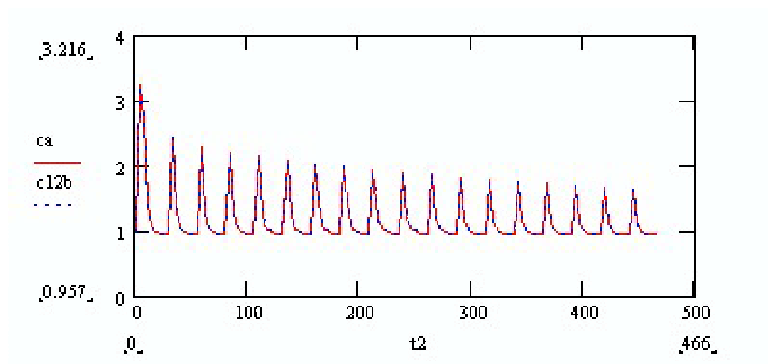


Fig. 33. With Gap Junction Clone 9 Cell 2

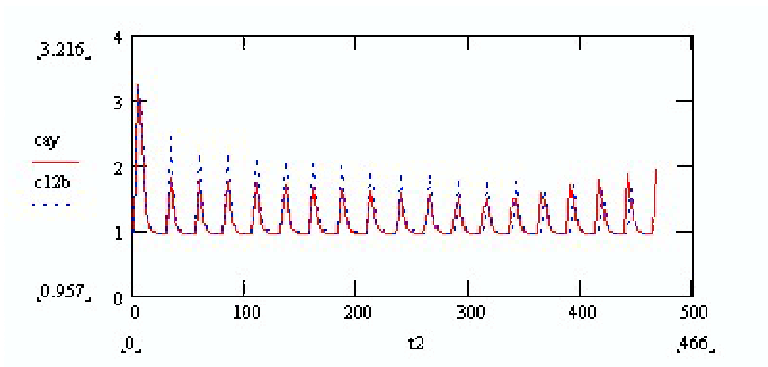


Fig. 34. Without Gap Junction Clone 9 Cell 2

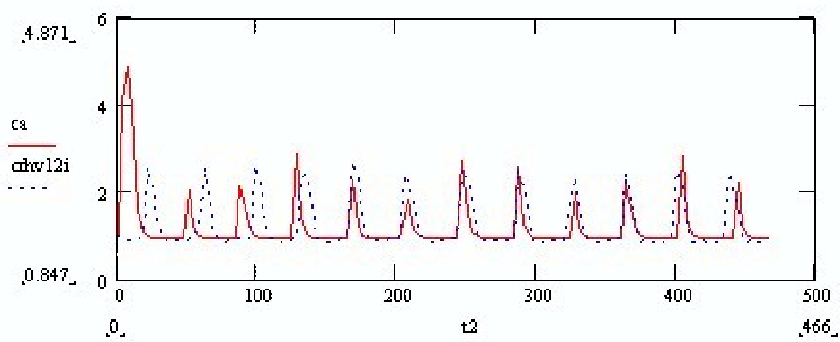


Fig. 35. With Gap Junction Clone 9 Cell 3

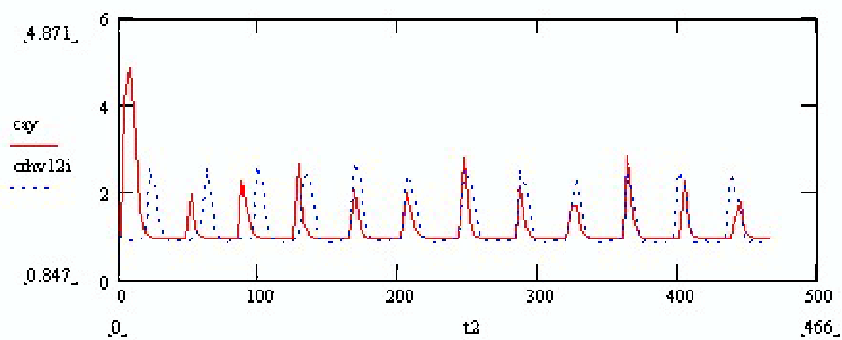


Fig. 36. Without Gap Junction Clone 9 Cell 3

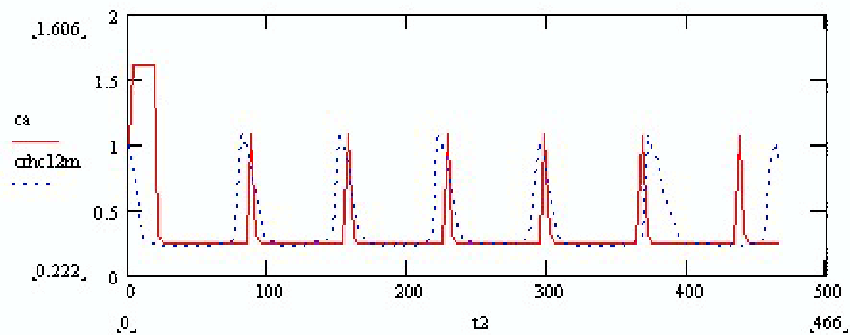


Fig. 37. With Gap Junction Clone 9 Cell 4

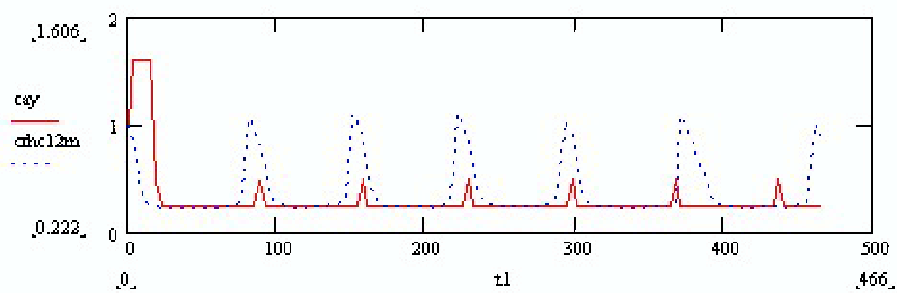


Fig. 38. Without Gap Junction Clone 9 Cell 4

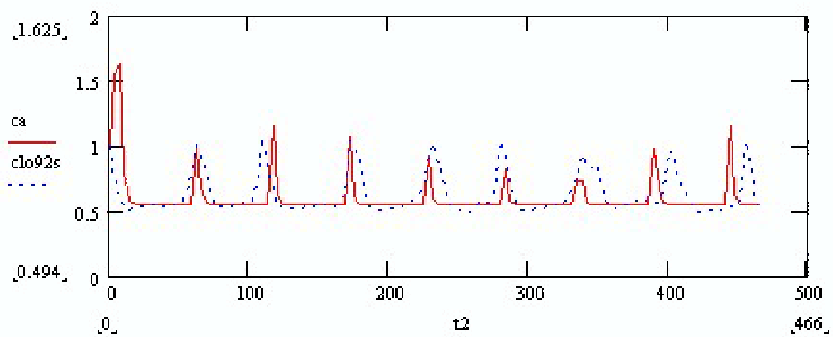


Fig. 39. With Gap Junction Clone 9 Cell 5

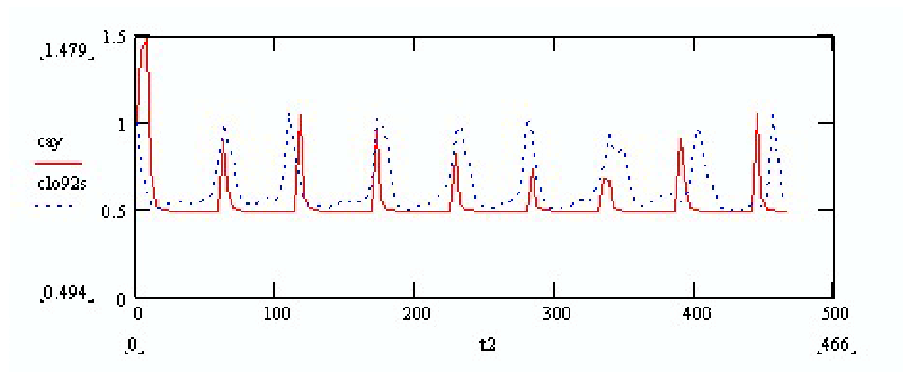


Fig. 40. Without Gap Junction Clone 9 Cell 5

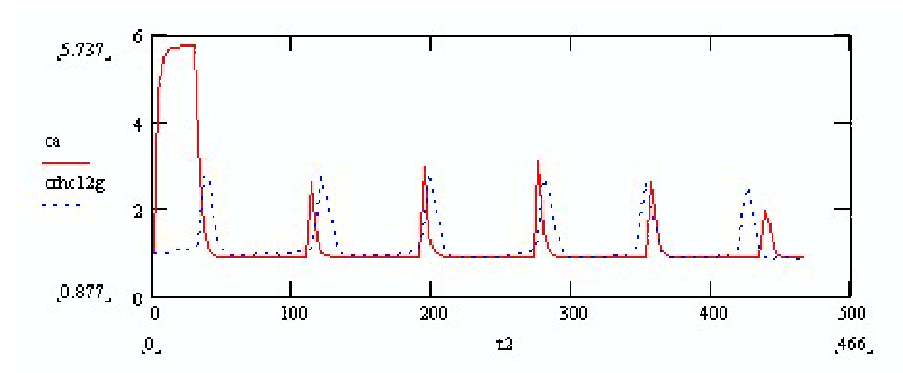


Fig. 41. With Gap Junction Clone 9 Cell 6

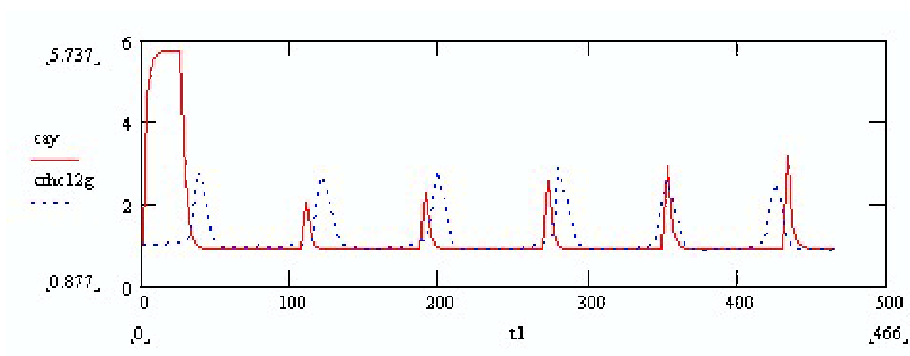


Fig. 42. Without Gap Junction Clone 9 Cell 6

3. Time Domain Statistical Tests

As in the case of the excitable cells, time domain tests are carried out on the model as well as experimental data to check if their pairing in the time series is effective. Wilcoxon signed rank t-test was performed on the above set of cells. The following table, Table VI shows the results of the test:

Table VI. Time Domain Test For Non-Excitable Cell Line.

No.	Name of cell	Was the pairing significantly effective?
1	Cell 1	Yes
2	Cell 2	Yes
3	Cell 3	Yes
4	Cell 4	Yes
5	Cell 5	Yes
6	Cell 6	Yes
7	Cell 7	Yes
8	Cell 8	Yes
9	Cell 9	Yes
10	Cell 10	Yes
11	Cell 11	Yes
12	Cell 12	Yes
13	Cell 13	Yes
14	Cell 14	Yes
15	Cell 15	No
16	Cell 16	No

Table VI. Continued.

No.	Name of cell	Was the pairing significantly effective?
17	Cell 17	Yes
18	Cell 18	Yes
19	Cell 19	Yes
20	Cell 20	Yes
21	Cell 21	No
22	Cell 22	Yes
23	Cell 23	Yes
24	Cell 24	Yes
25	Cell 25	Yes
26	Cell 26	Yes
27	Cell 27	Yes
28	Cell 28	Yes
29	Cell 29	Yes

The cells 5, 16, 21 and 22 didn't pair effectively hence were discarded.

4. Frequency Domain Statistical Tests

i) Frequency Test:

The fundamental frequencies of the Ca^{2+} oscillations (both model and experimental) were obtained by writing a LabView code to extract the fundamental frequencies from the oscillations. The following table, Table VII lists the frequencies of the experimental and model data.

Table VII. Fundamental Frequencies Of Non-Excitable Cell Line.

No.	Name of cell	Fundamental Frequency(Expt)	Fundamental Frequency(Model)
1	Cell 1	109.639	110.804
2	Cell 2	189.638	190.371
3	Cell 3	142.861	142.861
4	Cell 4	98.654	98.704
5	Cell 6	578.122	600.782
6	Cell 7	469.360	450.043
7	Cell 8	435.106	424.717
8	Cell 9	676.162	772.678
9	Cell 10	323.264	289.030
10	Cell 11	219.612	188.326
11	Cell 12	563.750	661.878
12	Cell 13	535.549	432.007
13	Cell 14	617.633	545.238
14	Cell 15	403.399	377.721
15	Cell 17	568.007	473.466
16	Cell 18	183.392	302.701

Table VII. Continued.

No.	Name of cell	Fundamental Frequency(Expt)	Fundamental Frequency(Model)
17	Cell 19	166.278	84.990
18	Cell 20	194.506	259.740
19	Cell 23	284.890	178.903
20	Cell 24	458.404	352.833
21	Cell 25	316.281	472.580
22	Cell 26	257.451	139.427
23	Cell 27	460.928	647.758
24	Cell 28	167.285	191.437
25	Cell 29	98.845	400.830

Table VIII. Statistical Frequency Test For Non-Excitable Cell Line.

Analysis Parameters	Results
P value	0.8035
Exact or approximate P value?	Gaussian Approximation
P value summary	Ns
Are medians significantly different?($P \leq 0.05$)	No
One- or two-tailed P value?	Two-tailed
Sum of positive, negative ranks	153.0, -172.0
Sum of signed ranks (W)	-19.00
How effective was the pairing?	
rs (Spearman, Approximation)	0.8578
P Value (one tailed)	$P < 0.0001$
P value summary	***
Was the pairing significantly effective?	Yes

Table VIII gives the results of the statistical t-test (Wilcoxon signed rank test) that was performed on the above table to verify the validity of the proposed model for frequency.

ii) Amplitude Test:

The amplitudes for the fundamental frequencies of the calcium oscillations were obtained using LabView 6 software. The following table, Table IX lists the amplitudes of the experimental and model data.

Table IX. Fundamental Amplitudes Of Excitable Cells.

No.	Name of cell	Fundamental Amplitude(Expt)	Fundamental Amplitude(Model)
1	Cell 1	245.417	326.581
2	Cell 2	242.944	393.786
3	Cell 3	315.989	315.989
4	Cell 4	122.843	118.575
5	Cell 5	460.928	647.758
6	Cell 6	167.285	191.437
7	Cell 7	198.845	400.830
8	Cell 8	99.637	202.198
9	Cell 9	578.122	600.782
10	Cell 10	469.360	450.043
11	Cell 11	435.106	424.717
12	Cell 12	676.162	772.678
13	Cell 13	323.264	289.030
14	Cell 14	219.612	188.326

Table IX. Continued.

No.	Name of cell	Fundamental Amplitude(Expt)	Fundamental Amplitude(Model)
15	Cell 15	535.549	432.007
16	Cell 16	617.633	545.238
17	Cell 17	358.196	367.702
18	Cell 18	403.399	377.721
19	Cell 19	145.225	250.029
20	Cell 20	183.392	302.701
21	Cell 22	166.278	84.990
22	Cell 23	194.506	259.740
23	Cell 24	284.890	178.903
24	Cell 25	458.404	352.833
25	Cell 26	257.451	139.427

The following table, Table X gives the results of the statistical t-test(Wilcoxon signed rank test) that was performed on the above table to verify the validity of the proposed model for amplitude.

Table X. Statistical Amplitude Test For Excitable Cells.

Analysis Parameters	Results
P value	0.2155
Exact or approximate P value?	Gaussian Approximation
P value summary	Ns
Are medians significantly different?($P \leq 0.05$)	No
One- or two-tailed P value?	Two-tailed
Sum of positive, negative ranks	172.0 , -293.0
Sum of signed ranks (W)	-121.0
How effective was the pairing?	
rs (Spearman, Approximation)	0.8234
P Value (one tailed)	$P < 0.0001$
P value summary	***
Was the pairing significantly effective?	Yes

C. DISCUSSION

The results of the data fitting prove that the model Ca^{2+} oscillations fit the experimental data well. All the statistical tests including the time domain and the frequency domain tests show that the pairing of the two sets of data is significant. There were a number of observations made during the course of preparing the model and fitting it to the data. Some of them are listed as under:

1. The model produced pulsatile shaped oscillations with the shape and amplitude of the oscillations almost constant and increase in frequency of oscillations due to increase in agonist concentration.
2. In the non-excitabile cells, it is found that when a group of cells is each treated with an agonist, the nature of the oscillations changes due to the effect of gap junctional diffusion of IP_3 between neighboring cells causing an increase of IP_3 in one cell and reduction in another. On adjusting the values of the gap junction permeability, rcc , it was found that inclusion of this factor caused improvements in the fit of many non-excitabile cells. The same was not observed with excitable cells. When it was assumed that instead of IP_3 , Ca^{2+} is the diffusing agent between cells, the results were almost the same as those got using IP_3 .
3. Increasing kd or ld and decreasing Kg increased the frequency of oscillations without changing the amplitude of the oscillations.
4. The nature of the model oscillations was found to be pulsatile, hence more in tune with non-excitabile cells as compared to excitable cells which have a quasi-sinusoidal shape. Hence, as can be seen in some examples of excitable cells above, although the frequency of the model fits that of the experimental, the shape of oscillations could vary slightly.

5. The second equation, which is the change in the rate of IP_3 production, causes very slight changes in the shape of the oscillations.
6. All the statistical tests conducted on both excitable and non-excitable cells showed that the pairing of the model and experimental data was significant. Hence, considering that the criteria for assessing a model should go beyond mere matching of oscillations, and having included factors like agonist concentration, pulse shape and statistical tests, the robustness of the model has been validated.

CHAPTER V

RESULTS OF DATA ANALYSIS

A. FAST FOURIER TRANSFORM

Fourier Analysis is a mathematical technique for transforming signals in time-domain to the frequency-domain. In a fourier series, the time-domain signal is expressed in terms of functions of sines and cosines. If the signal is periodic then, the fourier series is used to represent the signal over an interval but if the signal is aperiodic, then fourier series cannot be used to represent it for all values. For such signals, the Fast Fourier Transform is ideal since it is an integral defined from $-\infty$ to $+\infty$. For many signals, Fast Fourier Transform is very useful because the signal's frequency content is very important but there are several drawbacks of the Fourier Transform listed as under:

- One of the most important deficiencies of the Fast Fourier Transform is that in transforming to the frequency domain the time information is lost. It is impossible to say when a particular event occurred, looking at the Fourier transform.
- It cannot be computed in real-time.
- Even a very small perturbation of the signal on the time axis influences all the points on the frequency axis.
- It cannot display time-frequency information effectively.
- It can only be computed for one frequency at a time.

Nevertheless, the FFT analysis is very useful in the study of calcium oscillations because it is used to identify the frequencies that occur in the oscillations. The

FFT analysis involves conversion of the experimental calcium acquired in an interval of time into a steady state intensity signal that represents the stable calcium level within the cell at any given time during an experiment.

The following graphs show the Fourier Transform and Inverse Fourier Transforms of the above experimental data and of the calcium content in the proposed model. Here again, the solid line represents the model while the dotted line represents the experimental data.

For each cell, the first graph shows the cell in the time domain, second graph shows Fast Fourier Transform (FFT) of the experimental and model data and the second graph shows the Inverse FFT of the experimental and model data.

Legend: Dotted line-experimental data, solid line-model data.

Here, the X-axis (j (for the FFT) and k (for the Inverse FFT) variables) represents the frequency (number of sample points) and the Y-axis (b and c (for the FFT) and a and d (for the Inverse FFT)) represents the amplitude at that frequency. The analysis was done using Mathcad6 software. The total number of samples is 128. But, for real data in the time domain, the Fourier transform has conjugate symmetry. Because of this, the `fft` function in Mathcad will drop the redundant second half of the result. This is why the vector returned by `fft` is half the size of the original vector. i.e. over 64-sample points. The difference between the original and the reconstructed oscillations (after performing IFFT) for both the experimental and model calcium were found to be very small values. The *Nyquist Theorem* states that an analog waveform may be uniquely reconstructed, without error, from samples taken at equal intervals. For this, the sampling rate must be equal to, or greater than, twice the highest frequency component in the analog signal. This means that the highest frequency in any of the cells should not exceed the sampling frequency. Shown below (Fig.43 to Fig.60) are the FFT and IFFT graphs of 7 cells out of the total 37 analyzed excitable cells.

(experimental and model) since the rest of the cells follow the same pattern of analysis.

1. Analysis Of Excitable Cells Using FFT

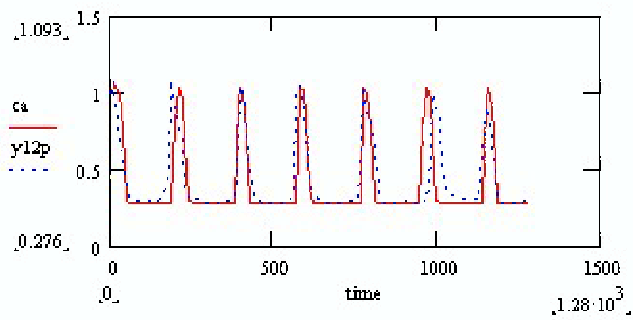


Fig. 43. Original Cell 1 In Time Domain

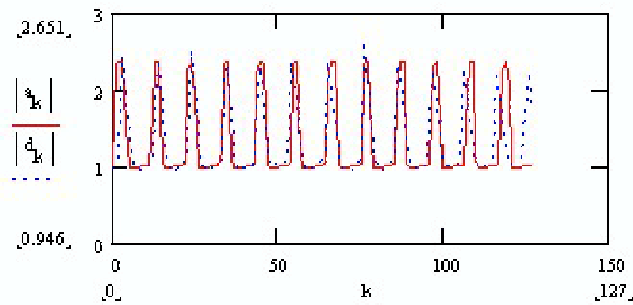


Fig. 44. Fast Fourier Transform(FFT) Of Cell 1

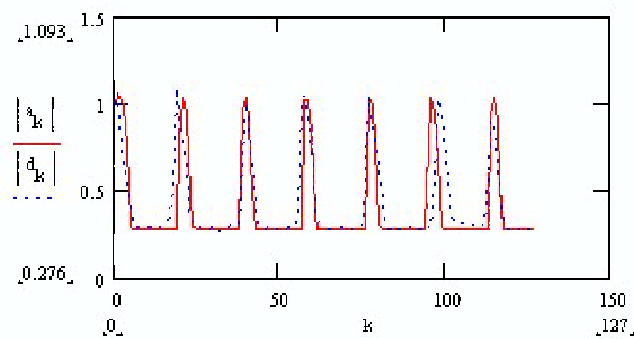


Fig. 45. Reconstructed Cell 1 After IFFT

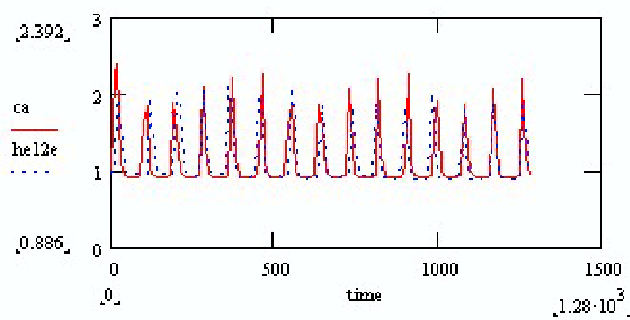


Fig. 46. Original Cell 2 In Time Domain

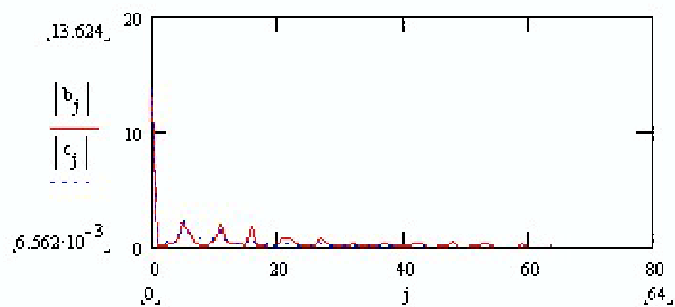


Fig. 47. Fast Fourier Transform(FFT) of Cell 2

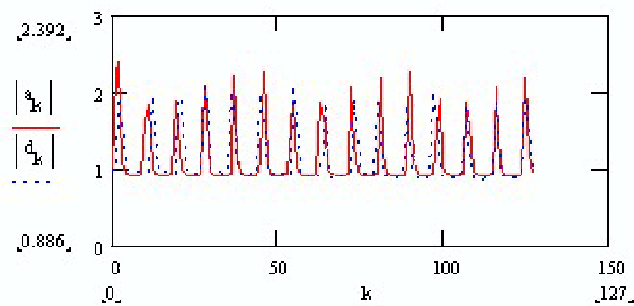


Fig. 48. Reconstructed Cell 2 After IFFT

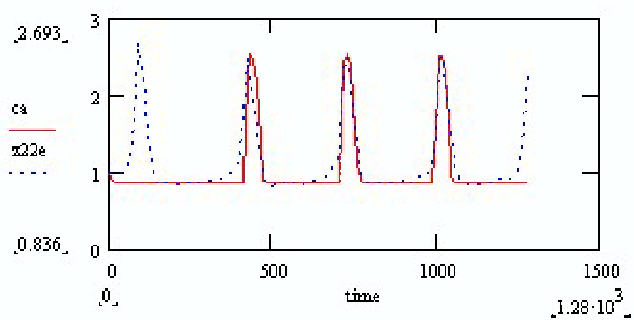


Fig. 49. Original Cell 3 In Time Domain

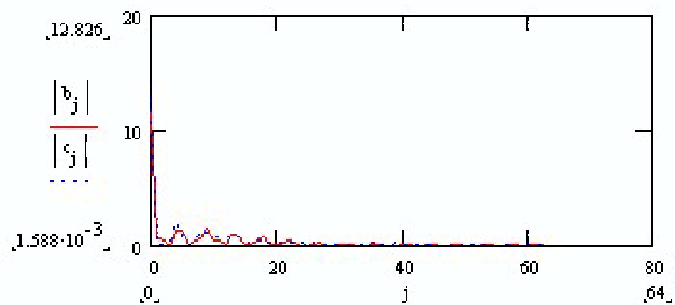


Fig. 50. Fast Fourier Transform(FFT) Of Cell 3

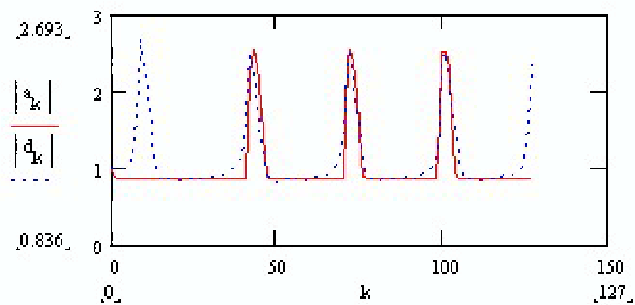


Fig. 51. Reconstructed Cell 3 After IFFT

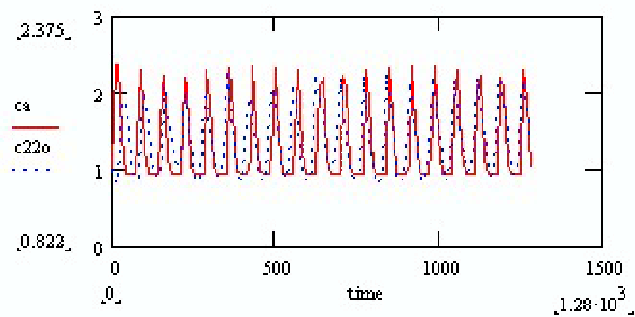


Fig. 52. Original Cell 4 In Time Domain

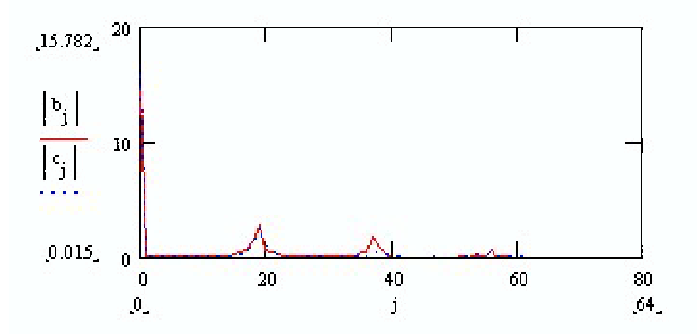


Fig. 53. Fast Fourier Transform(FFT) Of Cell 4

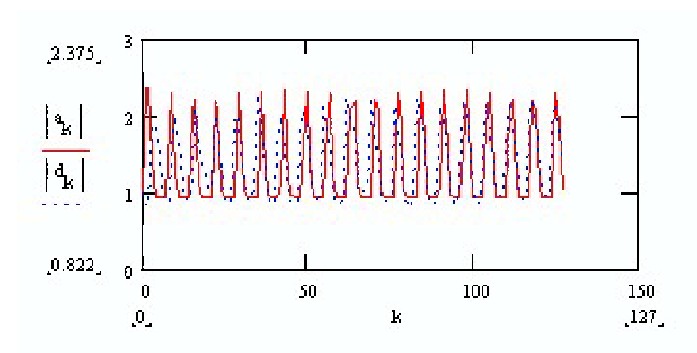


Fig. 54. Reconstructed Cell 4 After IFFT

The difference between the original and the reconstructed oscillations (after performing IFFT) for both the experimental and model calcium were found to be very small values. Also, the difference between the reconstructed model calcium oscillations and reconstructed experimental calcium oscillations were very small values, which means that the original and reconstructed values in the time domain are very close.

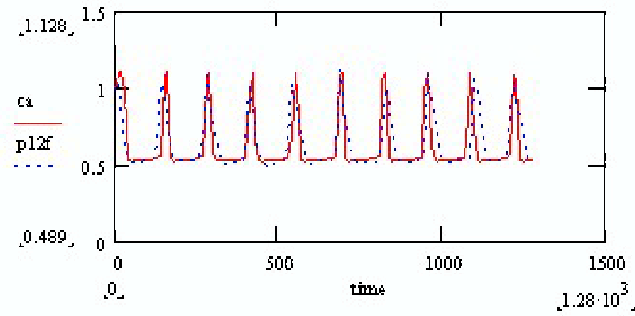


Fig. 55. Original Cell 5 In Time Domain

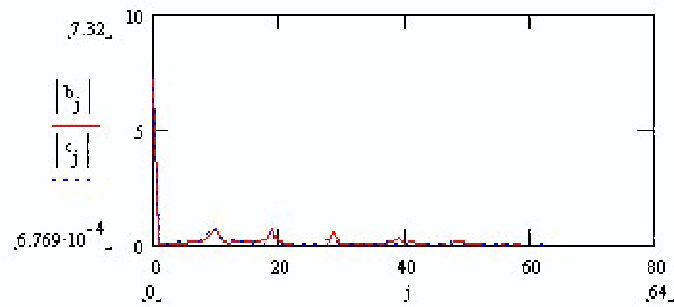


Fig. 56. Fast Fourier Transform(FFT) Of Cell 5

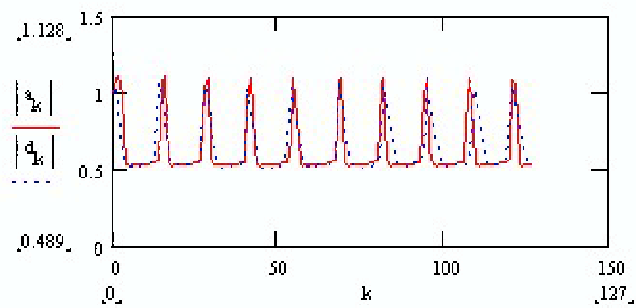


Fig. 57. Reconstructed Cell 5 After IFFT

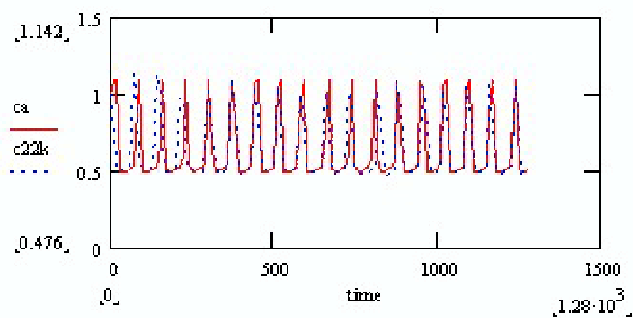


Fig. 58. Original Cell 6 In Time Domain

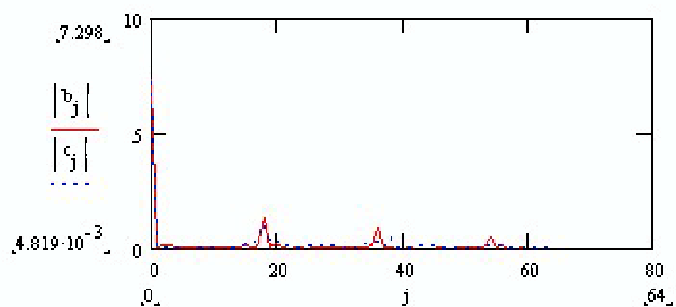


Fig. 59. Fast Fourier Transform(FFT) Of Cell 6

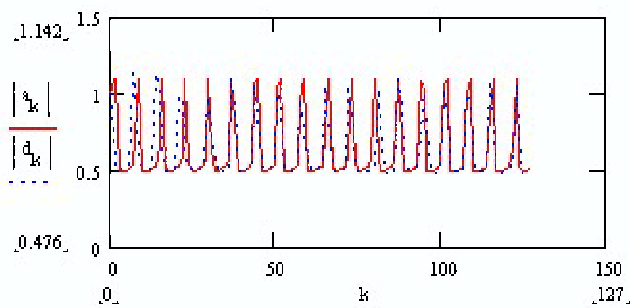


Fig. 60. Reconstructed Cell 6 After IFFT

2. Analysis Of Non-Excitable Cells Using FFT

Like the excitable cells, the non-excitable cells are subjected to FFT to identify the frequency of the calcium oscillations. In the case of non-excitable cells, the sampling frequency was found to be 0.333s. The following figures(Fig.61 to Fig.72) show the result of FFT and IFFT on the calcium oscillations:

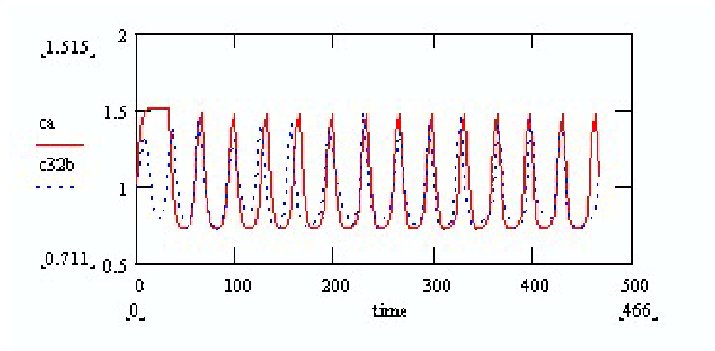


Fig. 61. Original Cell 1 In Time Domain

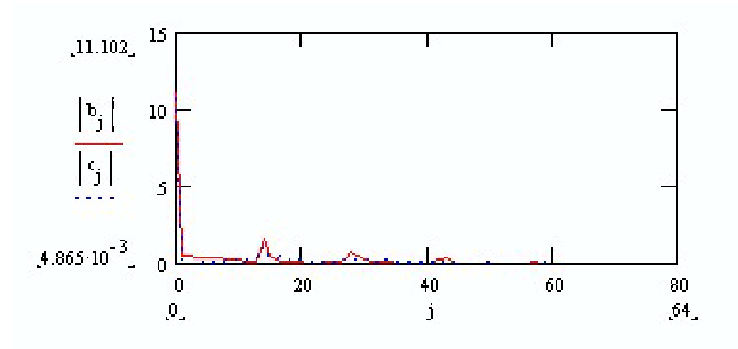


Fig. 62. Fast Fourier Transform(FFT) Of The Cell 1

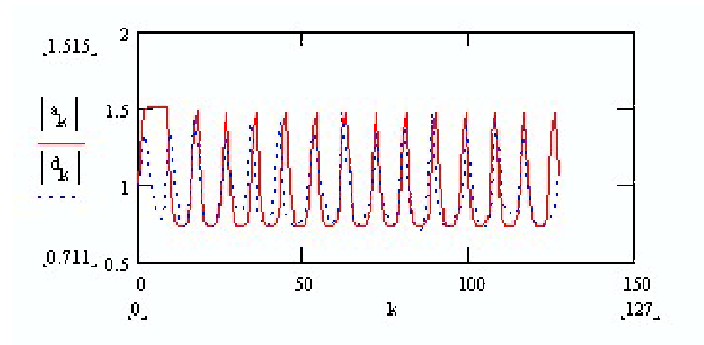


Fig. 63. Reconstructed Cell 1 After IFFT

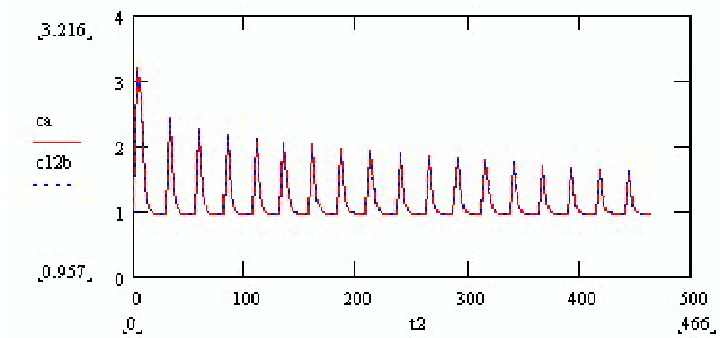


Fig. 64. Original Cell 2 In Time Domain

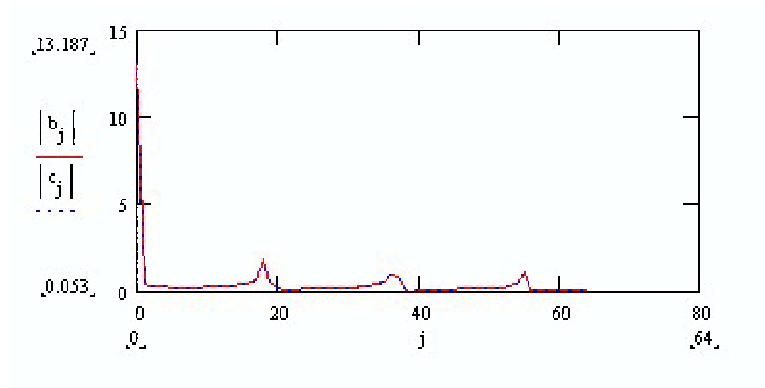


Fig. 65. Fast Fourier Transform(FFT) Of The Cell 2

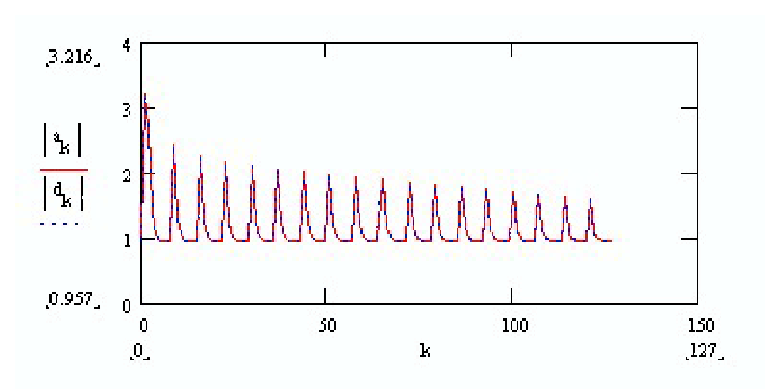


Fig. 66. Reconstructed Cell 2 After IFFT

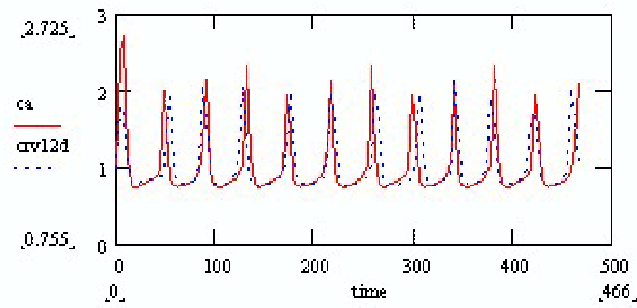


Fig. 67. Original Cell 3 In Time Domain

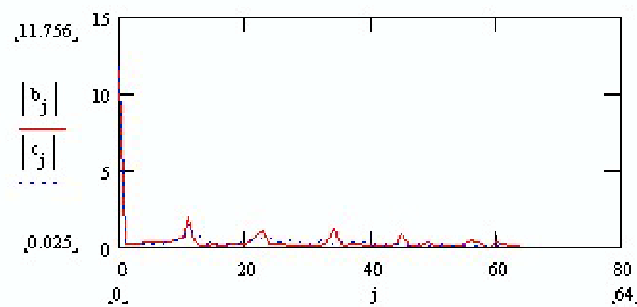


Fig. 68. Fast Fourier Transform(FFT) Of The Cell 3

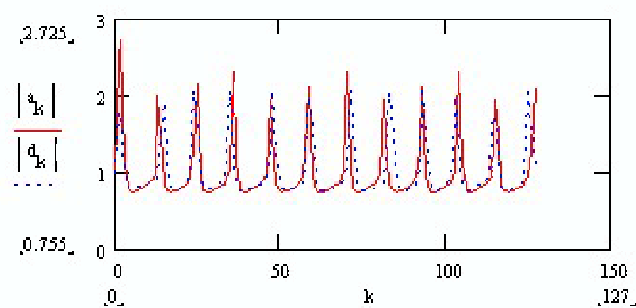


Fig. 69. Reconstructed Cell 3 After IFFT

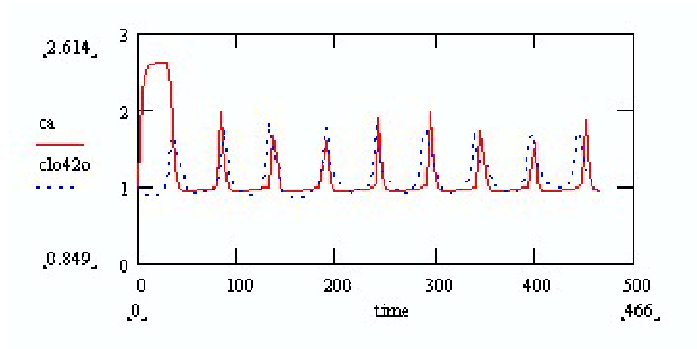


Fig. 70. Original Cell 4 In Time domain

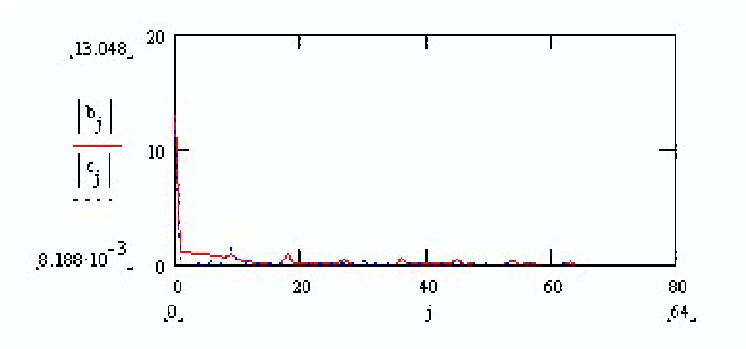


Fig. 71. Fast Fourier Transform(FFT) Of The Cell 4

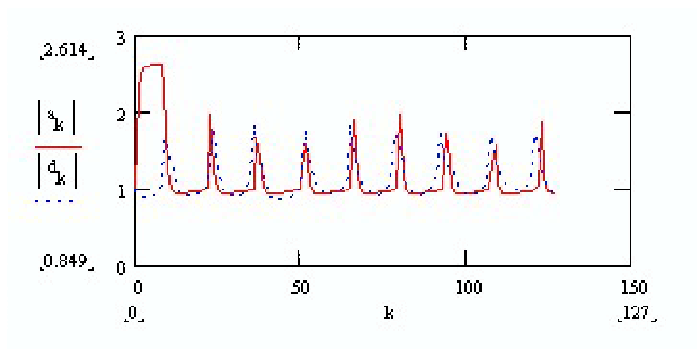


Fig. 72. Reconstructed Cell 4 After IFFT

B. WAVELET TRANSFORMS

Wavelets are a new set of tools developed to account for the inadequacies of the Fourier Transform. Wavelets can be used to extract time-frequency information from a given signal. A wavelet is a waveform of effectively limited duration that has an average value of zero[19]. Just as Fourier Transform involves the breaking up of the signal into sine waves of various frequencies, in a similar way wavelet analysis is the breaking up of a signal into shifted and scaled versions of the original (or mother) wavelet. Thus, using wavelets one has the flexibility of selecting variable sized regions for analysis and subsequently long time intervals can be used when we want precise low-frequency information and shorter regions when we want high frequency regions. *Scaling* a wavelet means stretching(or compressing) it(Fig.73). The scale factor "a" is inversely related to the frequency. Thus low scale means compressed wavelet which implies rapidly changing details i.e.high frequency. High scale, means stretched wavelet implying slowing changing, coarse features, hence low frequency.

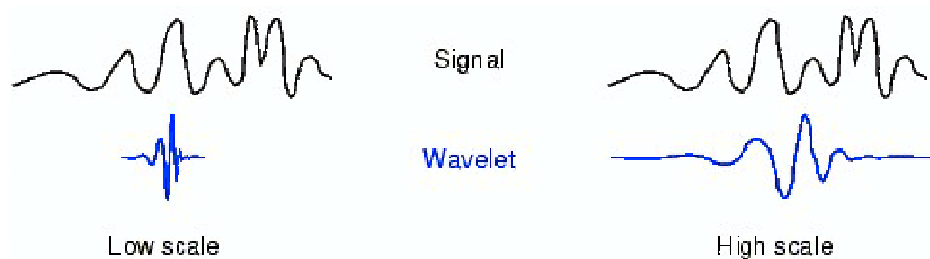


Fig. 73. Scaling[19]

Shifting a wavelet simply means delaying (or hastening) its onset(Fig.74). Mathematically, delaying a function $f(t)$ by k is represented by $f(t-k)$:

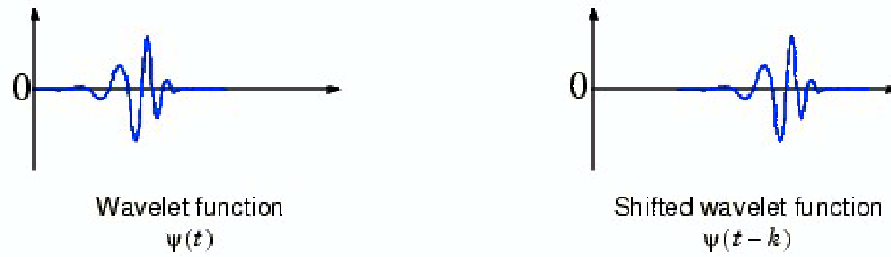


Fig. 74. Shifting[19]

The choice of the mother wavelet determines the nature of the wavelet analysis. There are two kinds of wavelet transform: the continuous wavelet transform (CWT) and the discrete wavelet transform (DWT). The continuous wavelet transform (CWT) is defined as the sum over all time of the signal multiplied by scaled, shifted versions of the wavelet function as follows ψ :

$$C(\text{scale}, \text{position}) = \int f(t)\psi(\text{scale}, \text{position}, t)dt \quad (5.1)$$

The results of the CWT are many wavelet coefficients C , which are a function of scale and position. Multiplying each coefficient by the appropriately scaled and shifted wavelet yields the constituent wavelets of the original signal. Calculating all these coefficients involves a fair amount of work, hence if we choose scales and positions based on powers of two – so-called dyadic scales and positions – then our analysis will be much more efficient and just as accurate. We obtain such an analysis from the discrete wavelet transform (DWT). When the signal is recorded in continuous time and all the values of the decomposition are needed to reconstruct the original signal then the CWT is preferred. When the energy of the signal is finite and not all the values of the decomposition are required to reconstruct the signal, DWT is preferred

since the CWT is redundant in this case. The one-dimensional DWT is implemented using a set of filters developed by Mallat[20]. Most signals consist of high-frequency and low-frequency components. The approximations(A) the high-scale, low-frequency components of the signal. The details(D) the low-scale, high-frequency components. The filtering process looks as shown in the Fig.75 below:

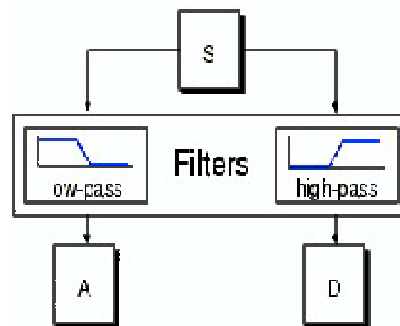


Fig. 75. Continuous Wavelet Transform.[19]

The A's and D's obtained are then downsampled (process of reducing the number of samples to equal the number of samples present in the original signal). This process then produces the DWT coefficients. (consisting of coefficients of A, cA and coefficients of D, cD). This decomposition process can then be iterated with successive A's being decomposed in turn to form the wavelet tree. The following figure, Fig.76 illustrates that.

The decomposition can proceed only until the individual details consist of a single sample or pixel. In practice, one can select a suitable number of levels based on the nature of the signal. The process of assembling back these coefficients to produce the original signal is called synthesis or reconstruction and is achieved using *inverse discrete wavelet transform*.

Just as wavelet analysis involves filtering and downsampling, synthesis involves

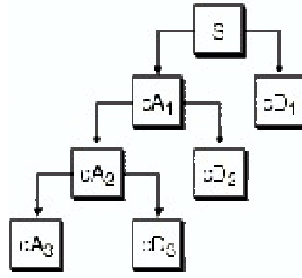


Fig. 76. Filtering For One-d Discrete Wavelet Transform.[19]

upsampling and reconstruction. Upsampling is the process of lengthening the signal by inserting zeroes between samples. Hence using the coefficients of approximations and details and passing them through appropriate filters, the original signal can be reconstructed.(Refer to Fig.77)

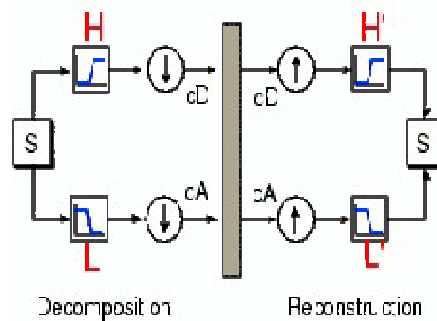


Fig. 77. Decomposition And Reconstruction.[19]

In the present study, the Daubechies four-coefficient 1-D discrete wavelet transform was selected as the mother wavelet since it closely resembles the nature of the calcium oscillations. Also, it was found that using the 1-D IDWT gave an almost exact reconstruction of the original which meant that the choice of the mother wavelet

was appropriate. The Matlab 1-D Wavelet Toolbox as well as MathCAD 6 were used for the analysis.

1. Analysis Of Excitable Cells Using 1-D DWT

The following are the results of the Wavelet analysis on the experimental data as well as the calcium content in the proposed model for an some excitable cell. As before the solid line represents the model calcium oscillations while the dotted line represents the experimental calcium oscillations. The following figures (Fig.78 to Fig.82) are the results of the Wavelet analysis on the experimental data as well as the calcium content in the proposed model for an some excitable cell. As before the solid line represents the model calcium oscillations while the dotted line represents the experimental calcium oscillations.

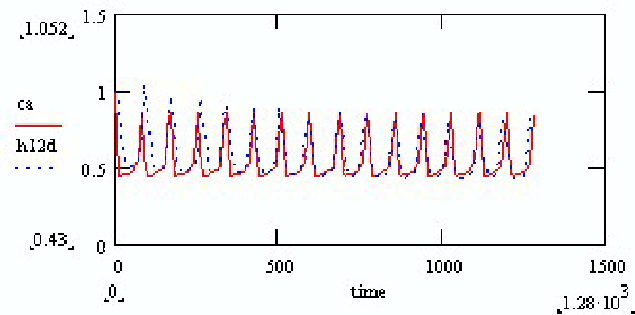


Fig. 78. Original Cell 1 In Time Domain

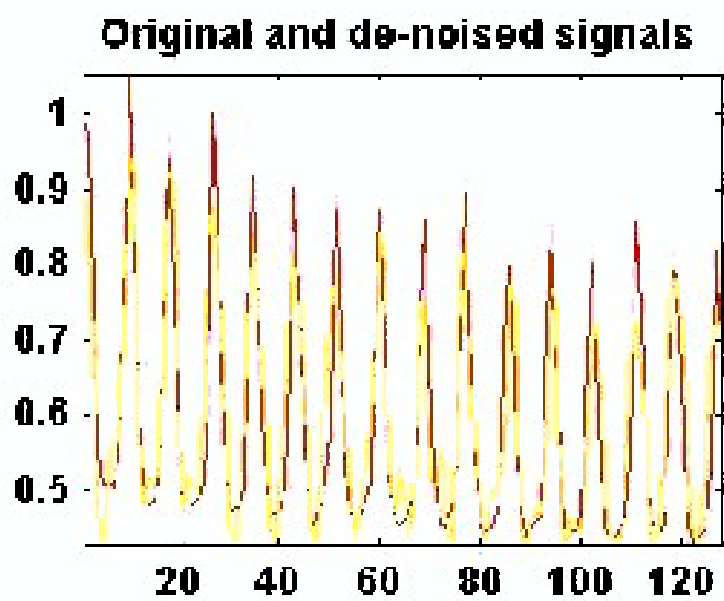


Fig. 79. Denoised Experimental Cell 1

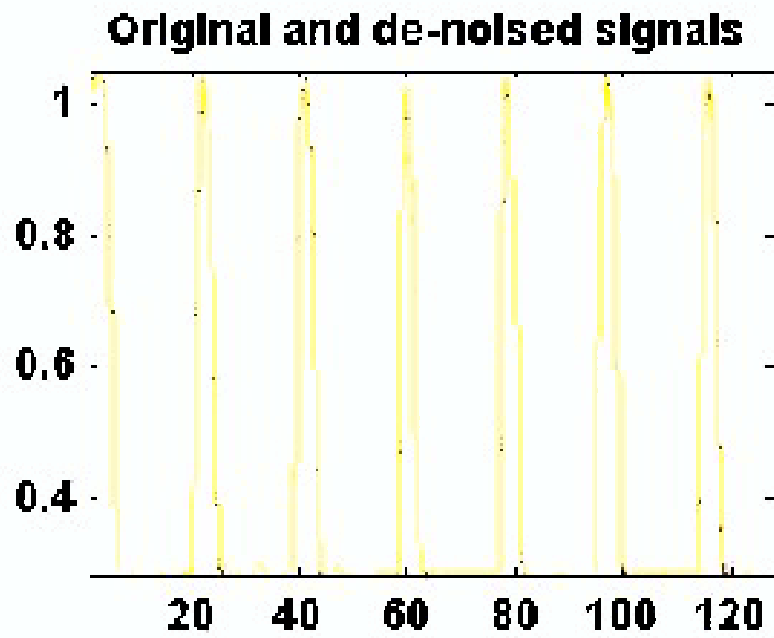


Fig. 80. Denoised Model Cell 1

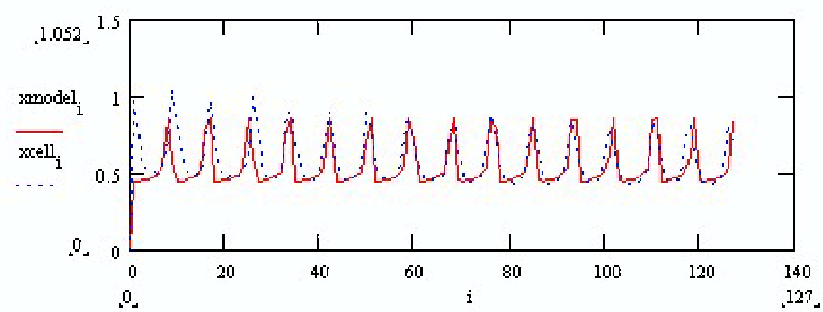


Fig. 81. 1-D DWT Of Cell 1

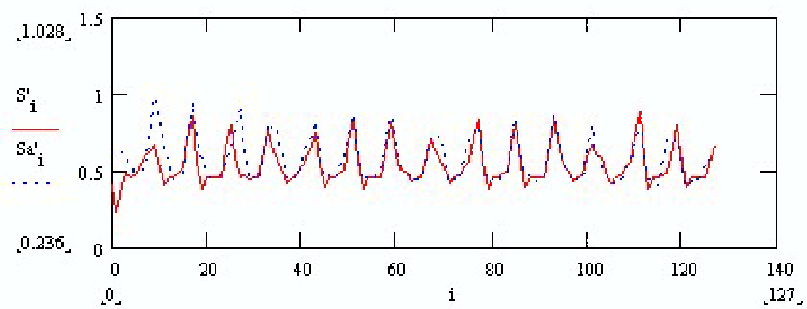


Fig. 82. 1-D Inverse DWT Of Cell 1

There are 7 levels in this decomposition. In the coefficients graph (cfs), the X-axis is the time axis, the Y-axis is the scale axis and each X-Y pt on the graph corresponds to a certain frequency, and the color represents the value of the coefficient on a color scale which goes from dark(Min value) to light(Max value). Hence by using this analysis, it is easy to say what frequency occurs in the signal at a certain time and scale.

$$\begin{aligned}
 S &= a_1 + d_1 \\
 &= a_2 + d_2 + d_1 \\
 &= a_3 + d_3 + d_2 + d_1 \\
 &= a_4 + d_4 + d_3 + d_2 + d_1 \\
 &= a_5 + d_5 + d_4 + d_3 + d_2 + d_1 \\
 &= a_6 + d_6 + d_5 + d_4 + d_3 + d_2 + d_1 \\
 &= a_7 + d_7 + d_6 + d_5 + d_4 + d_3 + d_2 + d_1
 \end{aligned}$$

The following figures, Fig.83, Fig.84 and Fig.85 show wavelet decomposition of the experimental signal of cell 1 into approximations, details and the subsequent coefficients. Also shown is the synthesized signal. As can be seen from the graphs, the approximations are the low frequency components, while the details are the higher frequency components. Also, the original signal S can be decomposed as follows:

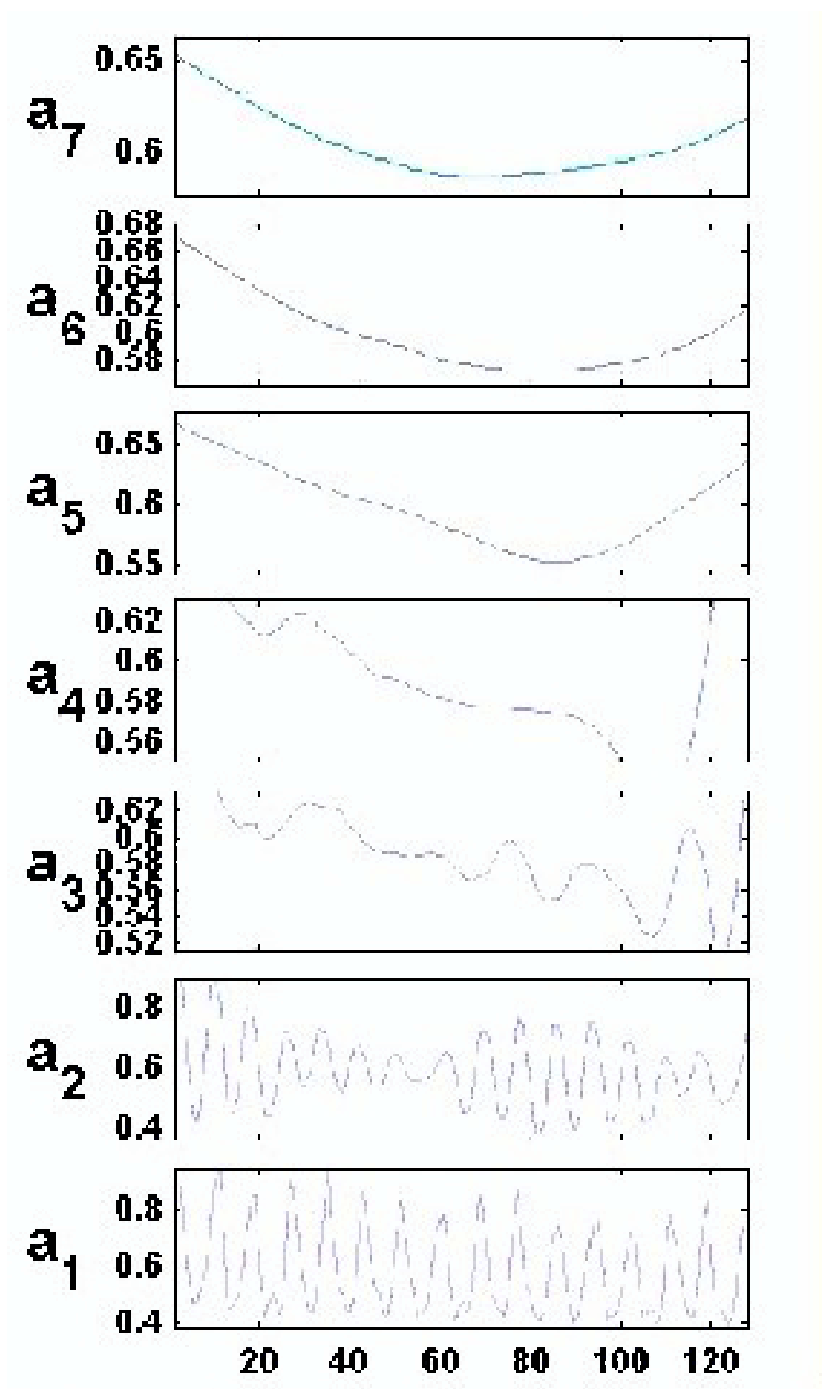


Fig. 83. Expt Cell 1 Decomposition: Approximations

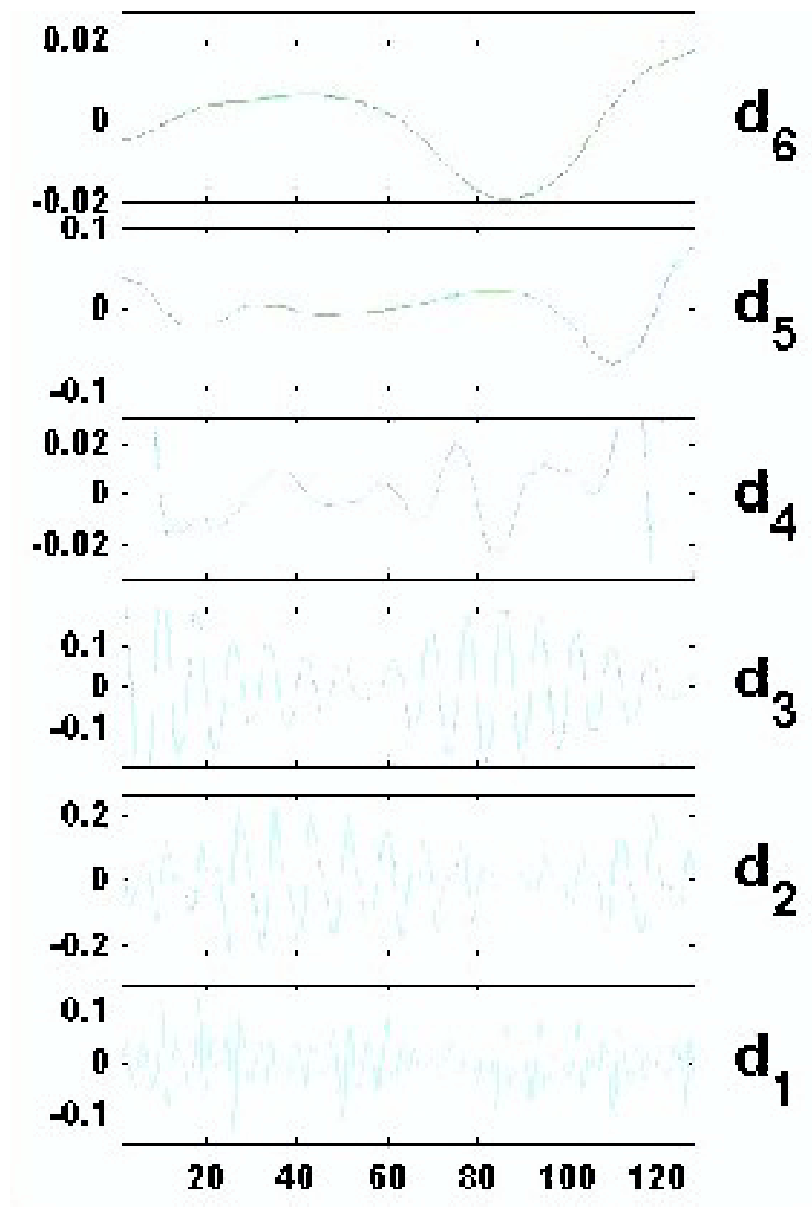


Fig. 84. Expt Cell 1 Decomposition: Details

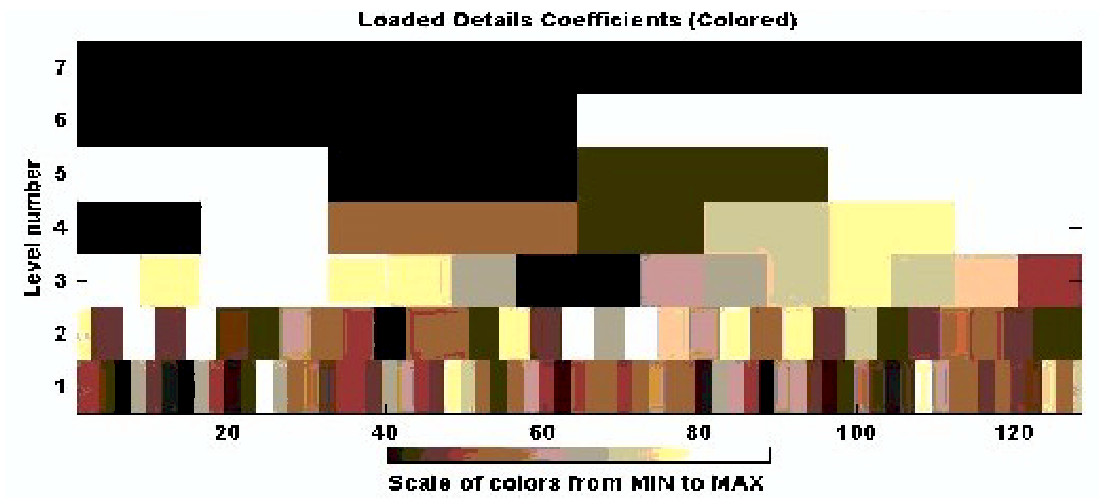


Fig. 85. Details Of Coefficients Of Expt Cell 1

The next three figures, Fig.86, Fig.87 and Fig.88 show decomposition of the model cell 1 data and its subsequent details, and coefficients.

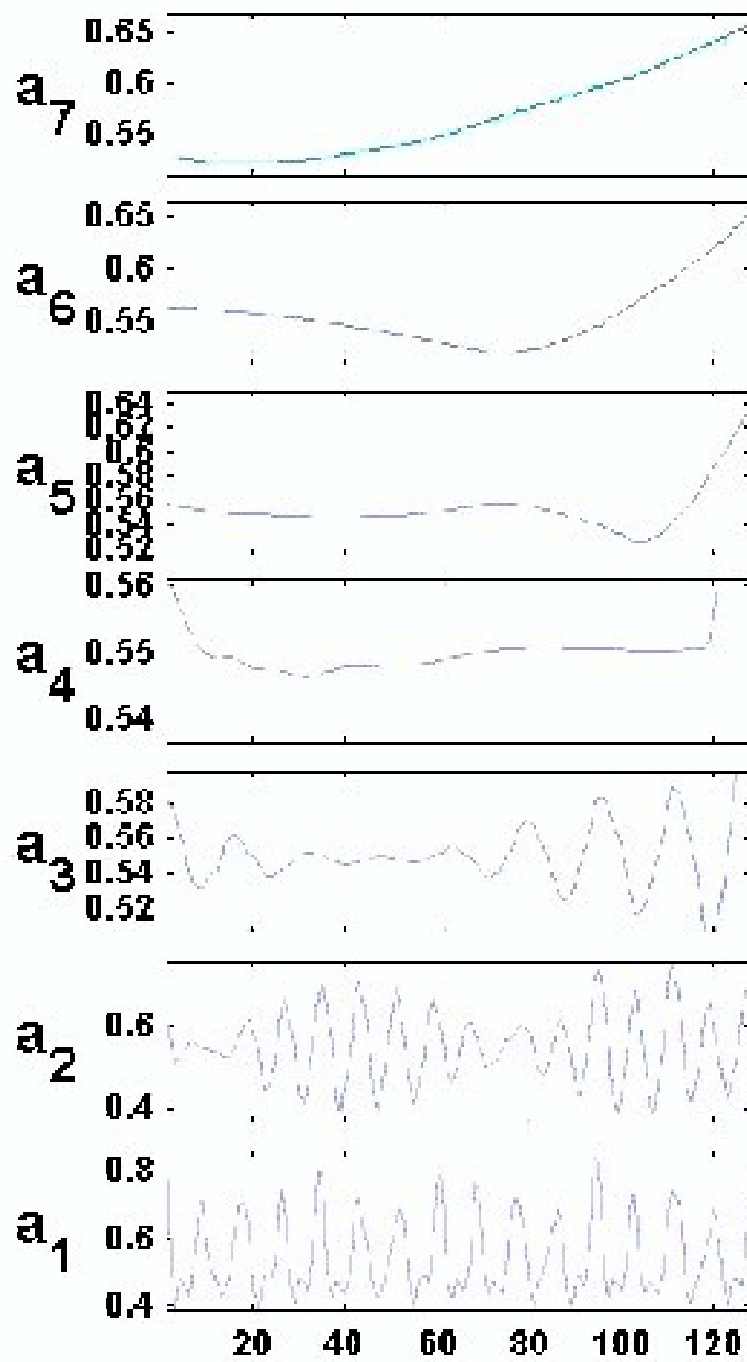


Fig. 86. Model Cell 1 Decomposition: Approximations

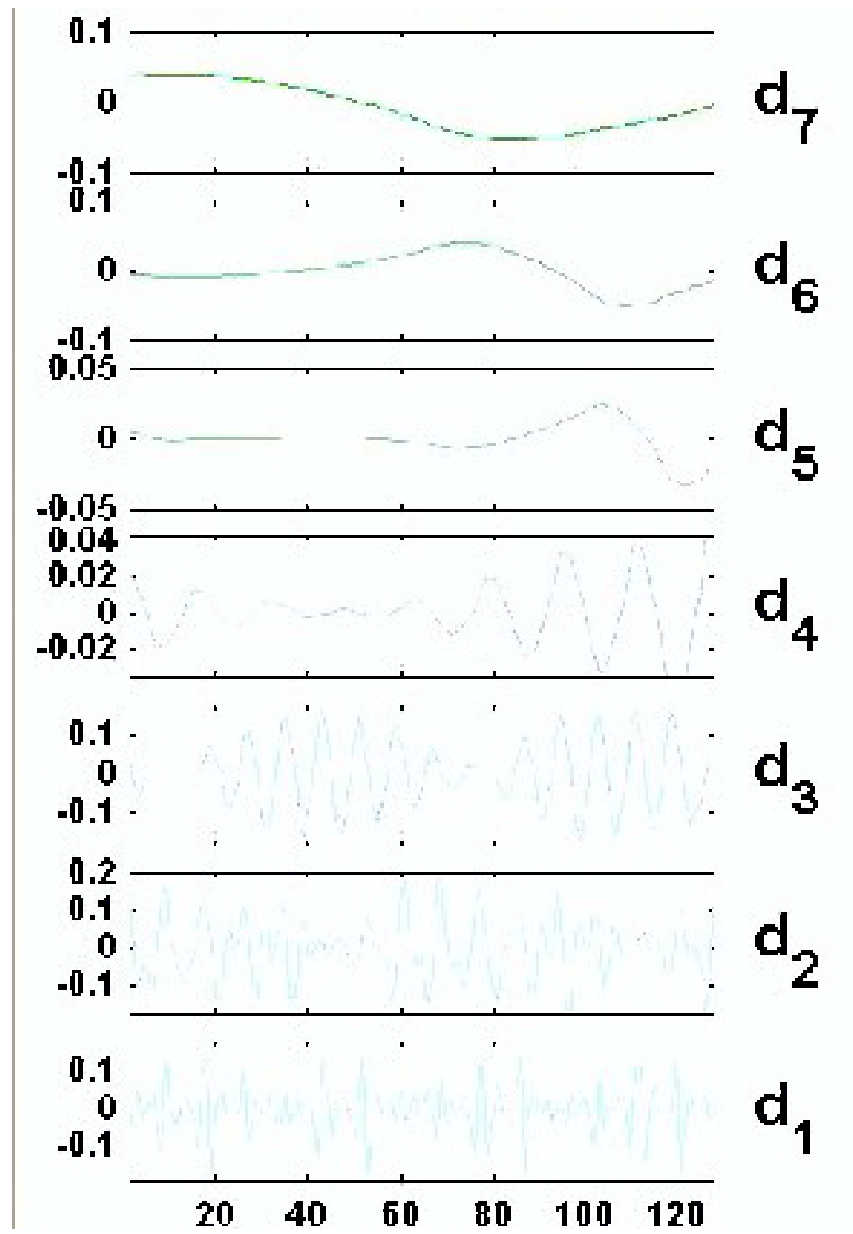


Fig. 87. Model Cell 1 Decomposition: Details

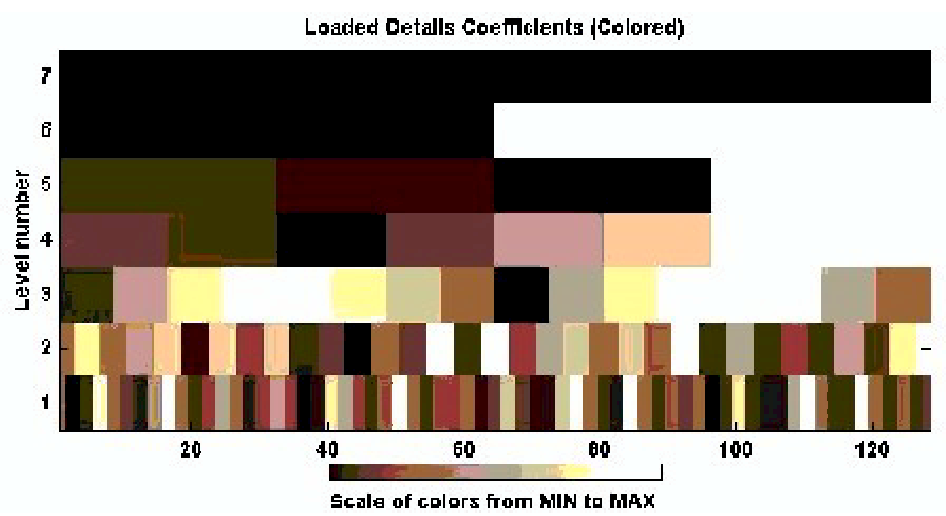


Fig. 88. Details Of Coefficients Of Model Cell 1

Note the similarity in the coefficients of experimental and model cell data. The next few figures(Fig.89 to Fig.93) illustrate the same wavelet decomposition as above.

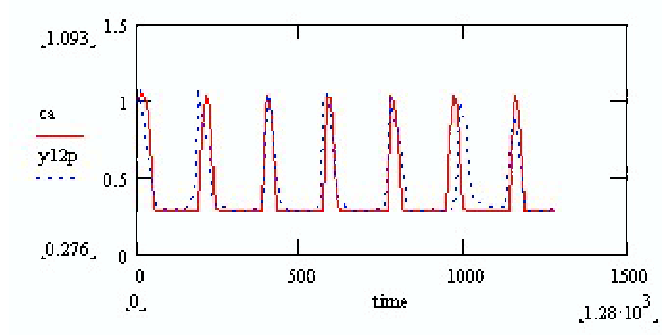


Fig. 89. Original Cell 2 In Time Domain

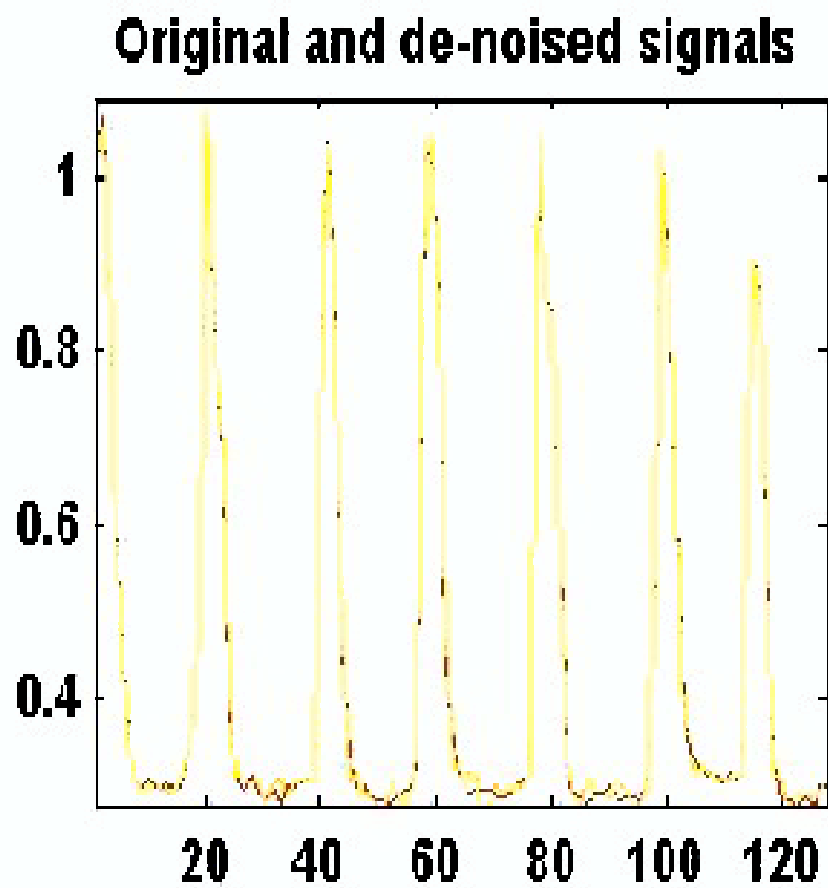


Fig. 90. Denoised Experimental Cell 2

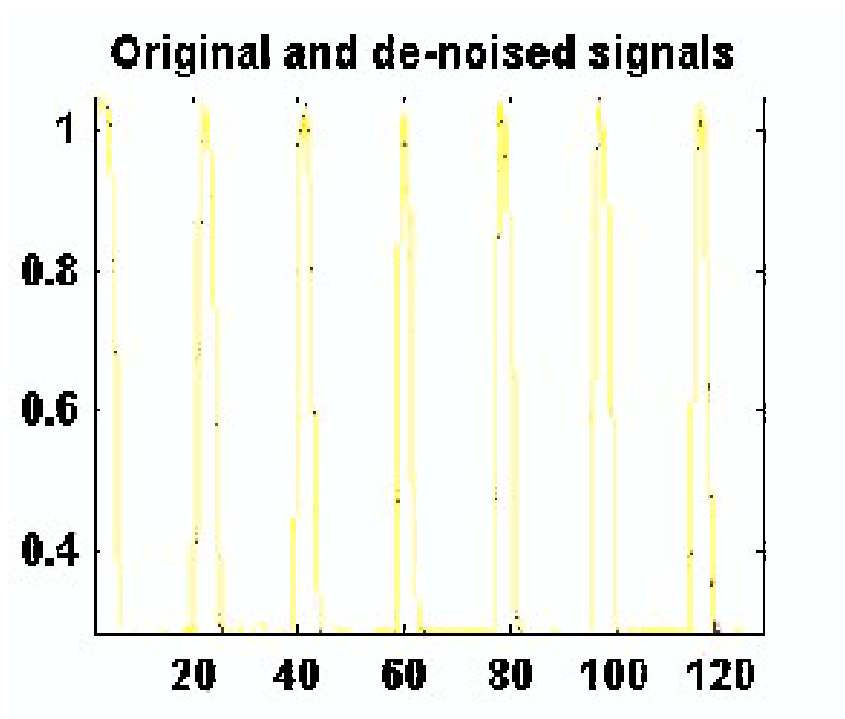


Fig. 91. Denoised Model Cell 2

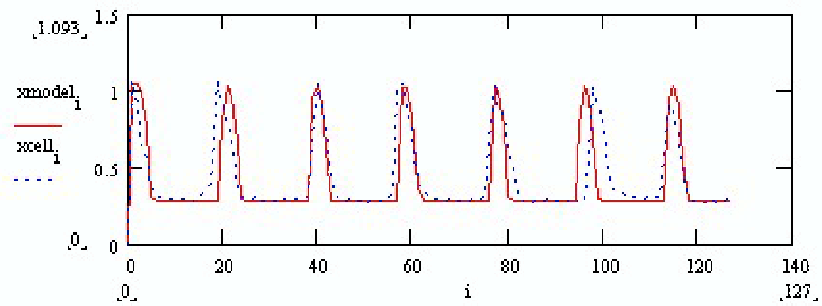


Fig. 92. 1-D DWT Of Cell 2

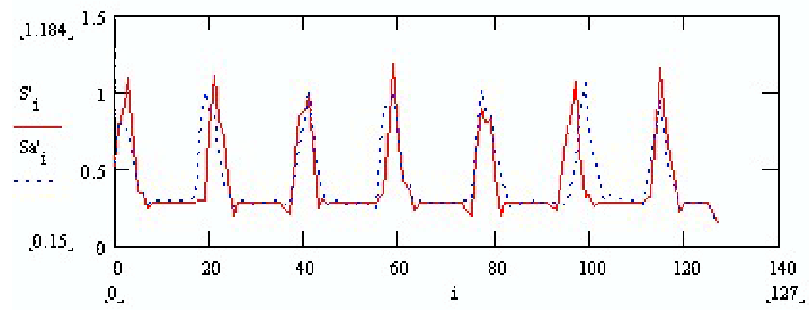


Fig. 93. 1-D Inverse DWT Of Cell 2

The next few figures (Fig.94 to Fig.99) shows decomposition of experimental cell 2: Graphs include original signal, coefficients, approximations and details. Note the nature of approximations and details.

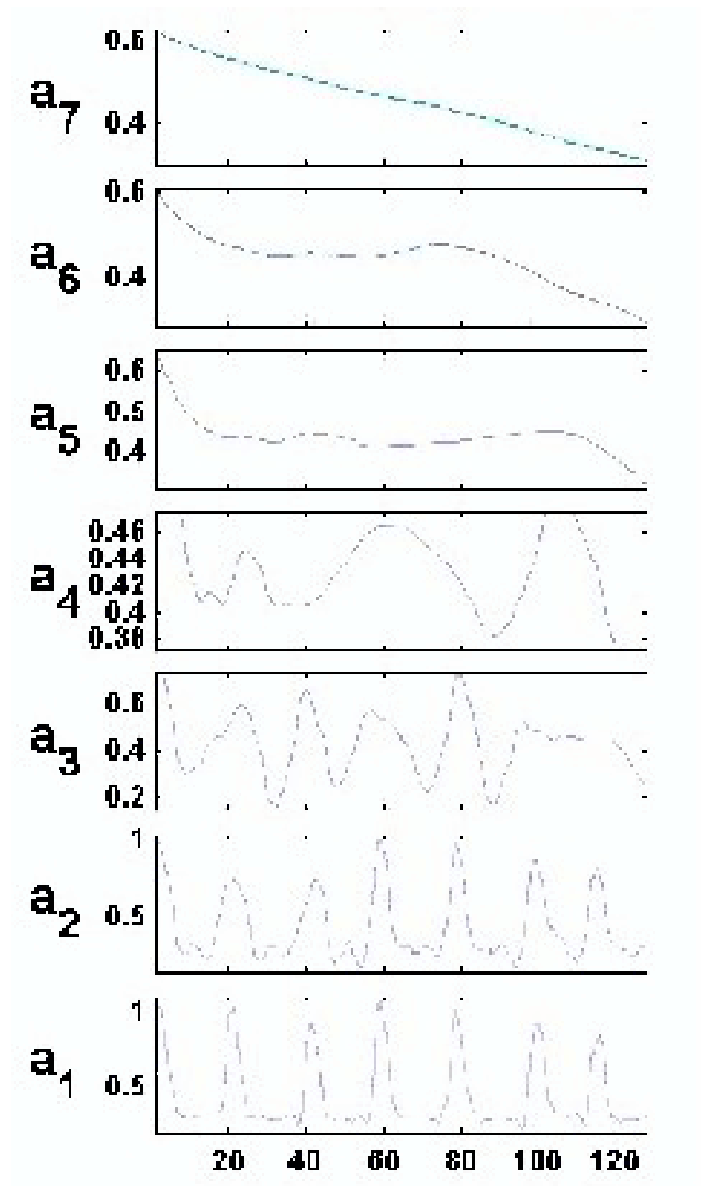


Fig. 94. Expt Cell 2 Decomposition: Approximations

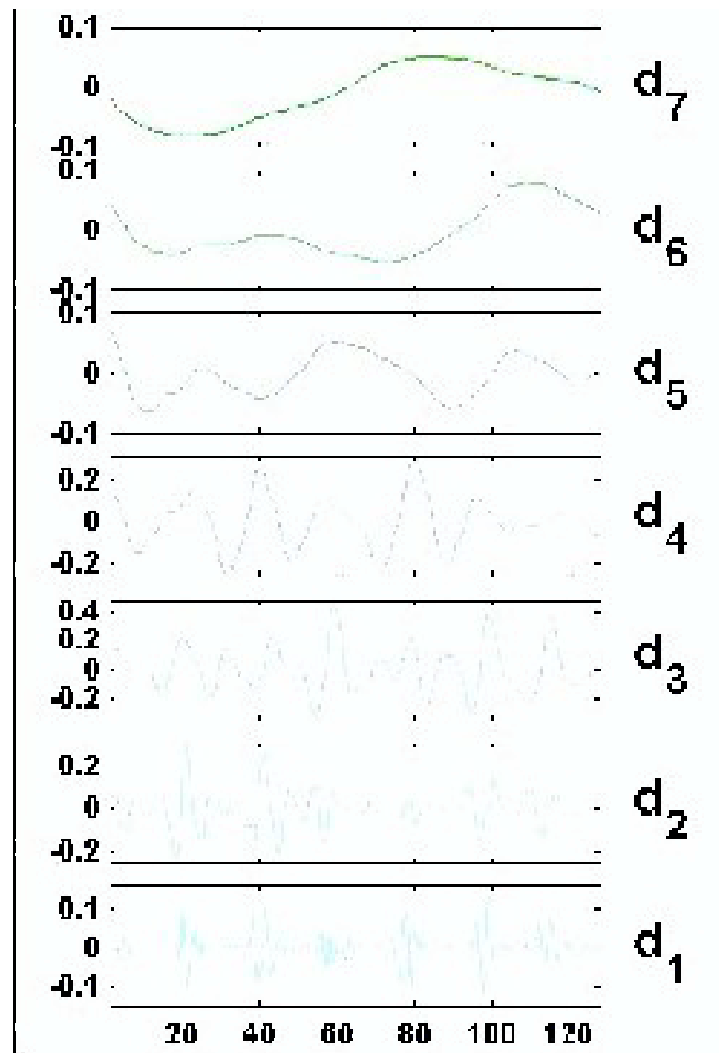


Fig. 95. Expt Cell 2 Decomposition: Details

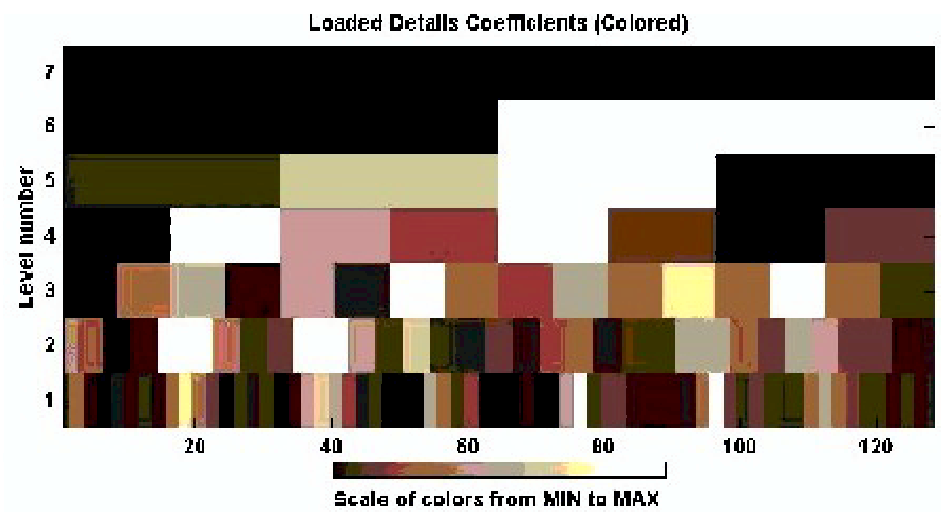


Fig. 96. Details Of Coefficients Of Expt Cell 2

Note the similarity of coefficients of model cell 2 data to experimental cell 2 data.

Here again, the coefficient patterns of both experimental and model cells are similar.

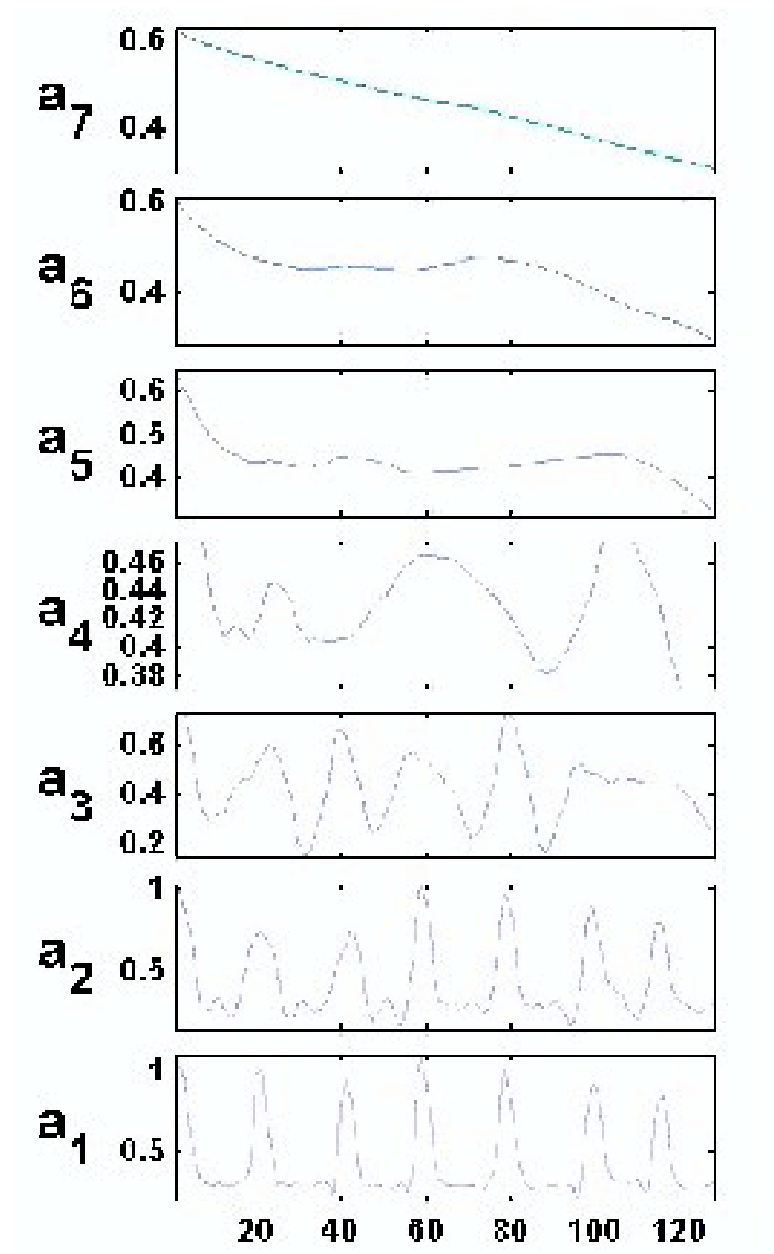


Fig. 97. Model Cell 2 Decomposition: Approximations

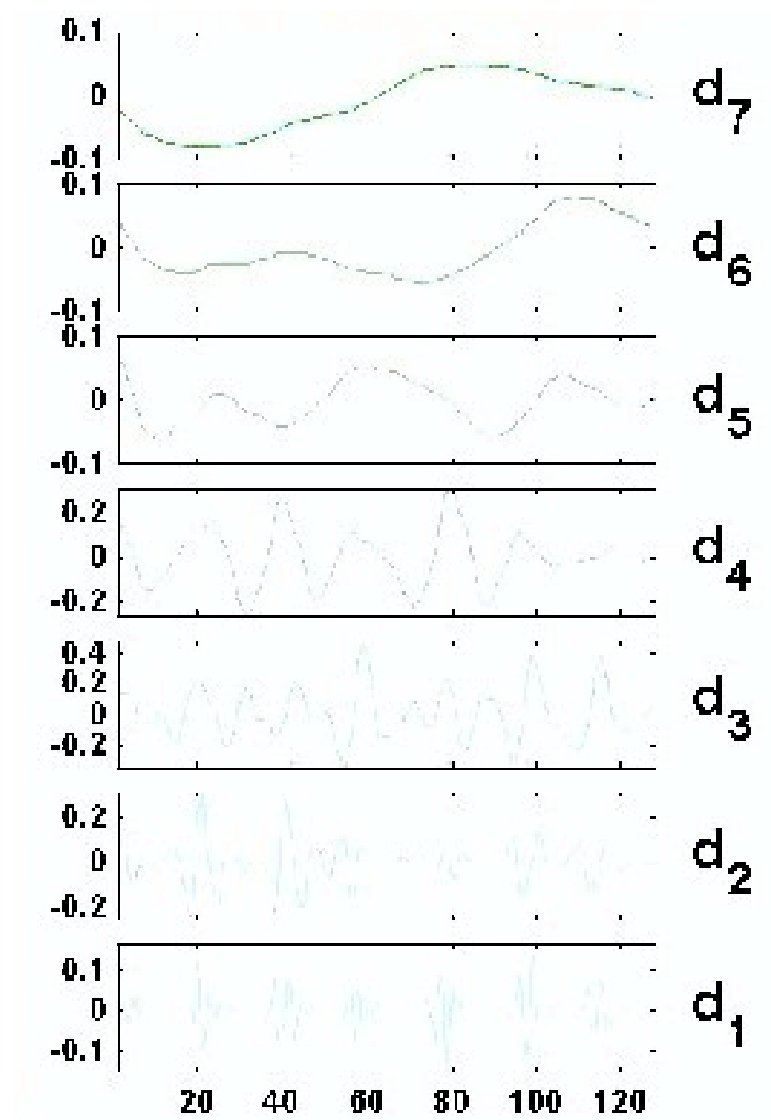


Fig. 98. Model Cell 2 Decomposition: Details



Fig. 99. Details Of Coefficients Of Model Cell 2

C. DISCUSSION

The results obtained by the Fourier Analysis give us important information regarding the mean fundamental frequencies and amplitudes that are shown by calcium oscillations in the period of around 500s for non-excitable cells and around 1300s for excitable cells. This is an interesting result as we can use this information for future experiments. Also, the experimental and model reconstructed data matched with the original data which again proves the validity of the model in the frequency domain. The results of the Wavelet Analysis prove that the model and experimental results match well as is easily seen in the detailed coefficients graph. The minor differences that are observed are due to unavoidable experimental errors. Here again, the original experimental and reconstructed model calcium oscillations fit effectively. Hence the validity of the model is established for both excitable and non-excitable cells. It was observed that denoising the signals and then decomposing them did not give as good a match to the model as expected. This is due to the various thresholding parameters present which resulted in the experimental signal and model signal being thresholded at different levels and having different threshold values which caused the two original signals to become much different from each other than what they initially were. Hence, although the denoised signals have been shown above, the above wavelet analysis was done using the original experimental and model data and was found to give a satisfactory fit. The 1-D DWT proves to be an effective tool, as good as and in many ways much more informative than the Fourier Transform since we are exactly able to tell what frequency is occurring at a particular time using the coefficients graph and the colorscale.

CHAPTER VI

SUMMARY AND CONCLUSIONS

The first part of this chapter presents a summary of all the previous chapters. The latter part of this chapter presents the conclusions of the present study.

A. SUMMARY

1. Chapter 1 presents an introduction to calcium signaling and a detailed description of the four components of the calcium signaling toolkit viz. generation of Ca^{2+} -mobilizing signals, ON mechanisms, Ca^{2+} -sensitive processes and OFF mechanisms. The last part of the chapter includes a discussion on some important aspects of calcium signaling like spatial aspects, temporal aspects, cell proliferation and cell death.
2. The first part of Chapter 2 deals with the need for models for Ca^{2+} oscillations. Next, a background of the existing models for describing Ca^{2+} oscillations is given. The models discussed are as follows: The calcium-induced-calcium-release model by Cuthbertson and Chay, the IP_3 - Ca^{2+} crosscoupling model by Meyer and Stryer, the ICC-CICR combination model by Shen and Larter and the Dupont model to explain intercellular Ca^{2+} wave propagation in non-excitable cells.
3. In Chapter 3, the experimental procedures for obtaining the image data in both excitable and non-excitable cell lines is described. The latter part of the chapter presents a detailed description of the proposed model for both the excitable and non-excitable cell line. The changes made to the model in order to incorporate gap junction diffusion in non-excitable cells has also been discussed in detail.

4. Chapter 4 presents the results of the data modeling. The first part of the chapter presents the results for the excitable cell line which include statistical time and frequency domain tests in order to verify the validity of the model. The latter part of the chapter presents the results for the non-excitable cell line with similar time and frequency domain tests.
5. Chapter 5 gives the details of the results of the data analysis of the excitable and non-excitable cell line. The first part of the chapter presents an introduction to Fourier Transform and describes the results of the analysis of excitable and non-excitable cell lines using Fast Fourier Transform and Inverse Fast Fourier Transform. The second part of the chapter presents an introduction to Wavelet Transforms and goes on to present the results of the analysis of both the excitable and non-excitable cell lines using 1-D Discrete Wavelet Transforms and 1-D Inverse Discrete Wavelet Transforms.

B. CONCLUSIONS

Although there are a number of models in the literature, the need to develop a new model to fit the hepatocyte and myometrial cell data arose from the fact that experimental conditions were different from those being used in the literature. The need to develop a model for a large group of cells, each being treated with an agonist rather than just an isolated cell or two or three cells, was the motivation behind developing a new model. The frequency spectrum is significant in light of recent studies that have identified cellular targets capable of integrating or decoding frequency-encoded intracellular Ca^{2+} signals. The FFT is an important tool which could be used to identify cellular targets to decode the frequency-encoded calcium signals into a cellular function. The results of the data analysis using the Wavelet Transform seem to be very promising too as knowing the time-frequency information of a signal can help to unravel important information about any defects that may have occurred in the signal at certain times, eliminate noise from the signals for purer frequency determination and also help in long-term prediction of evolution or trend of the signal which could reveal new information about the role and significance of calcium oscillations.

REFERENCES

- [1] M. Berridge, P. Cobbold, K. Cuthbertson, "Spatial and temporal aspects of cell signalling." *Philos Trans R Soc Lond B Biol Sci.*, vol.320, no.1199, pp. 325–343, Jul 26 1988.
- [2] M. Bootman, T. Collins, C. Peppiatt, L. Prothero, L. MacKenzie, P De Smet, M. Travers, S. Tovey, J. Seo, M. Berridge, F. Ciccolini, P. Lipp, "Calcium signalling—an overview." *Semin Cell Dev Biol.*, vol.12, no.1, pp. 3–10, Feb 2001.
- [3] M. Berridge, P. Lipp, M. Bootman, "The versatility and universality of calcium signalling." *Nat Rev Mol Cell Biol.*, vol.1, no.1, pp. 11–21, Oct 2000.
- [4] A. Genazzani, A. Galione, "A Ca^{2+} release mechanism gated by the novel pyridine nucleotide, NAADP" *Trends Pharmacol Sci.*, vol.18, no.4, pp. 108–110, Apr 1997.
- [5] C. Mao, S. Kim, J. Almenoff, X. Rudner, D. Kearney, L. Kindman, "Molecular cloning and characterization of SCaMPER, a sphingolipid Ca^{2+} release-mediating protein from endoplasmic reticulum." *Proc Natl Acad Sci U S A.*, vol. 93, no.5, pp. 1993–1996, Mar 5 1996.
- [6] M. Berridge, M. Bootman, P. Lipp, "Calcium- a life and death signal." *Nature*, vol. 395, pp. 645–648, Oct 1998.
- [7] J. Sneyd, J. Keizer, M. Sanderson, "Mechanisms of Calcium Oscillations and Waves: A Quantitative Analysis." *FASEB J.*, vol. 9, pp. 1463–1472, Nov 1995.
- [8] M. Berridge, "Inositol Trisphosphate and Calcium Signalling." *Nature.*, vol. 361(6410), pp. 315–325, Jan 28 1993.

- [9] G. Dupont, T. Tordjmann, C. Clair, S. Swillens, M Claret, L Combettes, “Mechanism of receptor-oriented intercellular calcium wave propagation in hepatocytes.” *FASEB J.*, vol. 14, no.2, pp. 279–289, Feb 2000.
- [10] K. Cuthbertson and T. Chay, “Modeling receptor-controlled intracellular calcium oscillators.” *Cell Calcium*, vol. 12, no.2–3, pp. 97–109, Feb-Mar 1991.
- [11] M. Endo, M. Tanaka, Y. Ogawa, “Calcium induced release of calcium from the sarcoplasmic reticulum of skinned skeletal muscle fibres.” *Nature*, vol. 228, no.5266, pp. 34–36, Oct 3, 1970.
- [12] A. Goldbeter, G. Dupont, M. Berridge, “Minimal model for signal-induced Ca^{2+} oscillations and for their frequency encoding through protein phosphorylation.” *Proc Natl Acad Sci U S A*, vol. 87, no.4, pp. 1461–1465, Feb 1990.
- [13] T. Meyer, L. Stryer, “Calcium spiking.” *Annu Rev Biophys Biophys Chem.*, vol. 20, pp. 153–174., 1991.
- [14] P. Shen, R. Larter, “Chaos in intracellular Ca^{2+} oscillations in a new model for non-excitable cells.” *Cell Calcium.*, vol. 17, no.3, pp. 225–232, Mar 1995.
- [15] R. Burghardt, R. Barhoumi, B Sanborn, J Andersen, “Oxytocin-induced Ca^{2+} responses in human myometrial cells.” *Biol Reprod.*, vol. 60, no.4, pp. 777–782, Apr 1999.
- [16] R. Barhoumi, Y. Mouneimne, T. Phillips, S. Safe, R. Burghardt, “Alteration of oxytocin-induced calcium oscillations in clone 9 cells by toxin exposure.” *Fundam Appl Toxicol.*, vol. 33, no.2, pp. 220–228, Oct 1996.
- [17] M. Monga, C. Ku, K. Dodge, B. Sanborn, “Oxytocin-stimulated responses in a pregnant human immortalized myometrial cell line.” *Biol Reprod.*, vol. 55, no.2,

- pp. 427–432, Aug 1996.
- [18] R. Hutchinson, R. Barhoumi, J. Miles, R. Burghardt, “Attenuation of gossypol cytotoxicity by cyclic AMP in a rat liver cell line.” *Toxicol Appl Pharmacol.*, vol. 151, no.2, pp. 311–318, Aug 1998.
- [19] www.mathworks.com, The MathWorks Release 2.1 Documentation, Accessed date: August 2002
- [20] J. Putney Jr., “Calcium signaling: up, down, up, down...what’s the point?” *Science*, vol. 279, no.5348, pp. 191–192, Jan 9 1998.
- [21] R. Tsien, “Fluorescent probes of cell signaling.” *Annu Rev Neurosci.*, vol. 12, pp. 227–253, 1989.
- [22] T. Meyer, L. Stryer, “Transient calcium release induced by successive increments of inositol 1,4,5-trisphosphate.” *Proc Natl Acad Sci U S A*, vol. 87, no.10, pp. 3841–5, May 1990.

APPENDIX A

DATA MODELING RESULTS

The following are some more data modeling results for both the cell lines:

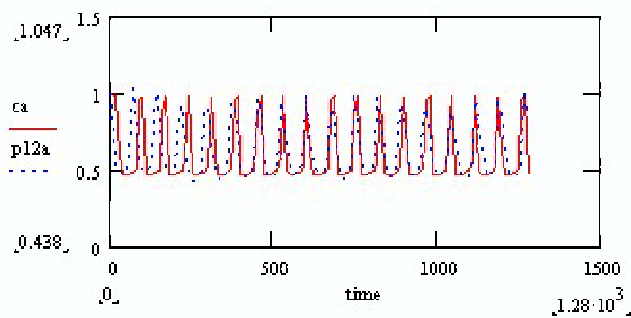


Fig. 100. PHM1 Cell 11

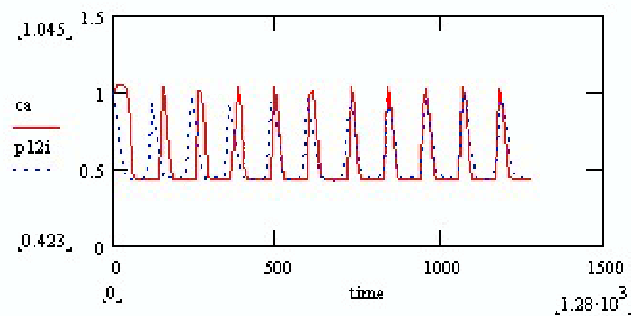


Fig. 101. PHM1 Cell 12

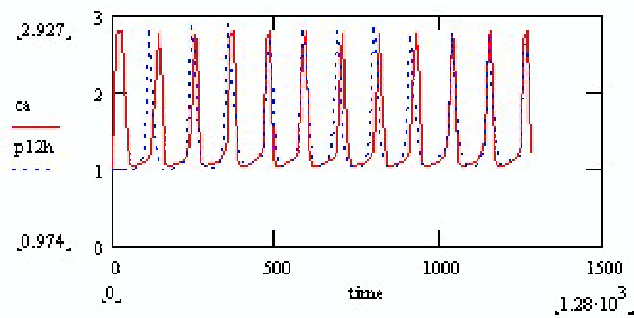


Fig. 102. PHM1 Cell 13

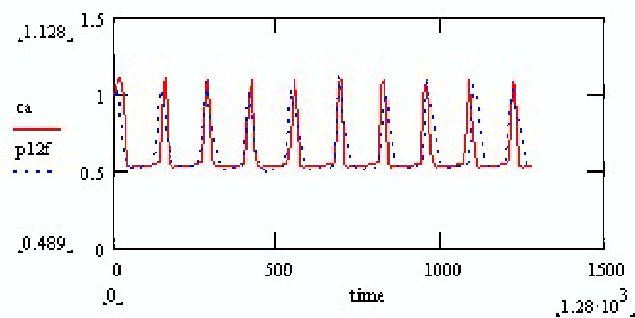


Fig. 103. PHM1 Cell 14

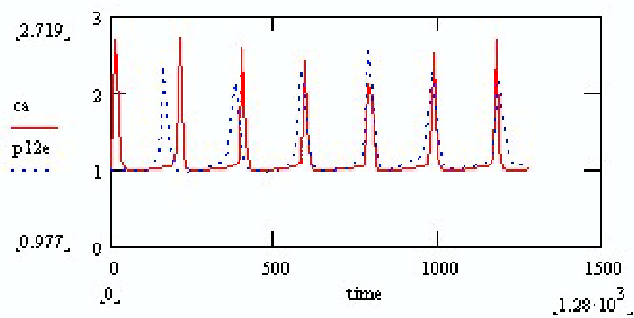


Fig. 104. PHM1 Cell 15

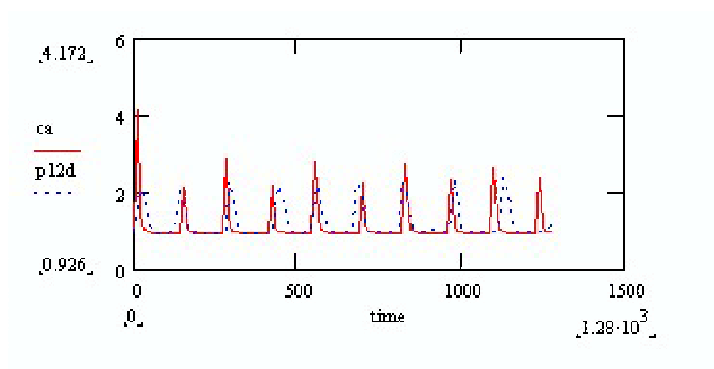


Fig. 105. PHM1 Cell 16

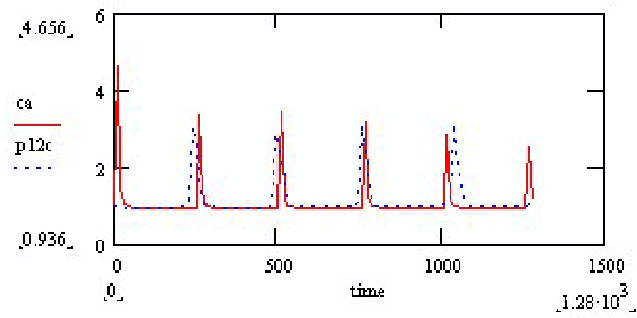


Fig. 106. PHM1 Cell 17

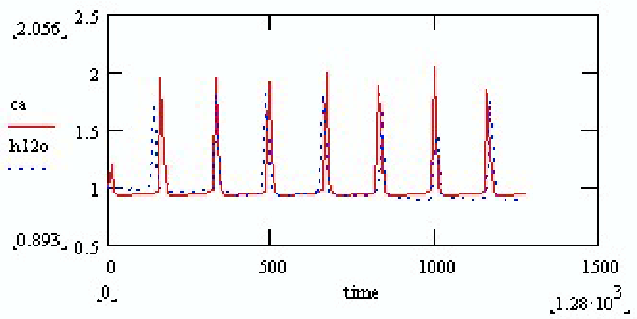


Fig. 107. PHM1 Cell 18

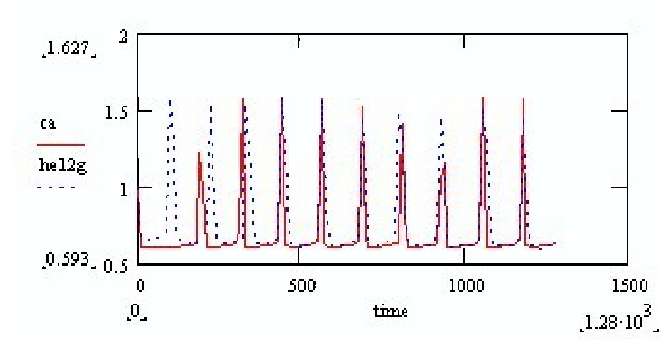


Fig. 108. PHM1 Cell 19

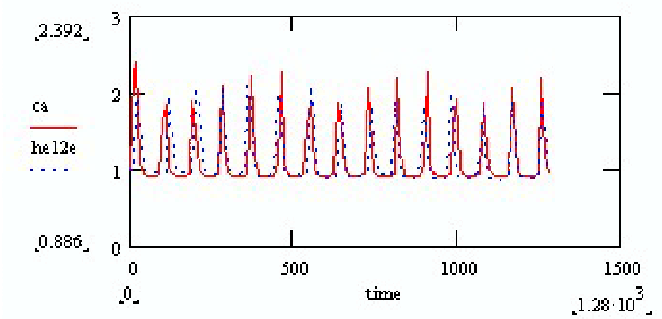


Fig. 109. PHM1 Cell 20

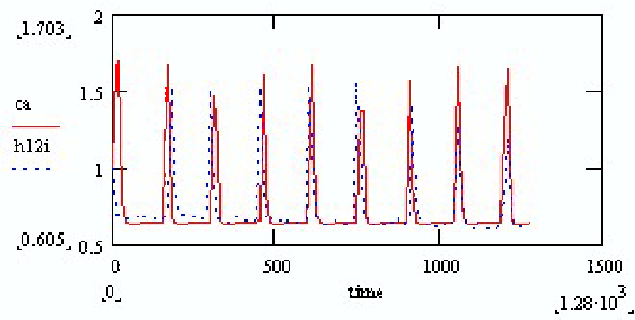


Fig. 110. PHM1 Cell 21

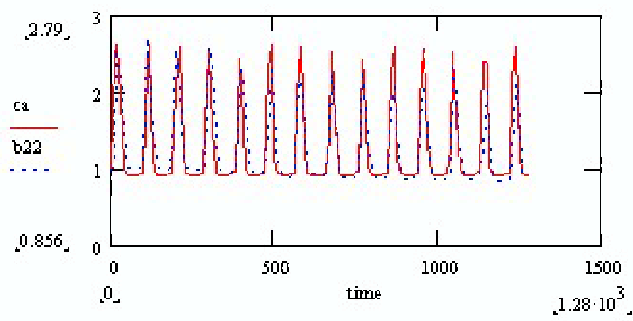


Fig. 111. PHM1 Cell 22

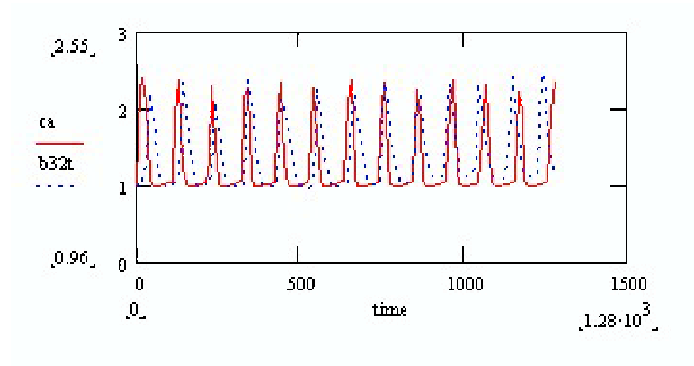


Fig. 112. PHM1 Cell 23

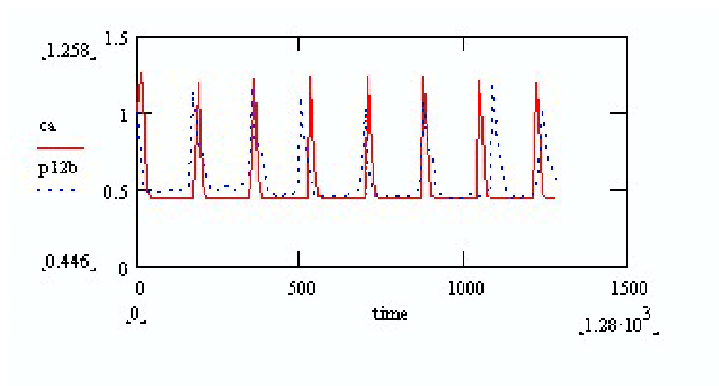


Fig. 113. PHM1 Cell 24

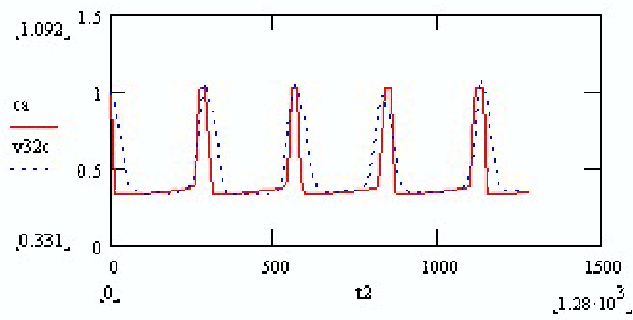


Fig. 114. PHM1 Cell 25

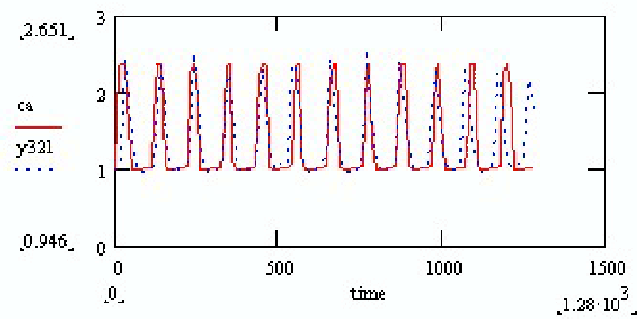


Fig. 115. PHM1 Cell 26

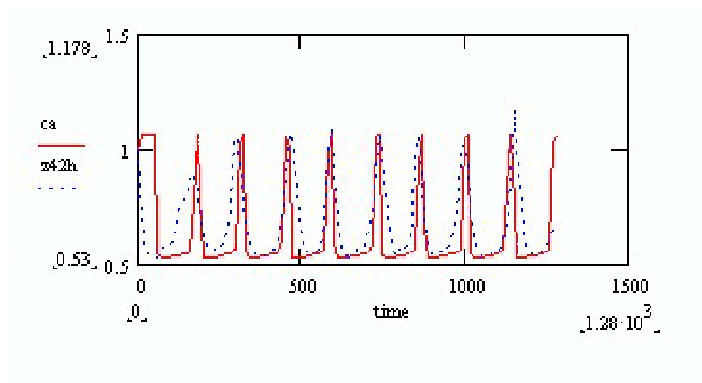


Fig. 116. PHM1 Cell 27

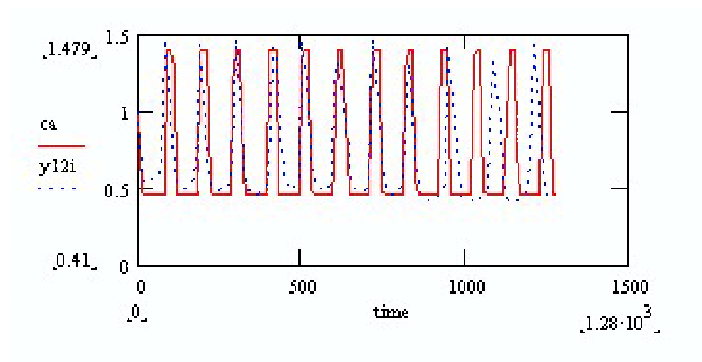


Fig. 117. PHM1 Cell 28

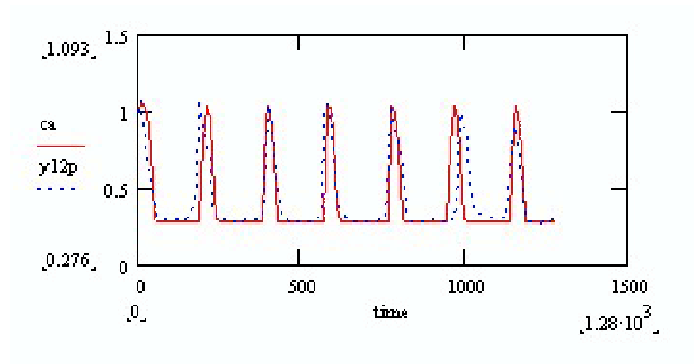


Fig. 118. PHM1 Cell 29

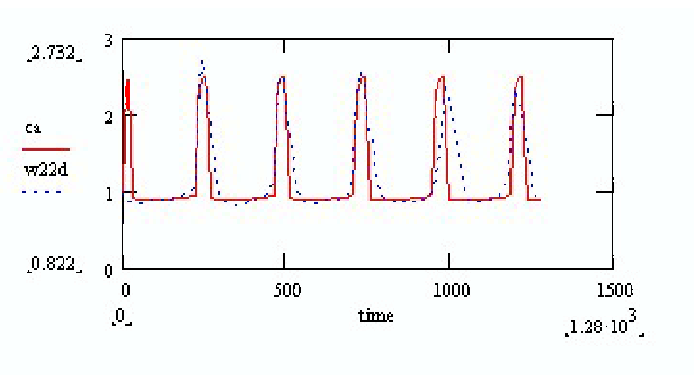


Fig. 119. PHM1 Cell 30

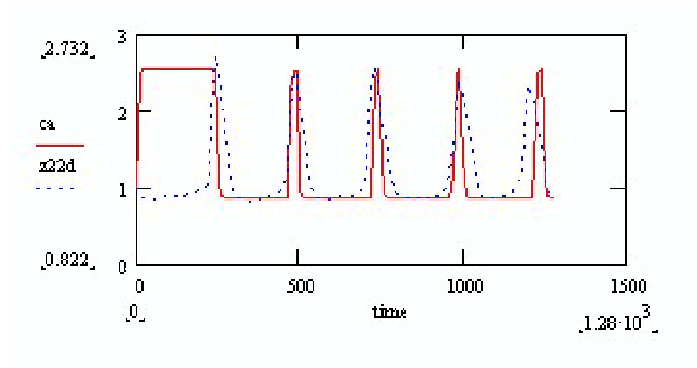


Fig. 120. PHM1 Cell 31

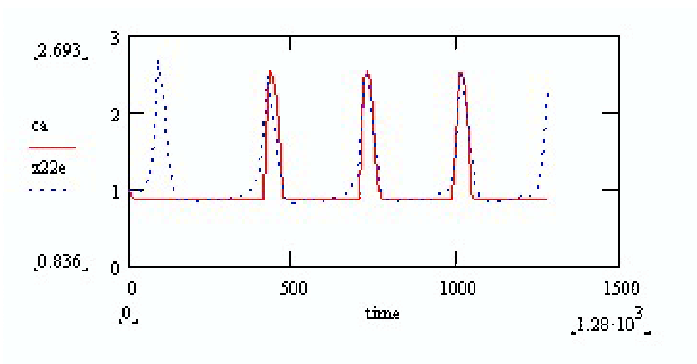


Fig. 121. PHM1 Cell 32

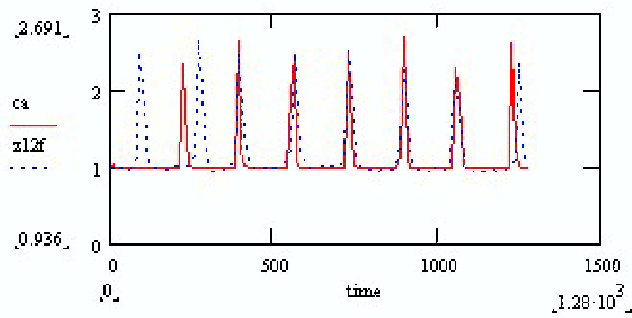


Fig. 122. PHM1 Cell 33

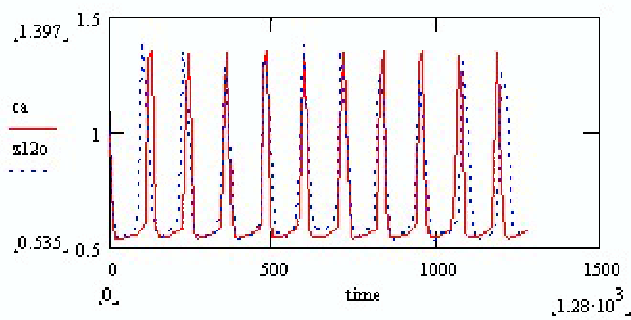


Fig. 123. PHM1 Cell 34

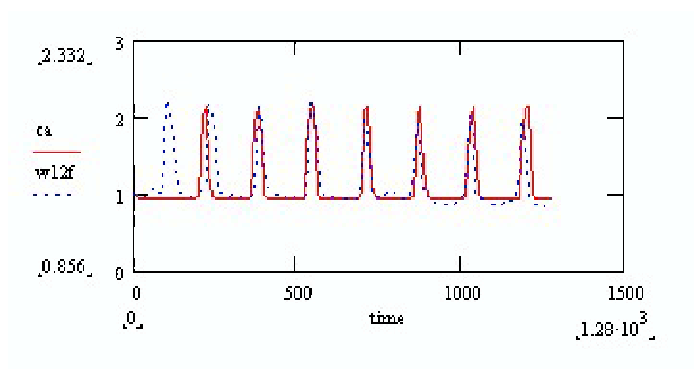


Fig. 124. PHM1 Cell 35

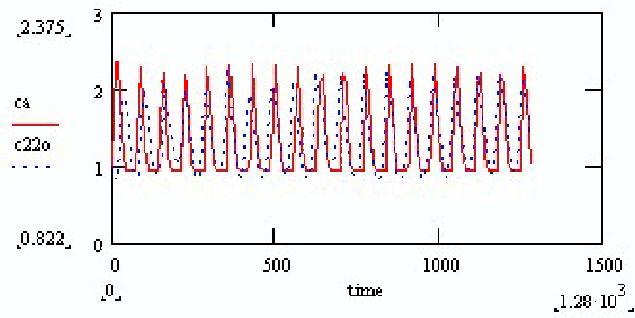


Fig. 125. PHM1 Cell 36

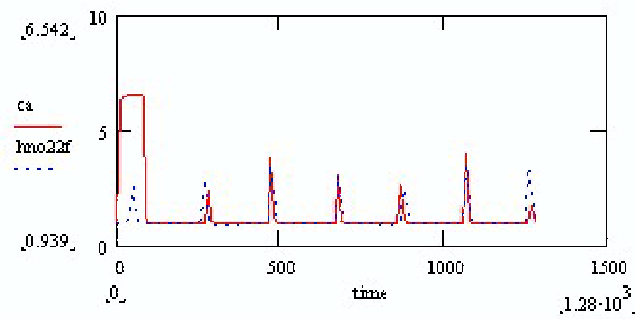


Fig. 126. PHM1 Cell 37

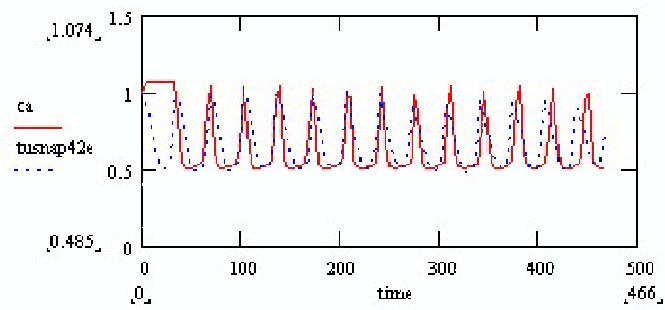


Fig. 127. Clone 9 Cell 19

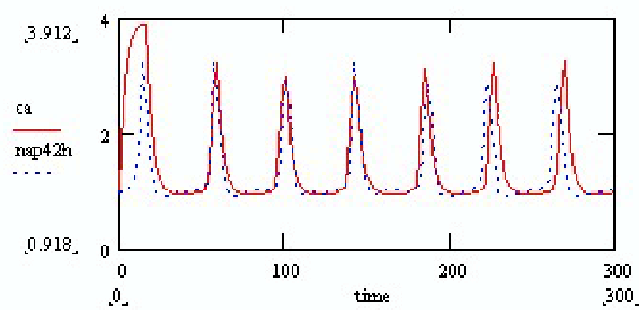


Fig. 128. Clone 9 Cell 20

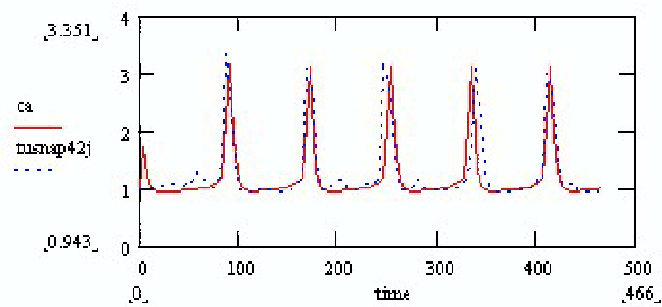


Fig. 129. Clone 9 Cell 21

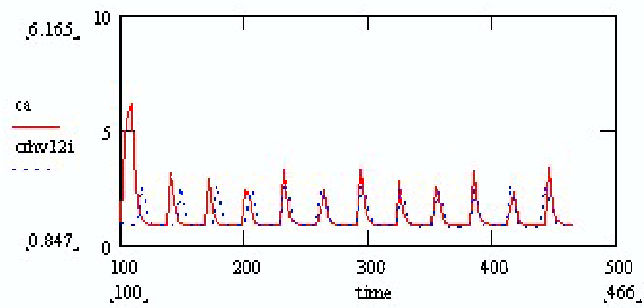


Fig. 130. Clone 9 Cell 22

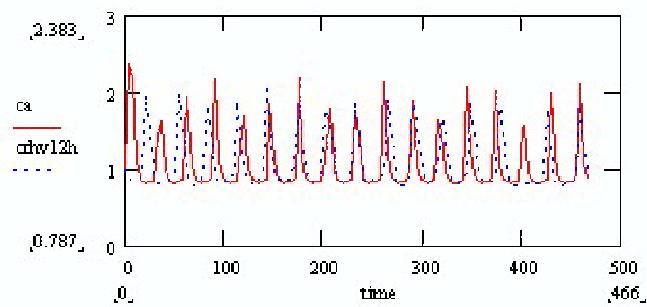


Fig. 131. Clone 9 Cell 23

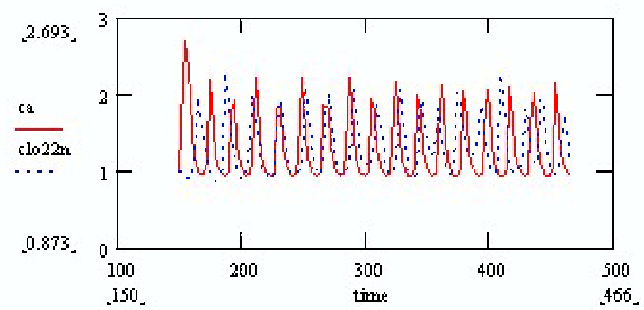


Fig. 132. Clone 9 Cell 24

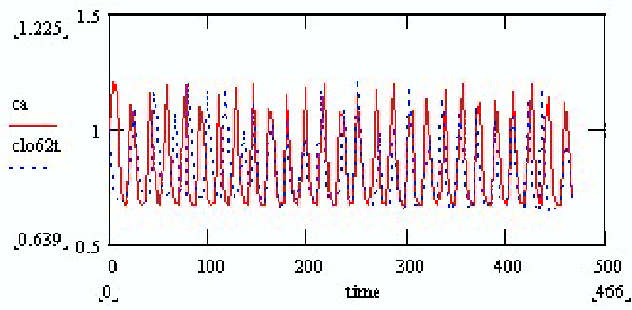


Fig. 133. Clone 9 Cell 25

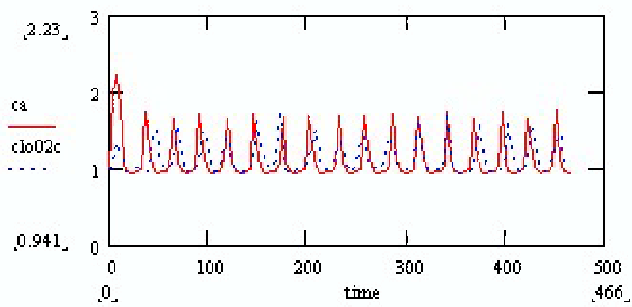


Fig. 134. Clone 9 Cell 26

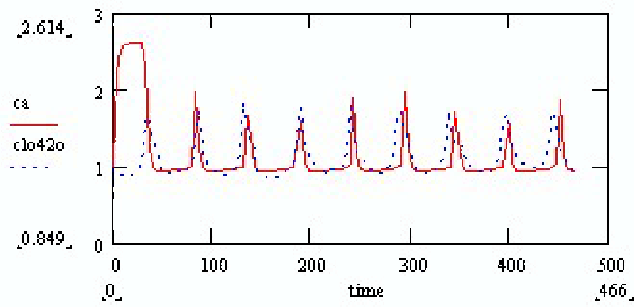


Fig. 135. Clone 9 Cell 27

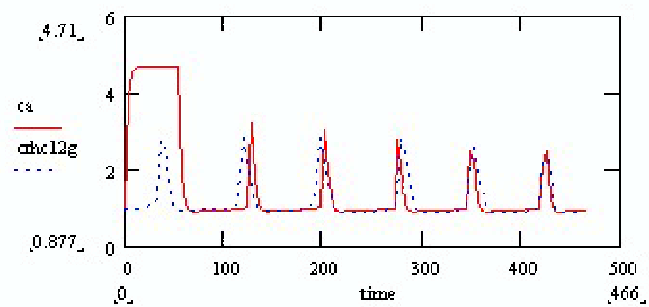


Fig. 136. Clone 9 Cell 28

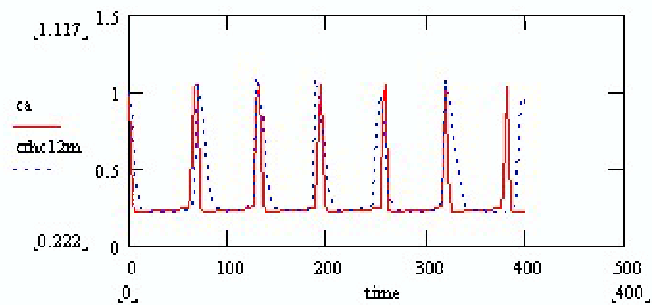


Fig. 137. Clone 9 Cell 29

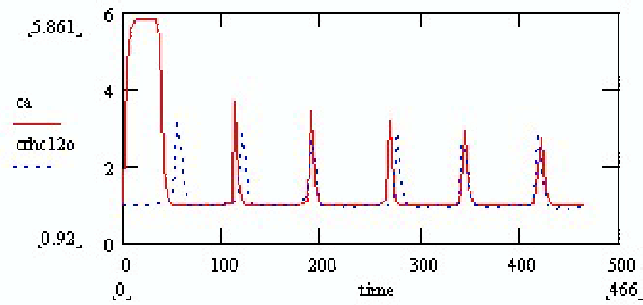


Fig. 138. Clone 9 Cell 30

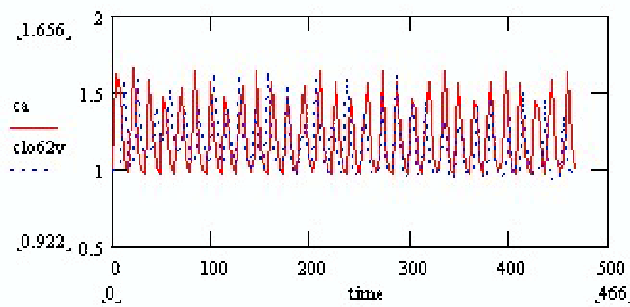


Fig. 139. Clone 9 Cell 31

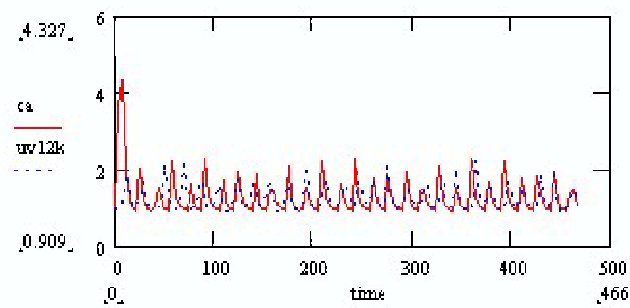


Fig. 140. Clone 9 Cell 32

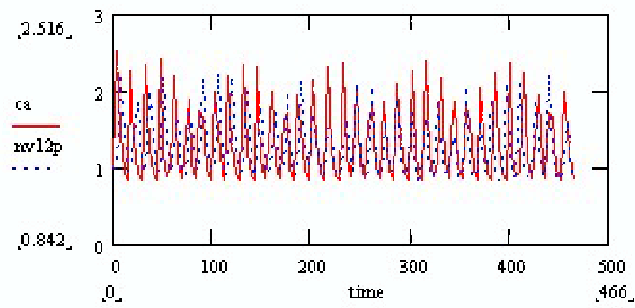


Fig. 141. Clone 9 Cell 33

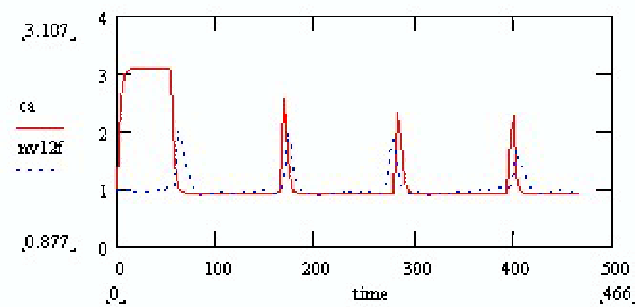


Fig. 142. Clone 9 Cell 34

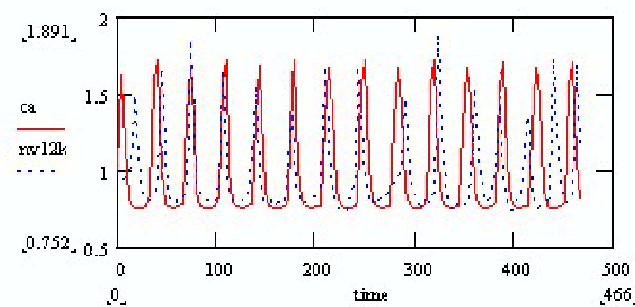


Fig. 143. Clone 9 Cell 35

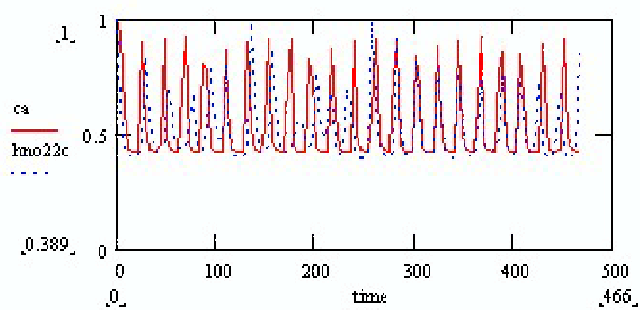


Fig. 144. Clone 9 Cell 36

VITA

Bharati Krishna Hegde was born in Sirsi, Karnataka, India. She received her B.E. degree in Electronics Engineering from Vishwakarma Institute of Technology, University of Pune, India in 1999. She worked as a Programmer Analyst with Cognizant Technology Solutions, Pune, India from July 1999 to July 2000. She joined the Department of Biomedical Engineering at Texas A&M University in August 2000 to pursue her Master's degree.

Permanent Address:

407, College Main, Apt.4,

College Station, TX- 77840

The typist for this thesis was Bharati Krishna Hegde.